

POLITECNICO DI TORINO



Master of Science in Civil Engineering

Thesis title:

“POST-PEAK BEHAVIOR OF RUBBERIZED  
CONCRETE IN COMPRESSION”

**Supervisor:** Alessandro Pasquale Fantilli (DISEG)

**Student:** Noussaiba Ben Ayed

**Matricola:** s249192

Academic year: 2019-2020

## Sommario

Summary: .....	4
1. Introduction : .....	5
2. Literature review : .....	10
2.1 compressive strength as a function of rubber content : .....	13
3. Pre-peak and Peak behavior of rubberized concrete: .....	17
3.1. Test number One: .....	18
3.1.1. Materials and method : .....	18
3.1.2. Specimen preparation and testing: .....	19
3.1.3. Results and discussion: .....	20
3.2. Test number Two: .....	23
3.2.1. Materials and method: .....	23
3.2.2. Specimen preparation and testing: .....	25
3.2.3. Results and discussion: .....	25
3.3. Test number Three : .....	27
3.3.1. Materials and method: .....	27
3.3.2. Specimen preparation and testing : .....	28
3.3.3. Results and discussion : .....	29
4. Post-Peak behavior of rubberized concrete : .....	32
4.1. Test number one : .....	33
4.1.1. Materials and method: .....	33
4.1.2. Specimen preparation and testing: .....	34
4.1.3. Results and discussion : .....	36
4.2. Test number Two: .....	44
4.2.1. Materials and methods: .....	44
4.2.2. Concrete mixes: .....	45
4.2.3. Results and discussion: .....	46
4.3. Test number Three: .....	51
4.3.1. Materials and method: .....	51
4.3.2. Test setup: .....	52
4.3.3. Results and discussion : .....	53

4.4.	Test number Four :	57
4.4.1.	Materials methods:	57
4.4.2.	Specimen preparation and testing:	58
4.4.3.	Results and discussion:	59
4.5.	Test number Five:	63
4.5.1.	Materials:	63
4.5.2.	Mix design and testing arrangement :	63
4.5.3.	Results and discussion:	65
5.	Characterization of post-peak branch :	69
5.1.	The normalized stress and the inelastic displacement diagram:	69
5.2.	The area A(f):	71
5.3.	The experimental results:	72
5.3.1.	Test number One:	72
5.3.2.	Test number Two:	78
5.3.3.	Test number Three:	81
5.3.4.	Test number Four :	85
5.3.5.	Test number Five:	88
6.	Conclusion :	91
	Bibliography:	97

## Summary:

After water, concrete is the most widely used substance on earth. If the cement industry were a country, it would be the third largest carbon dioxide emitter in the world with up to 2.8bn tonnes, surpassed only by China and the US, and therefore unfortunately, concrete is not an environmentally friendly material, either to make, or to use, or even to dispose of. To gain the raw materials to make this material, much energy and water must be used, and quarrying for sand and other aggregates causes environmental destruction and pollution.

Hence, a large number of researchers have focused on the development of a new concrete materials that would be more suitable with environmental necessity than ordinary Portland concrete. Among these materials, one of the most discussed is rubberized concrete. Waste tire rubber can be incorporated in self-compacting concrete by partially replacing the natural fine and coarse aggregate, reducing consumption of sand and gravel and preserving these natural materials. In addition, recycling and reusing waste tire rubber is one of the major ecological problem of the near future.

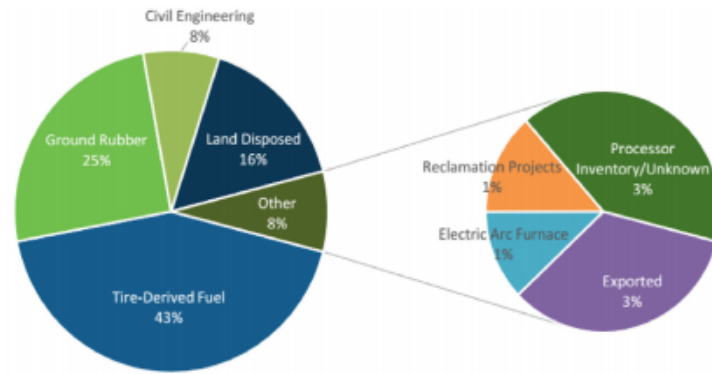
Replacement of natural aggregate with waste tire rubber can have an undesirable influence on the mechanical properties of self-compacting concrete, i.e., compressive strength, flexural strength, splitting tensile strength, and modulus of elasticity, however. On the other hand, replacing natural gravel or sand with waste tire rubber can improve impact resistance, ductility, and fatigue resistance. This paper presents an overview of the literature investigating recycled waste tire rubber used as a fine and/or coarse aggregate replacement in self-compacting concrete and its influence on several essential fresh and hardened self-compacting concrete properties.

## 1. Introduction :

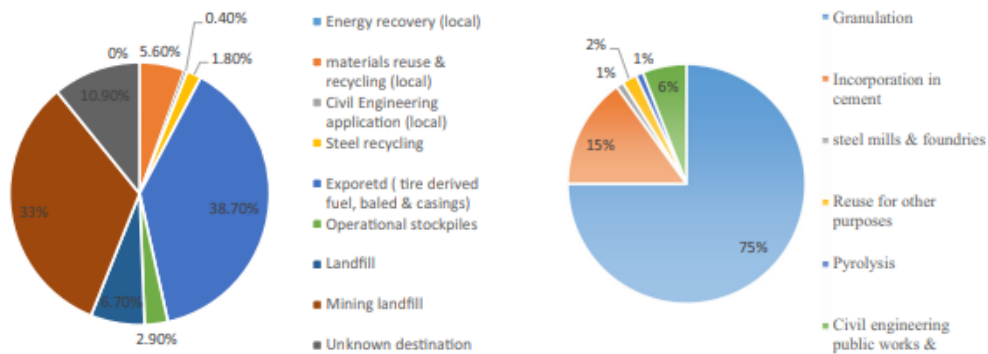
The number of unusable waste tires from different kinds of vehicles is rapidly growing and is in fact turning out as one of the major ecological and environmental problems of the present day. Nearly one-billion waste tires are discarded each year, and are predicted to be almost 1.2 billion per year by 2030. Nearly 8.3 million tons of waste tires are discarded per year just in Europe and United States of America (USA), some of which were probably disposed illegally, compromising human health as the aesthetics of nature. In the US, 289 million of waste tires are disposed annually. In Australia, this number is near 51 million and because of the overwhelming number of disposed tires, landfills are being cluttered with scrap tires and causing additional exposure to potential environmental threats, such as mosquitoes, mice, other insects, rats, and an increased risk of fire hazards.

Tire rubber contains styrene, a strongly toxic component that is highly damaging to humans. Therefore, dumping of waste tires may be very dangerous to human health. Recycling of waste in any way is beneficial. In recent years, researchers have attempted to establish a proper guideline for recycling tire waste in different ways. The global tire recycling market was valued at USD 0.95 billion in 2016 and is expected to grow at a compound annual growth rate of 2.1% during the forecast period. The same report revealed that North America accounts for approximately 31% of the revenue share of the global tire recycling market.

In response to the growing environmental concerns, waste tires are now being recycled in a manner that not only benefits the environment but also contributes to economic growth. As shown in Figure 1.



Disposal of scrap tires in the US (2017) [6]



Destination of waste tires in Australia (2016-2017) [7]

Materials recovery from waste tires in the EU (2016) [8]

Figure 1: Recycling status of waste tires in developed countries

based on the report of the US Tire Manufacturers Association , only 16% of scrap tires are dumped in landfills while the rest are being recycled in different ways. The energy recovered from waste tires also contribute to the economy of industries in developed countries. Around 6% to 8% of waste tires are being recycled as civil engineering materials in the US and in EU countries, but only around 0.4% of waste tires are being recycled in Australia.

The concrete industry is one of the biggest industries in the world. According to the European Ready Mixed Concrete Organization statistics (ERMCO), the average concrete production in 2015 in the European Union (EU), Russia, USA, and Japan was 344.3, 62.0, 365.0 and 138.0 million m<sup>3</sup>, respectively. Overall, the world produces around 5 billion tonnes of concrete a year. From an ecological point of view, by implementing rubber derived from waste tires in concrete, the amount of disposed waste tires would become smaller and provide a source of eco-friendly concrete. From an engineering point of view, adding waste tire rubber into concrete could produce a material with improved dynamic and durability properties, such as

ductility, damping capacity, chloride-ion penetration resistance, carbonation resistance, etc.

Given the good strength, ductility, and strain control properties of tire waste, it may be utilized as a substitute for concrete components. Rubber can be applied to concrete and mortar by replacing fine aggregates (FA) and coarse aggregates (CA) or used as binder. The advantages of incorporating crumb rubber (CR) into any engineering cementitious composite (ECC) include lowering the CO<sub>2</sub> emissions and increasing the greenness of the environment .

Moreover, the collection of natural sand is changing the direction of river flow and causing the loss of river bed stability. Such effects could be minimized through saving natural sand by supplanting it with CR in construction purpose. The addition of flexible rubber into rigid concrete alters the overall performance and properties of concrete and may help produce low self-weight structures with cost sustainability by reducing the use of natural aggregates. A 14–28% reduction in unit weight of concrete can be obtained by replacing 10–30% sand with CR.

The properties of crumb rubber concrete were significantly affected by rubber content. Several studies have shown that the compressive strength of concrete with different replacement ratios of crumb rubber by volume (5%, 10% and 15%) decreased with the addition of crumb rubber.

Properties, testing, and design of rubber as an engineering material were investigated in 2004 (Siddique and Naik ) they used the crumb rubber particles as concrete aggregates where fine aggregates were replaced by waste materials of crumb rubber in several percentages (20%, 40%, 60%, 80%, and 100%) in separate concrete and these specimens were tested for compressive strength and they found that as the percentage of crumb rubber content increases the specimens have a reduction in compressive strength , The use of rubber particles in the concrete influence the mechanical properties of the specimen and the compressive strength was found to be reduced with the increase of rubber content.

However, the replacement of up to 15% in the CS mixture was not very severe (Aymen Mostafa). According to (D.V Bompá)\_rubbercrete usually shows a clear reductions in strength and stiffness with the increase of rubber content. The strength is approximately halved with each 20% increment increase of aggregate replacement.

Ali R. Khaloo reported that the failure state or softening phases of C specimens were accompanied by a larger deformation compared to F specimens at the same loading condition. C specimens exhibited higher strength compared to F specimens at the

failure state for the same strain condition. This extra strength is due to the existence of fibers in coarse tire–rubber particles. The CF specimen stress–strain curves located between the C and F specimens stress–strain curves contain the same tire concentration. The combined stress–strain curve demonstrated stress values which were close to those of the F mixture, but the curve’s shape dominantly resembled the C mixture curve. This suggests that the ultimate stress of CF tire–rubber concrete depends on the fine aggregate concentration, while the shape of the stress–strain curve is primarily affected by the coarse aggregate concentration. These observations imply the stress–strain response for CF tire–rubber concrete is located between the corresponding C and F stress–strain curves equaling the total respective tire particles concentration. Hence any desired stress–strain curve between the C and F curves can be obtained by tuning coarse and fine tire concentrations.

Ilker Bekir Topçu report that the rubberized concretes absorb more energy, they can show more strain at the time of fracture. Examination of  $\epsilon_{max}$  values obtained from  $\sigma$ - $\epsilon$  diagrams show that these values can reach to 0.007 and 0.008. So tire–rubber concrete specimens present large deformations compared to plain concrete specimens. During the unloading process, the flexible behavior of tire particles decreases the internal friction among the concrete elements, and recovers extra strain. Tire–rubber concretes are able to withstand loads beyond the peak load, which is referred to as post-failure strength.

Ahmed Tareq Noaman report a change in the shape of the stress–strain curves was also observed. The behaviour of rubberized concrete specimen differed from that of normal concrete, which exhibited ductile behaviour rather than the brittle one. This behaviour was concluded by comparing the shapes of rubberized concrete curves with those of normal concrete. A further increase in rubber content led to increase in the ductility. The failure state of rubberized concrete was accompanied by high deformations in descending curves. Another difference between rubberized concrete curves was the increase in strain capacity (which can be defined as the strain at the maximum stress). Hence, the rubberized concrete mixtures showed a decrease in the slope of the descending portion of the stress–strain curve by the addition of crumb rubber. A high strain was measured at the peak stress, although the maximum stress was reduced with rubber replacement ratio. The change in the shape of the stress–strain curves would also affect the energy absorbed.

Danda Li has demonstrated from his study that the post-peak behavior presents other differences. For reference mix or the normal concrete, the softening branch has a high reduction of stiffness, when compared with rubberized concrete. With increased rubber content this post peak behavior has an increase in the softening stiffness leading to a higher ultimate strain varying between 0.004 and 0.011. However, mixes with rubber fail with less pronounced cracks, in more uniform manner, which is in accordance with previously analyzed strain-strain curves, i.e., post peak behavior. Namely, after reaching peak stress test specimens could withstand further increase of strain without sudden loss of force.

D.V Bompá reported that the post-peak axial compression behaviour exhibits increased softening with the decrease in strength. Tests showed softer post-crushing behaviour which typically leads to similar or higher energy dissipation in the post-peak regime. Tire-rubber concretes are able to withstand loads beyond the peak load, which is referred to as post-failure strength. So with increased rubber content this post peak behavior has an increase in the softening stiffness leading to a higher ultimate strain varying between 0.004 and 0.015.

Of course, the introduction of artificial aggregates much more deformable than natural aggregates induces reductions in the mechanical features of the resulting concrete. In different studies, authors have found that the size of rubber particles, their proportion in the mixture and different surface texture have a significant effect on concrete strength properties.

## 2. Literature review :

Disposal of waste tires has been a major issue to the cities all around the world. Generally, the cheapest and easiest way to decompose the used tires is by burning them. However, the pollution due to enormous amount of smoke makes this method so unacceptable that it is prohibited by law in many countries. Therefore, recycling of the waste tires and , the feasibility of using elastic and flexible tire–rubber particles as aggregate in concrete is investigated in this study. Tire–rubber particles composed of tire chips, crumb rubber, and a combination of tire chips and crumb rubber, were used to replace mineral aggregates in concrete.

Inclusion of rubber into concrete to replace a certain percentage of aggregate can change its mechanical properties and consequently influence the shape of the stress-strain curve, compared to commonly used concrete. Due to induced changes, available constitutive stress-strain models for concrete are not valid in case of rubberized concrete, and available modified models need to be experimentally verified on more compositions. Considering specific aspects of rubberized concrete, this paper will present previous studies of rubberized concrete’s behavior, new and literary available

experimental investigations, and stress-strain curve analytical models. The main contribution of this paper is based on the applicable constitutive compressive axial model and direct guidelines of utilization of rubberized concrete.

Rubber tyres (from cars and trucks) have heterogeneous composition (approx. 22% of synthetic fibre, 18% steel wire and more than 60% rubber mixture). They are subjected to mechanical grinding and used in the mixture as crumbs, without textile parts and without steel fibres. Before their use in the mixture, crumbs can be often subjected to chemical or natural treatments and cryogenic process.

Studies of many researchers have shown that concrete containing rubber aggregates has several interesting properties that encourage its use as construction material, some- times very different from those of standard concrete. The replacement of natural aggregates with rubber reduces the Young’s Modulus, allowing the material to absorb energy with small deformations (Skripiunas et al. 2007a; 2007b). The use of crumb rubber in the mixture produces various changes in acoustic properties as well, with a noise reduction effect as observed in (Venslovas et al. 2011). The high vibration damping capacity, the impact resistance and the high thermal and acoustic insulation of rubbercrete allow its use for specific applications including sub-foundations, road pavements, trench filling. According to

(Chung and Hong 2009) rubbercrete usually exhibits better freezethaw resistance and better weathering properties compared to ordinary concrete. Moreover, thanks to a reduced specific weight compared to ordinary concrete, rubbercrete represent an interesting option for architectural applications. Of course, the introduction of artificial aggregates much more deformable than natural aggregates induces reductions in the mechanical features of the resulting concrete. In different studies, authors have found that the size of rubber particles, their proportion in the mixture and different surface texture have a significant effect on concrete strength properties. Siddique and Naik (2004), Skripkiunas et al. (2007a; 2007b) observed a deterioration in concrete strength properties when fine aggregates is replaced with crumb rubber. Moreover, a greater reduction in concrete strength is observed when coarse aggregate is replaced with crumb rubber (Eldin & Senouci 1993; Fattuhi and Clark 1996; Fedroff et al. 1996; Khatib and Bayomy 1999; Lee et al. 1993; Siddique and Naik 2004; Topçu 1995; Topçu and Avcular 1997). On the other hand, Hernandez-Olivares et al. (2002) found that natural aggregate replacement with waste tyre rubber less than 5% did not imply any particular changes in the performance of the material. Moreover, using rubber with rougher surface texture instead of rubber with smooth surface and spherical shape leads to lower reductions in strength (Benazzouk et al. 2006), due to a better adhesion among rubber particles and cement matrix. More precisely, many tests demonstrated that a higher decrease is observed in compressive strength rather than bending strength in rubberised concrete (Bignozzi and Sandrolini 2006; Colom et al. 2006; Gesoglu and Güneyisi 2007; Güneyisi et al. 2004; Hernández-Olivares and Barluenga 2004; Hernández-Olivares et al. 2002; Li et al 2004; Papakonstantinou and Tobolski 2006; Taha et al 2008; Zhu et al 2002). Eldin and Senouci (1993; 1994) observed that the compressive strength dropped by 85% when replacing coarse aggregate with waste rubber, instead of 65% when replacing fine aggregate. In addition, (Albano et al. 2005; Benazzouk et al. 2006; Güneyisi et al. 2004; Papakonstantinou and Tobolski 2006) noticed that compressive strength reduces the more the higher amount of crumb rubber is added. Despite the loss of strength, these concretes may be extensively used in civil engineering as subfoundations, road pavements and insulating screeds. The aim of this article is to investigate the reduction in compressive strength when a partial replacement of the natural aggregates is operated in a concrete mixture, using waste tyre rubber. The reduction in the concrete compressive strength can be explained as follows. Rubber particles have lower strength than concrete matrix around them so, under load condition, cracks first appear in the contact zone between rubber and concrete matrix and then gradually propagate until concrete crumbles. Such performance makes rubber particles act like voids into concrete. (Benazzouk et al. 2006; Bignozzi and Sandrolini 2006; Eldin and Senouci 1993; Eldin and Senouci 1994; Güneyisi et al. 2004;

Khatib and Bayomy 1999; Lee et al. 1993; Papakonstantinou and Tobolski 2006; Topçu and Avcular 1997). Rubber aggregates are characterized by a very low modulus of elasticity compared to that of concrete and to that of natural aggregates. (Aiello and Leuzzi 2010; Batayneh et al. 2008; Eldin and Senouci 1993; Hernandez et al. 2004). There is poor adhesion between the rubber and the cement paste, due to the hydrophobic nature of the rubber, which contributes to further weaken the mechanical resistance of the whole mixture. (Güneyisi et al. 2004; Li et al. 2004; Segre and Joekes 2000; Siddique and Naik 2004). Soaking waste tyre rubber in NaOH solution is recommended to increase the adhesion (Güneyisi et al. 2004; Li et al. 2004; Papakonstantinou and Tobolski 2006; Segre and Joekes 2000; Siddique and Naik 2004). Rostami et al. (1993) washed rubber with pure water, water and carbon tetrachloride solvent, water with latex admixture cleaner. Results showed that concrete containing rubber particles washed in water exhibited a 16% increase of the compressive strength with respect to the mixture containing untreated rubber, and a further improvement (higher than 57 %) was found when rubber aggregates were treated with carbon tetrachloride. Researchers as Li (Li et al. 2004) and Albano (Albano et al. 2005) confirmed that rubber pre-treatment might increase the compressive strength of the mixture. To this purpose, Yilmaz and Degirmenci (2009) studied the use of fly ash and waste tyre rubber in building materials reporting an improvement of the compressive strength loss with increasing percentages of fly ash introduced in the mixture. Youssef et al. (2016) investigated the compressive strength of the rubbercrete confined with Fibre Reinforced Polymers (FRP) for structural seismic applications. They demonstrated the overall behaviour of the FRP-confined rubberized concrete to be very similar to that of FRP-confined conventional concrete, with even less damage and spalling up to a drift of 4%. In particular, the confinement effectiveness for the rubbercrete was found to be higher than in case of conventional concrete at the same confinement pressure, this encouraging the use of rubbercrete for structural applications. Using two different types of cement (Magnesium Oxide Cement and Portland cement) Biel and Lee (1996) reported the cement type to have an influence on the final compressive strength of the rubbercrete. The cement type, the volume fraction, the type and the size of the rubber particles are all relevant in affecting concrete strength and it would be extremely useful to recognize and to assess the individual effects of all these factors on the strength reduction. However, some difficulties arise in determining the gradation curves of the rubber particles adopted by the authors for most of the studies found in the literature (Khatib and Bayomy 1999; Güneyisi et al. 2004). In the best case, authors state the natural aggregates (both fine and coarse) to have been replaced with rubber particles characterized from a gradation simply close to that of the substituted natural aggregates and not being exactly the same.

## 2.1 compressive strength as a function of rubber content :

In this paragraph, the reduction of compressive strength of rubberised concrete mixture is investigated, in relation to the content of rubber.

The search for a mathematical model for the Strength reduction factor (SRF) is necessary as guide for procedures of mix design. In fact, through a mathematical model, predictions on the mixture can be made and the starting mixture mix design can be set in order to get the required performance. The strength reduction factor is defined as the ratio between the compressive strength of the rubbercrete with a certain percentage of rubber and the compressive strength of the concrete without rubber.

$$SRF = \frac{R_{c[\%]}}{R_{c0}}$$

In the tested mixtures, the percentage of rubber considered refers to the total volume of aggregates. In literature there are several laws proposed by various authors for the calculation of the Strength Reduction Factor and they are shown in Table 1.

Reference	Range of replacement [%]	Model proposed <sup>a</sup>	R <sup>2</sup>
Khatib and Bayomy(1999)	0-100	$SRF = 0.1 + 0.9(1 - x)^7$	0.94
Guneyisi et al.(2004)	0-50	$SRF = 0.125 + 0.875(1 - x)^{4.55}$	0.91
Khaloo et al.(2008)	0-100	$SRF = 0.02 + 0.98(1 - x)^{12}$	0.99
Mohammed and Azmi (2014)	0-30	$SRF = 0.422 + 0.605(1 - x)^{15}$	0.98
		$SRF = 0.327 + 0.691(1 - x)^{14}$	0.97
		$SRF = 0.379 + 0.619(1 - x)^{18}$	0.97

Table 1: Models of SRF proposed by in the literature

In this study, literature data are collected together with new experimental data from mixes made by the authors of this paper in Italcementi (Mesagne - BR - Italy) as shown in Table 2. All data have been classified and plotted, distinguishing replacement of fine aggregate, replacement of coarse aggregate and simultaneous replacement of fine and coarse aggregate, operated at different rubber percentages. As shown in Figure 2, distributions of the SRF data are not uniform, but a common trend stands out. A greater decrease in compressive strength with the use of coarse rubber chips can be observed, rather than fine rubber crumbs.

Reference	Pre-treatments	C	F	C&F	Range of replacement [%]
Eldin and -senouci (1993)	Soaked in water	x	x		0-100
Topcu(1995)		x	x		0-45
Toutanj (1996)		x			0-100
Khatib and Bayomy(1999)		x	x	x	0-100
Guneyisi et al.(2004)				x	0-50
Khaloo et al.(2008)		x	x	x	0-100
Aiello and Leuzzi(2010)		x	x		0-75
Godfrey (2012)	Soaked in water		x		0-40
Grinys et al.(2012)			x		0-30
Tung-Chai Ling(2012)			x		0-30
El-Gamma et al.(2010)			x		0-100
Batayneh et al.(2008)			x		0-100

Table 2:Experimental Data

Considering in a single figure (Figure 2) all the SRF values corresponding to different percentages of replacement, a “fan shaped” point cloud is obtained. Regression analyses have been carried out to calculate the upper and the lower bound curves of this point cloud, respectively. These two curves are identified with polynomial laws such as those proposed by other authors (Guneyisi et al. 2004; Khatib and Bayomy 1999; Khaloo et al. 2008; Mohammed and Azmi 2014).

The least squares method was applied to estimate the regression parameters a, b and m of each proposed model. Following equations 1) and 2) represent the mathematical expression of the upper and lower bound curve respectively:

$$SRF = 0.2447 + 0.753(1 - x)^{2.308} \quad (1)$$

$$SRF = 0.001 + 0.999(1 - x)^{9.855} \quad (2)$$

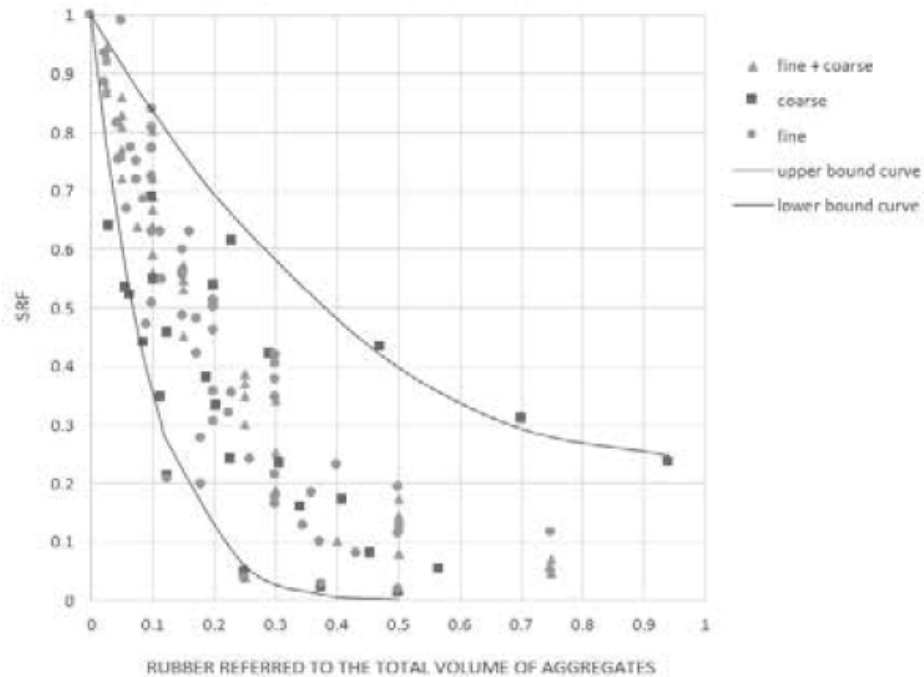


Figure 2: Whole dataset of the Strength reduction factor - SRF vs. the content (by volume) of the natural aggregates replaced with rubber aggregates.

Therefore, replacements of coarse aggregates may have less predictable consequences in terms of concrete compressive strength reduction compared to cases in which replacements is operated only on the fine fraction or, simultaneously, on the fine and coarse fraction of the aggregates.

This study analyses some key aspects of concrete mixtures modified by partial replacement of natural aggregates with rubber particles from waste tyres. The resulting material, known as rubbercrete in the literature, has mechanical and rheological properties suitable for civil and industrial applications such as subfoundation, insulating screeds, road pavements, and, at the same time, is an effective way of recycling discarded tyres.

Based on several literature studies and laboratory experiments, analytical formulas to describe the behaviour of these modified concretes are proposed as a function of type, size and content of rubber particles in the mix.

Results obtained from this experimental investigation can be used to refine mixdesign procedures of rubbercrete. In this study, a greater reduction in the compressive strength is shown to be expected when replacement of the natural

aggregates with rubber is operated on coarse aggregates rather than on fine ones or on fine and coarse aggregates together. Also uncertainty of the predicted SRF values increase in this case compared to other type of replacements.

For this reasons, rubbercrete represents a suitable material mostly for non-structural purposes, including insulating screeds, lightweight masonry, external enclosure walls and filling materials. In structural applications - where specific requirements are introduced replacing fine aggregates with rubber particles should be performed with care, by limiting the replacement ratio to 10% and by enforcing strict quality controls. In any case, the trade-off between using rubber particles and using more cement to guarantee acceptable mechanical properties should be examined thoroughly.

### 3. Pre-peak and Peak behavior of rubberized concrete:

Modification of concrete properties by the addition of appropriate materials is a popular field of concrete research. The brittle nature of concrete and its low loading toughness compared to other materials, has prompted the use of waste tire particles as a concrete aggregate to possibly remedy or reduce these negative attributes. Elastic and deformable tire–rubber particles could improve concrete properties.

In this paper , the reduction of compressive strength of rubberised concrete mixture is investigated, in relation to the content of rubber.

as shown in Table 3. All tests have been classified, distinguishing replacement of fine aggregate, replacement of coarse aggregate and simultaneous replacement of fine and coarse aggregate, operated at different rubber percentages.

Author	Test Number	Rubber particle size[mm]	Rubber content	Specimen dimensions
D.V Bempa et al.	2	0.0–10.0	0	Φ100x200
			20	
			40	
			60	
			80	
Ayman Moustafa	3	8_30	0	Φ100x200
			5	
			10	
			15	
			20	
Siddique and Naik	1	0.15-4.75	0	Φ150x300
			20	
			40	
			60	
			80	
			100	

*Table 3: The experimental tests*

### 3.1. Test number One:

#### 3.1.1. Materials and method :

four sets of cylindric samples  $\varnothing 100 \times H 200$  [mm] were prepared to assess the compression behaviour of rubberised concrete with various replacement ratios of both fine and coarse mineral aggregates.

Such that the volumetric replacement ratio, which is the ratio between the replaced volume of mineral aggregates in the rubberised concrete and the total volume of mineral aggregates in the reference normal concrete mix, varying in the range of  $\rho_{vr} = 0-0.6$ .

The rubber particles used in the rubberized concrete mixes were obtained from two sources. Rubber aggregates with dimensions up to 10 mm, produced from car tyre recycling. As depicted in Figure 3a, they were supplied in the following size ranges : 0–0.5 mm, 0.5–0.8 mm, 1.0–2.5 mm, 2–4 mm and 4–10 mm, and were used in the concrete mix in the 5%, 5%, 15%, 20% and 10% ratio of the total added rubber content, respectively, with remaining 45% being comprised of particles with sizes in the range 10–20 mm.

The larger rubber particles were produced from truck or bus tyre recycling, with typically higher density than car tyre particles. This portion was identified following a study of the workability of rubberized concrete within a wider European research project. All rubber particles are reported to have 25% content of carbon black, polymers in the range of 40–55%, whereas the remaining constituents are softeners and fillers. The specific gravity of rubber was 1.1, whereas the water absorption 7.1% for 4–10 mm particles and 1.05 for 10–20 mm particles. Sand and gravel aggregates shown in Fig. 3a, from naturally occurring rock deposits consisting of combinations of various minerals, were used for the concrete mix shown in Figure 3b. The fine aggregates with sizes up to 5 mm had a specific gravity of 2.65 and a moisture content of 5%, whereas the coarse aggregate (5–10 mm) had a specific gravity of 2.65 and a moisture content of 3%. The particle size distribution of mineral aggregates and rubber particles was determined following EN 933-1:2012 as illustrated in Figure 4. In the trial mixes, CEM I 52.5N and CEM II 32.5N were used to assess their influence on the compressive concrete strength at 7 and 28 days. However, in the tests used for the assessment of the constitutive behaviour, the higher strength cement was used.

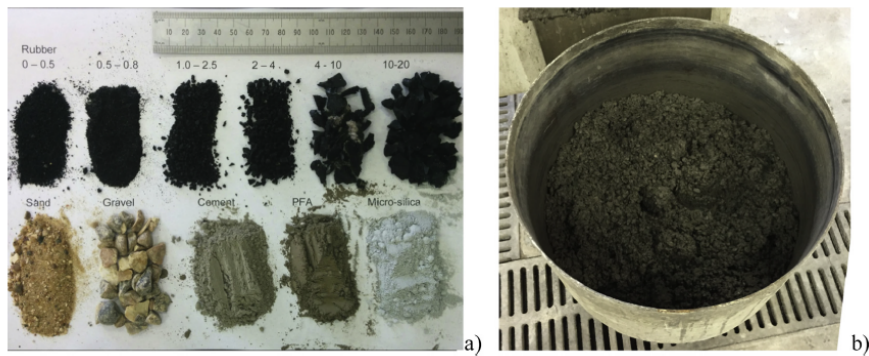


Figure 3: a) Rubberised concrete constituents b) Rubberised concrete mix.

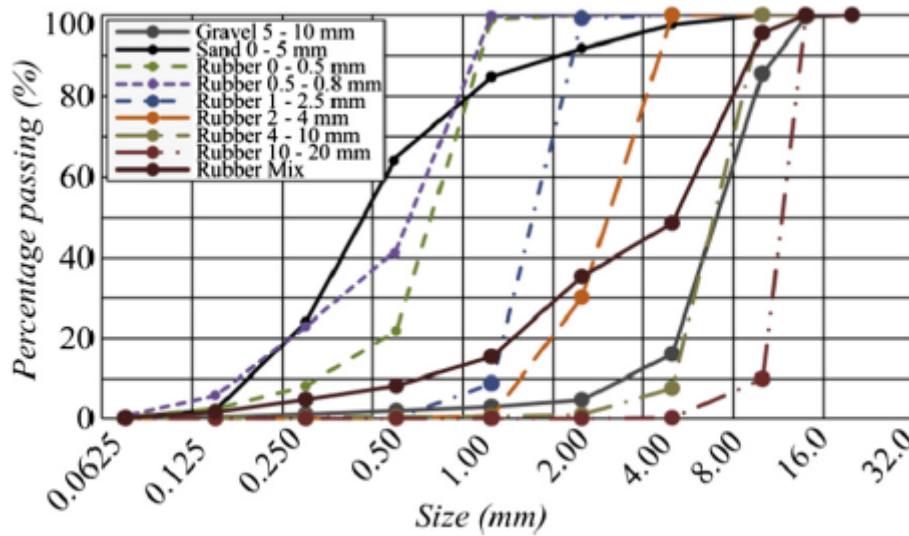


Figure 4: Sieve analysis for mineral aggregates and waste rubber.

### 3.1.2. Specimen preparation and testing:

A reference normal concrete mix with target compressive strength of 60 MPa was used. The normal concrete (NC) reference mix had 425 kg/m<sup>3</sup> of cement, 820 kg/m<sup>3</sup> of sand, 1001 kg/m<sup>3</sup> of gravel, 149 L of tap water, with 2.5 L/m<sup>3</sup> of plasticiser and 5.1 L/m<sup>3</sup> of super-plasticiser [43]. In the rubberized concrete mixes, 20% of the cement was replaced in equal quantities with EN 450-1 fineness category S fly ash and Grade 940 silica fume. They were primarily added to improve workability, segregation and slump, and to optimise the particle packing of the mixture. Rubberised concrete mixes with 20%, 40% and 60% rubber replacement by volume of mineral aggregates were produced to assess the full constitutive characteristics

of rubberized concrete. The rubber quantities used in the mixes were 110 kg/m<sup>3</sup>, 220 kg/m<sup>3</sup> and 330 kg/m<sup>3</sup>, respectively.

In this investigation, preliminary tests were carried out at 7 days, yet the fundamental observations from tests are made at 28 days from compression tests on 100 mm \_ 200 mm cylinders. The samples were cast directly in the size required in steel or plastic formworks and covered with plastic sheets until de-moulding. Two days after casting, the samples were placed in a water tank located in a curing room to ensure appropriate concrete hydration.

The cylindrical specimens, used in the pilot tests and for assessing the full constitutive behaviour, were tested in a stiff four-post Instron Satec 3500 kN machine. These tests were carried out in displacement control with a compressive displacement rate of 0.1 mm/min.

### 3.1.3. Results and discussion:

Material characterisation tests on rubberised concrete and normal concrete cylinders were carried out to assess the influence of rubber content on the constitutive behaviour. The investigated rubber replacement ratios were 20%, 40% and 60% of the total aggregate volume, as described previously in this section.

Figure 5a–d depict three axial and lateral stress-strain recorded test curves and their average but I focused only on the axial stress-strain recorded test. The stress-strain curves include both pre-peak and post-peak behaviour as recorded in the tests. The post-peak response is plotted down to 30% of the compressive strength  $f_{cr}$ .

Figure 5a–d shows clear reductions in strength and stiffness with the increase of rubber content. The strength is approximately halved with each 20% increment increase of aggregate replacement. The compressive strength of concrete  $f_{cr}$  with  $\rho_{vr} = 0.6$  (R60) is about 10% of the normal concrete R00. The elastic modulus  $E_c$  is also significantly affected with R60 exhibiting 20% of the modulus from R00.

A stronger influence on mechanical properties is typically observed for small replacement ratios and tends to stabilise as the rubber content increases.

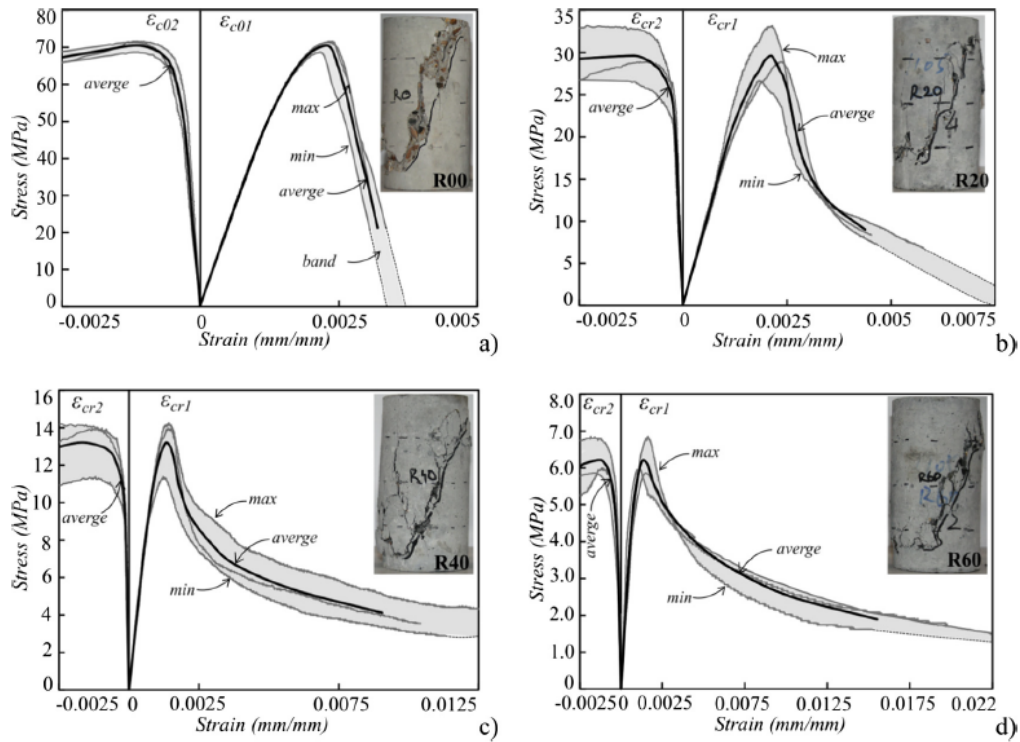


Figure 5: Stress-strain relationships for a) normal concrete R00, b) rubberised concrete with 20% replacement R20, c) rubberised concrete with 40% replacement R40, d)

The pre-peak behaviour of the concrete tests was strongly influenced by the rubber replacement of the mineral aggregates. As illustrated in Figure 6, elastic stiffness  $E_{cr}$  degraded with the increase in rubber content. Naturally, the rubber aggregates are softer and lighter in weight compared to mineral aggregates. In this case, the matrix, comprised of binders, water and admixtures, is much stronger than the rubber aggregates but may be weaker than the mineral aggregates.

Hence, for the rubberised concrete materials, the reduction in stiffness is a function of the stiffness ratio between the cement matrix and inclusions (rubber particles and voids). Around the peak, the tangent modulus decreases to zero and crushing occurs, which is generally triggered by de-bonding of the aggregates from the cement paste.

As depicted in Figure 6a–c, similarly to the stiffness  $E_{cr}$  degradation with rubber content as described above, test measurements of compressive strength  $f_{cr}$  and axial strain at crushing  $\varepsilon_{cr1}$  showed similar decreasing trends. For the concrete samples without rubber, the average  $E_{cr,R00} = 42.3$  GPa,  $f_{cr,R00} = 70.2$  MPa and the corresponding average  $\varepsilon_{cr1,R00} = 0.228\%$ . The average  $E_{cr}$  for samples with rubber was 19.6 GPa, 14.1 GPa and 9.03 GPa for R20, R40 and R60, respectively. The recorded  $f_{cr}$  and  $\varepsilon_{cr1}$  were 29.7 MPa and 2.13% for 20% replaced mineral aggregates, 13.3 MPa and 1.38% for 40% replacement, and 7.06 MPa and 1.37% for the material with the highest rubber content (60%).

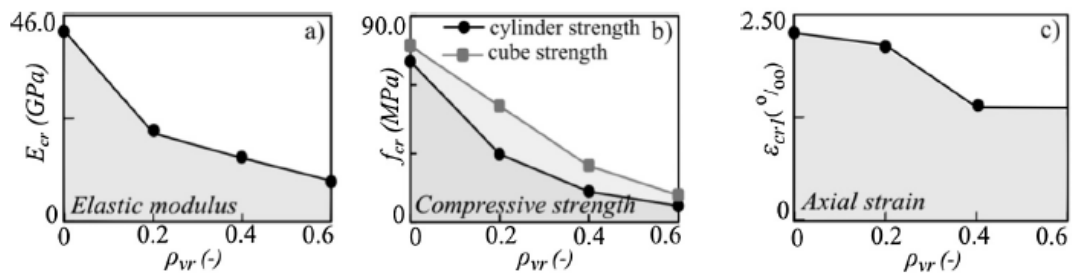


Figure 6: Influence of rubber content  $\rho_{vr}$  to the mechanical properties of concrete a) elastic modulus  $E_{cr}$  b) compressive strength  $f_{cr}$ , c) peak axial strain  $\varepsilon_{cr1}$

### 3.2. Test number Two:

#### 3.2.1. Materials and method:

A set of constant slump (CS) ,constant slump (CS) was designed to keep the workability the same, of rubberized concrete mixtures was designed and used during the course of this study.

This set was used to test the properties of concrete having 0%, 5%, 10%, 15%, 20%, and 30% volume replacement of sand with shredded rubber.

The mixture nomenclature in Table 4 consists of mixture set (CS) followed by the percentage of sand replacement with rubber by volume.

Materials[kg/m <sup>3</sup> ]	Water	Cement	Fly ash	Coarse aggregate	per-plastici	Sand	R(8-14)	R(14-30)	R(30-)
Normal concrete	142.4	336.39	112.13	1057.22	1.12	576.66			
CS 05	142.4	336.39	112.13	1057.22	1.33	544.63	10.09	3.2	0.7
CS 10	142.17	336.39	112.13	1057.22	1.33	519	20.18	6.41	1.41
CS 15	142.17	336.39	112.13	1057.22	1.55	490.16	30.27	9.61	2.11
CS 20	142.17	336.39	112.13	1057.22	1.65	461.33	40.37	12.81	2.82
CS 30	142.17	336.39	112.13	1057.22	1.76	403.67	60.55	19.22	4.23

*Table 4:Mixture proportions for the control concrete and for CS set*

The cement used in all mixtures is type I Portland cement meeting ASTM C150 specifications. Limestone washed coarse aggregate with nominal maximum size of 1[in] was used. The sand used was Missouri river sand. The rubber used was ground rubber with three different sizes of 8–14, 14–30, and 30- where the first number represents the sieve number of the passing particles and the second number represents the sieve number of the retained particles. Different trial mixtures including different grading of the shredded rubber were prepared and the grading that had the best workability and consistency was selected for all mixtures. Fig.8 shows the grading of the sand, coarse aggregate and ground rubber used during the course of this research. Figure 7 shows the used ground rubber. The material characteristics of the sand, coarse aggregate and rubber are shown in Table 5.



### 3.2.2. Specimen preparation and testing:

For each mix, cylinders of 100 mm diameter by 200 mm height were prepared to determine the compressive strength of the concrete at 7 and 56 days, The compressive strengths of the concrete cylinders were determined using an MTS machine. The average axial strains along a full specimen height were also measured using a Linear Variable Displacement Transducer (LVDT). The loading rate for both sets was 0.2 mm/min. The cyclic axial compressive loading, including loading/unloading cycles, was applied based on a prescribed pattern of progressively increasing levels of axial displacements until failure occurred. Three cycles of loading/unloading

were applied at each axial displacement level. Finally, the cylinders were tested for compressive strength at 56 days to represent the actual compressive strength of the beams on the test day.

### 3.2.3. Results and discussion:

The compressive behavior of CS mixtures was determined at 7 and 56 days. Figure 9 shows the compressive stress after 7 days of moist curing according to ASTM C192 and after 56 days.

the figure shows that for a replacement up to 15%, the 7 days compressive stress suffer very limited degradation and beyond that severe degradation was observed reaching 17.4% for 30% replacement.

For CS series at 7 days stress, replacing any percentage of sand resulted in a significant reduction in strength. Replacing up to 15% of sand with rubber resulted in a strength reduction of approximately 10%. At 30% replacement, the strength reduction was approximately 32%.

Figure 10 shows the stress strain curves for the monotonic loading at 56 days. The figure shows a very large difference in ductility between the conventional and the rubberized concretes. The conventional concrete failed in a brittle way once it reached the peak load. The addition of up to 15% rubber in the CS mix did not change the sudden failure.

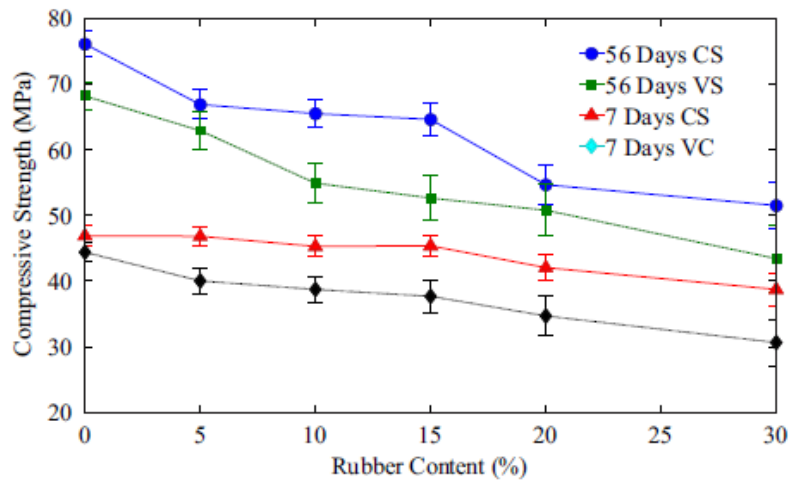


Figure 9: Average compressive stress for VS and CS cylinders.

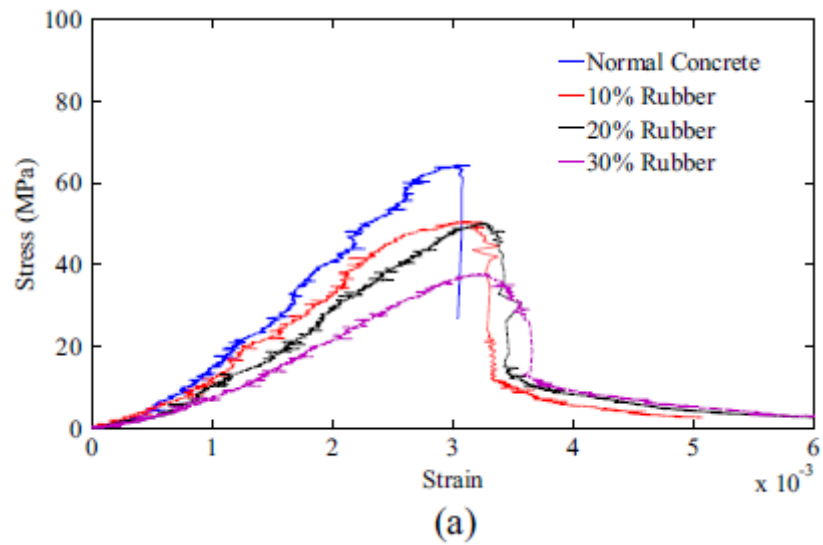


Figure 10: Stress–strain curves for (a) VS and (b) CS.

The mode of failure for the concrete changed with the addition of rubber. The high strength concrete with no rubber exhibited a brittle failure and shattered into small pieces when it reached the maximum load, while the rubberized concrete experienced a more ductile failure and was able to sustain loads after reaching its capacity.

### 3.3. Test number Three :

#### 3.3.1. Materials and method:

The raw materials used for the preparation of the concrete mix consist of Type I Ordinary Portland Cement, natural fine aggregate which is specified as natural silica sand, and coarse aggregates taken from crushed limestone, all of which were supplied from natural local resources in Jordan. Tap water at room temperature was used in all mixes. For each crumb rubber percentage, three batches of concrete were prepared but here I considered only one batch. Concrete with no additives was designated as the control mix. Various mix ratios of cement, water, fine, and coarse aggregates were used to achieve a workable concrete for a typical in situ concrete following ACI 211.1-91 (ACI, 2002).

Four types of scrap tire particles have been classified by the study carried out by Siddique and Naik (2004), which were graded according to particle size. These types consisted of slit tires (the tire is slit into two halves), shredded/chipped tires (the particle size is 300–400 mm long by 100–230 mm wide), ground rubber (19– 0.15 mm), and crumb rubber (4.75–0.075 mm). The crumb rubber has been reported to have a nominal size between 4.75 mm (No. 4 sieve) and 0.075 mm (No. 200 sieve). The waste tire particles used in this study were crumb rubber, which was obtained from a local industrial unit in Jordan. The scrap tires originated from a scrap yard of tires from different types of vehicles (a combination of cars and trucks) in Jordan. The physical properties of the crumb rubber relevant for this study are particle shape and size. Figure 11 shows the sieve analysis for both the crumb rubber particles and the fine aggregates (sand) used. The figure indicates that the gradation of the crumb rubber particles and the sand used fall between the minimum and maximum limits of the fine aggregates specified ACI gradation limits. The crumb rubber particle size varied from 0.15 to 4.75 mm. The crumb rubber was used in the concrete mix to partially substitute for fine aggregates (sand) in various percentages of 20%, 40%, 60%, 80%, and 100%.

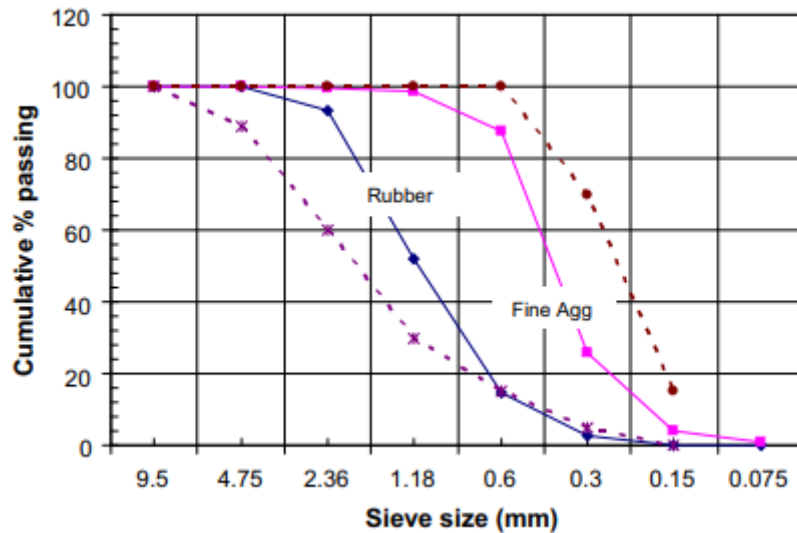


Figure 11: Sieve analysis of crumb rubber

### 3.3.2. Specimen preparation and testing :

In order to prepare the recycled crumb rubber concrete specimens, fine aggregates were replaced by waste materials of crumb rubber in several percentages (20%, 40%, 60%, 80%, and 100%) in separate concrete mixes. For each mix, cylinders of 150 mm diameter by 300 mm height were prepared. All specimens were fabricated and then cured in water for 28 days in accordance with ASTM/C192M-06 Standard practice (ASTM, 2006). For each concrete mix, slump tests were performed and recorded at the casting time of the specimens. A Universal Testing Machine with a maximum load capacity of 300 kN (load accuracy within  $\pm 0.5\%$ ) was used for testing. After curing, specimens were tested for compressive strength. The compression tests were performed according to ASTM C39 Standard Test Method.

### 3.3.3. Results and discussion :

The relationship between stress and strain is shown in Figure 12 for the different rubber contents in the concrete mix. Two different behavior patterns are shown for the stress–strain curves. The stress–strain behaviors of the specimens containing rubber of up to 40% behave in a similar trend to the control specimen, but having a smaller peak. From the figure, it can be observed that there is linear increase of stresses until it reaches its peak before energy is released by specimen's fracture. For this case, the specimens behaved like a brittle material of which the total energy generated upon fracture is elastic energy. However, nonlinear behavior is seen for the other two specimens containing 60% and 80% rubber. Here, once the peak stress is reached, the specimen continues to yield, as represented by the branch-line. This behavior is similar to the behavior of the tough materials having most of its energy generated upon fracture as plastic energy. Plastic energy is defined as the amount of energy required to produce a specified deformation after the elastic range, which increased the ability of the material to support loads even after the formation of cracks. Therefore, it can be stated that concrete with a higher percentage of crumb rubber possess high toughness, since the generated energy is mainly plastic.

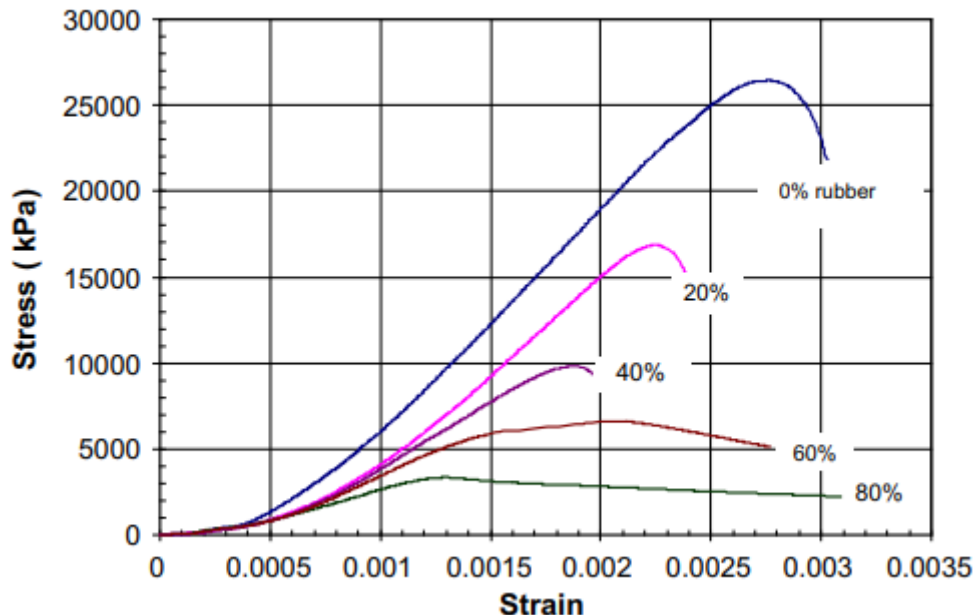


Figure 12: Relationship between stress and strain for different rubber

In order to study the effect on the compressive strength I consider the mix proportions and fresh rubber concrete properties plus the effect of crumb rubber on concrete strength is given in Table 6, and is demonstrated in Figure 13. The relationships between the percentage of crumb rubber content and the reduction in compressive, also the tensile and flexural strengths are shown but i focused only on the compressive strength.

Crumb rubber content (%)	Water [Kg/m <sup>3</sup> ]	Cement [Kg/m <sup>3</sup> ]	Coarse aggregates [Kg/m <sup>3</sup> ]	Fine aggregates [Kg/m <sup>3</sup> ]	Rubber	Compressive strength $f_c$ [Mpa]
0	252	446	961	585	0	25,33
20	252	446	961	468	67,51	18,96
40	252	446	961	351	135	12,27
60	252	446	961	234	202,5	8,07
80	252	446	961	117,2	270	4,47
100	252	446	961	0	337,6	2,5

Table 6:Effect of crumb rubber content on various strength results

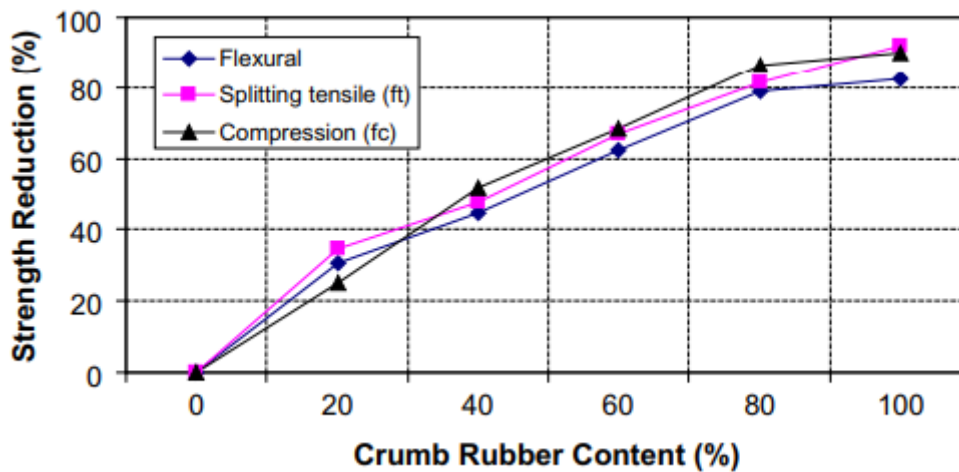


Figure 13:Comparison between strength reduction and rubber content.

in Figure 13. It can be seen that the use of crumb rubber reduced the compressive strength. As expected, the higher the rubber content in the mix, the higher the reduction in compressive ( $f_c$ ), Detailed examination of the figure shows that increasing the crumb rubber to a limit of 40% maintained a linear relationship between the increase of crumb rubber and the compressive strength, showing a loss of about 50% of the compressive strength at 40% rubber content. The inclination is lesser when rubber content is above 40%; however, rubber content

between 40% and 100% continues to reduce the strength to a maximum loss of strength of up to 90%. . Therefore, this result limits the use of the modified concrete when strength is the prime requirement.

The test results of this study indicate that there is great potential for the utilization of waste tires in concrete mixes in several percentages, including 20%, 40%, 60%, 80%, and 100%. Based on these results, the following can be concluded: The modified concrete mix using recycled tires performed satisfactorily on various tests, with acknowledgment to the proportional relationship between its rate of strength-loss and the content of the rubber in the mix. Mixing, casting and compacting the concrete mix using crumb rubber with local materials can be carried out in a similar fashion to that of the conventional concrete mix. Although the strength of modified concrete is reduced with an increase in the rubber content, its lower unit weight meets the criteria of light weight concrete that fulfill the strength requirements . Although it is not recommended to use this modified concrete in structural elements where high strength is required, it can be used in many other construction elements like partition walls, road barriers, pavement, sidewalks, etc. which are in high demand in the construction industry. With the addition of the crumb rubber, the reduction in strength can not be avoided. However, these data provide a preliminary guideline of the strength-loss of locally produced modified concrete in comparison with the conventional concrete of 25 MPa targeted strength. The amount of scrap tires being accumulated in third world countries has created a big challenge for their disposal, thus obliging the authorities to invest in facilitating the use of waste tires in concrete as the use of concrete is fundamental to the booming construction industry in these countries.

#### 4. Post-Peak behavior of rubberized concrete :

So far only compressive strength of concrete with varied rubber content is investigated and modelled. As seen before we concentrated on the pre-peak and peak behavior but now in the following paper I want to analyse and model the post-peak stage .

as shown in Table 7. All tests have been classified, distinguishing replacement of fine aggregate, replacement of coarse aggregate and simultaneous replacement of fine and coarse aggregate, operated at different rubber percentages.

Author	Test Number	Rubber particle size[mm]	Rubber content	Specimen dimensions
Ali R.Khaloo	1	2.0-15	0	Φ150 -300
			12.5	
			25	
			37.5	
			50	
Ilker Bekir Topcu	2	0-4	0	Φ150 -300
			15	
			30	
			45	
Ahmed Tareq Noaman	3	1.18-2.36	0	Φ100 -200
			5	
			10	
			15	
Danda Li	4	1.18-2.36	0	Φ100 -200
			6	
			12	
			18	
D.V Bompa	5	0.0-10	0	Φ100 -200
			20	
			40	
			60	

Table 7: Experimental tests

#### 4.1. Test number one :

##### 4.1.1. Materials and method:

In order to investigate the mechanical properties of tire–rubber concrete, specimens of a cylindrical shape 15 cm in diameter \_ 30 cm in height were fabricated. These specimens were different in the content and type of tire particles as a portion of total aggregates in concrete.

Constituent materials for concrete mixes included a type I Portland cement meeting ASTM C150 requirements, crushed stone gravel with a maximum size of 20 mm as a coarse aggregate, natural sand with a 4.75 mm maximum size as fine aggregate, and tire–rubber particles provided by the Yazd Tire Company in Iran. Tire particle specifications are summarized in Table 8 .

Rubber powder specification		
1	specific gravity	1.16[g/cm <sup>3</sup> ]
2	Ash content	5%
3	Plasticizer	10%
4	Carbon black	29%
5	Polymer	50%
6	Sieve residue on mesh 40	3.36%
7	Sieve residue on mesh 60	80%
Packing:bags of 30kg		

*Table 8:Rubber–tire specification*

These specifications were provided by tire manufacturers according to ANSI (American National Standard Institute) tests. Two types of scrap tire–rubber particles were used: crumb rubber, which was a fine material with grading close to that of the aforementioned sand, and coarse tire chips produced by mechanical shredding. Tire particle groups are shown in Figure 14. Particles of tire finer than 0.15 mm may disturb the cement paste reaction (Neville,1995); thus these particles were removed from the tire aggregate source using a sieve # 100 based on the ASTM C136 method. Tire particles were not pretreated before their incorporation into the concrete mixture. The properties of fine and coarse aggregates were determined according to ASTM standard test methods C127, C128, C129, and C136. The grading of tire–rubber materials was determined based on the ASTM C136 method. The grading curve of rubber materials was determined by using crushed

stones in each sieve in order to provide adequate pressure on tire-rubber particles to pass the sieves. Grading curves are presented in Figure 14. Data regarding the properties of the aggregates and the rubber particles are given in Table 9. The specific gravity of the cement was evaluated to be 3.15 g/cm<sup>3</sup>.

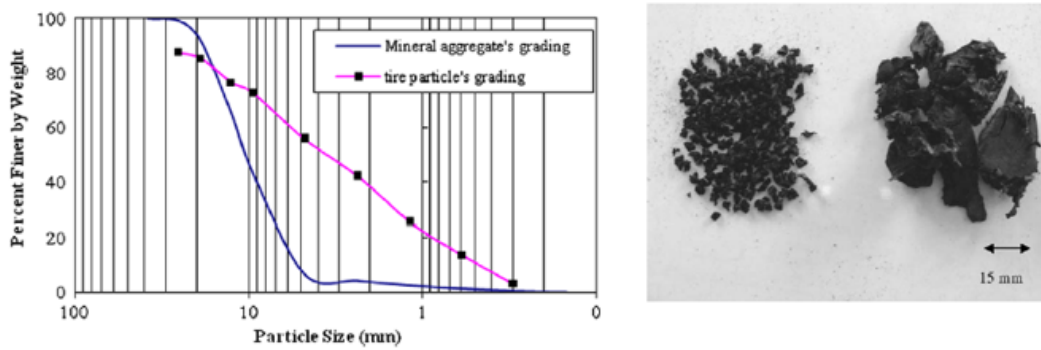


Figure 14: Grading of mineral aggregates and tire particles (in the left), Type of tire-rubber particles (in the right)

Aggregate type	Specific gravity	Absorption[%]	Fineness modulus	Unit weight[kg/m <sup>3</sup> ]
Coarse aggregate	2.65	2.66	NA	1701.3
Fine aggregate	2.67	5.01	4.35	1716.8
Rubber particles	1.16	49.56	NA	1150

Table 9: Properties of aggregate and rubber

#### 4.1.2. Specimen preparation and testing:

The experimental setup and specimen fabrication are summarized in Tables 10 and 11, respectively. To unify the rubber content, a designated percentage for each mix type was converted to a total aggregate volume percentage. The equivalent values of rubber content by total aggregate volume are given in Table 10. Specimens were demoulded 24 h after casting, and were then water cured for 7 days. Thereafter, the specimens were kept in a curing room at a temperature of 30°C, with a relative humidity of 60%, until the time of testing. A normal, non-air-entrained, Portland cement concrete, with a 30 MPa targeted compressive strength, was designed as the control mix following ACI Standard 211.1-81 (American Concrete Institute, 2002). The mix required a 0.45 water-cement ratio. Other constituents are given in

Table 10 for P specimens. This control mix was used as the basis for preparing three rubberized concrete mixes specified by C, F, and CF mixes. In the C mixes, the coarse aggregates of the control mix were replaced by rubber chips, and in the F mixes, the sand in the control mix was replaced by crumb rubber. In the CF mixes, chip and crumb rubber particles were used as replacements for gravel and sand, respectively. For a C50F50 mix, crumb rubber replaced 50% of the sand volume and tire chips replaced 50% of the coarse aggregate volume.

Several specimens were fabricated from each of the C and F mixes, where in the coarse or fine mineral aggregate was replaced by rubber aggregates in increments of 25% by volume. C25F25 and C50F50 were also fabricated.

Specimen designation	ire content[%] by total aggregate	Fine tire aggregate[%]	Coarse tire aggregate[%]	Fine mineral aggregate[%]	Coarse mineral aggregate[%]	Replicates in compressive test	Replicates in ultrasonic test
P	0	0	0	100	100	3	2
C25	12.5	0	25	100	75	3	2
C50	25	0	50	100	50	3	2
C75	37.5	0	75	100	25	3	2
C100	50	0	100	100	0	3	2
F25	12.5	25	0	75	100	3	2
F50	25	50	0	50	100	3	2
F75	37.5	75	0	25	100	3	2
F100	50	100	0	0	100	3	2
C25F25	25	25	25	75	75	3	2
C50F50	50	50	50	50	50	3	2

Table 10: Experimental program

Specimen	Water[lit]	Cement[Kg]	Coarse tire aggregate[Kg]	Fine tire aggregate[Kg]	Gravel[kg]	Sand[Kg]	Moisture of gravel[%]	Moisture of sand [%]
P	227	350	0	0	900	900	0	0
C25	229	350	152.375	0	675	900	2.6	5.5
C50	299	350	304.18	0	450	900	2	6.4
C75	356	350	456.3	0	225	900	3	8
C100	442	350	609.5	0	0	900	3	7
F25	215	350	0	149.5	900	675	3	7
F50	282	350	0	299	900	450	4	7.5
F75	384	350	0	452.1	900	225	3	2.5
F100	453	350	0	602.8	900	0	3	7
C25F25	298	350	152.375	149.5	675	675	3	6
C50F50	434	350	304.2	301.4	450	450	4	9

Table 11: Concrete mixture proportions

For the test method a compressive strain-control test was conducted for hardened concrete specimens to obtain the stress–strain curves for all of the specimens. The test was performed by a universal testing machine and a sensitive data acquisition system. The machine yielded a loading value variation due to a constant rate of specimen deformation. This rate was chosen to be 0.005 mm/sec. The ends of the cylinders were capped with traditional sulfur mortar following the requirements of ASTM C617 (ASTM, 1988) prior to testing. Compressive strengths of the cylindrical specimens were evaluated after 50 days.

#### 4.1.3. Results and discussion :

In order to investigate the mechanical properties of tire–rubber concrete, specimens of a cylindrical shape 15 cm in diameter \_ 30 cm in height were fabricated. These specimens were different in the content and type of tire particles as a portion of total aggregates in concrete as as demonstrated in Table 12.

To unify the rubber content, a designated percentage for each mix type was converted to a total aggregate volume percentage.

This control mix was used as the basis for preparing three rubberized concrete mixes specified by C, F, and CF mixes. In the C mixes, the coarse aggregates of the control mix were replaced by rubber chips, and in the F mixes, the sand in the control mix was replaced by crumb rubber. In the CF mixes, chip and crumb rubber particles were used as replacements for gravel and sand, respectively.

Test	Specimen	Cylinder sample		Tire content(%)by total aggregate	Fine tire aggregate(%)	Coarse tire aggregate(%)
		H[cm]	D[cm]			
#1	P	30	15	0	0	0
#2	C25	30	15	12,5	0	25
#3	C50	30	15	25	0	50
#4	C75	30	15	37,5	0	75
#5	C100	30	15	50	0	100
#6	F25	30	15	12,5	25	0
#7	F50	30	15	25	50	0
#8	F75	30	15	37,5	75	0
#9	F100	30	15	50	100	0
#10	C25F25	30	15	25	25	25
#11	C50F50	30	15	50	50	50

Table 12:Experimental program

The experimental results of the compressive stress–strain response of each specimen are summarized in the figure a and b as follow:

P	
Post-Peak	
$\epsilon$ [mm/mm]	$\sigma$ [Mpa]
0	0
0,0019	4,5052
0,005697	30,3736
0,006152	30,6484
0,006389	30,2614
0,007323	9,6519
0,010104	4,4548
0,011634	3,3223
0,01451	2,0287
0,018643	1,0455
0,03427	0,4146

(a)

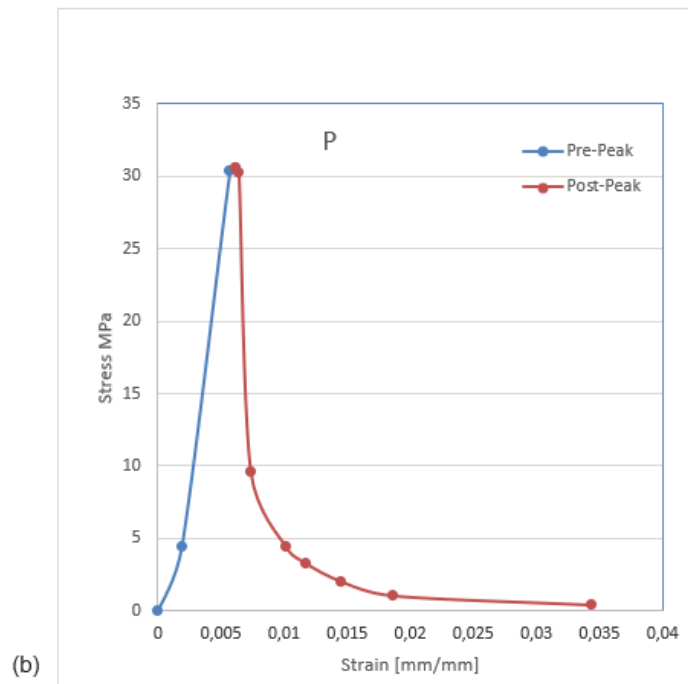
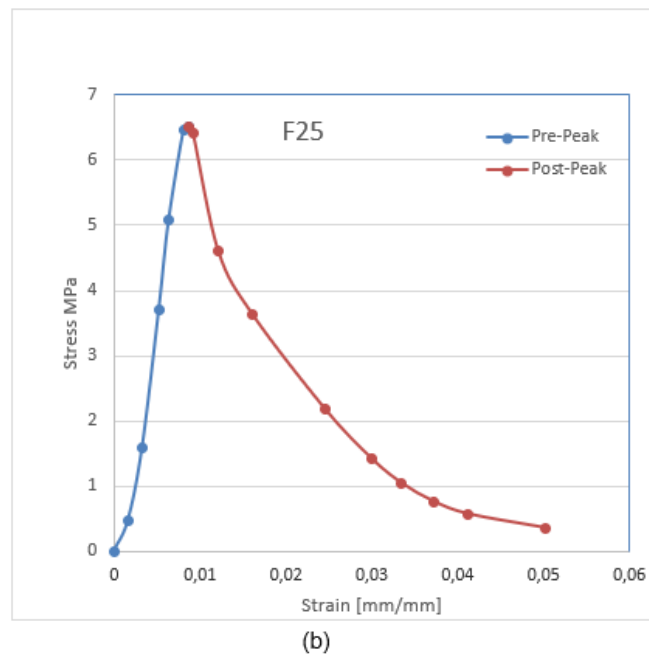


Figure 15: compressive stress–strain response of normal concrete ,(a) coordinates of  $\epsilon$ - $\sigma$  Post-Peak,(b) diagram of compressive  $\epsilon$ - $\sigma$

F25	
Post-Peak	
$\epsilon$ [mm/mm]	$\sigma$ [Mpa]
0	0
0,001627	0,4640
0,003281	1,5800
0,005232	3,7106
0,006365	5,0734
0,008112	6,4704
0,008623	6,5146
0,009179	6,4195
0,01213	4,6051
0,016118	3,6279
0,024587	2,1721
0,029956	1,4198
0,03346	1,0423
0,037118	0,7656
0,041227	0,5709
0,050227	0,3562

(a)

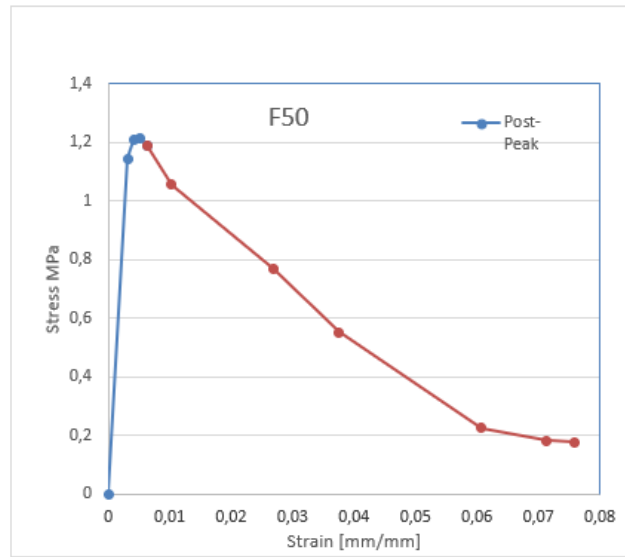


(b)

Figure 16: compressive stress–strain response of concrete with 25%,(a) coordinates of  $\epsilon$ - $\sigma$  Post-Peak,(b) diagram of compressive  $\epsilon$ - $\sigma$

F50	
Post-Peak	
$\epsilon$ [mm/mm]	$\sigma$ [Mpa]
0	0
0.003199	1.1445
0.004108	1.2063
0.005045	1.2134
0.006248	1.1877
0.01026	1.0556
0.026806	0.7701
0.037578	0.5511
0.060704	0.2255
0.07137	0.1824
0.075828	0.1789

(a)

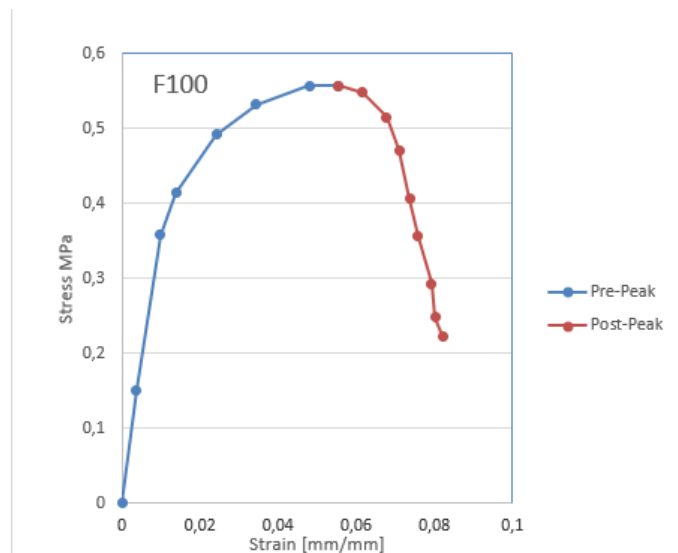


(b)

Figure 17: compressive stress–strain response of concrete with 50%, (a) coordinates of  $\epsilon$ - $\sigma$  Post-Peak, (b) diagram of compressive  $\epsilon$ - $\sigma$

F100	
Post-Peak	
$\epsilon$ [mm/mm]	$\sigma$ [Mpa]
0	0
0.003804	0.150735
0.009824	0.35801
0.013938	0.413799
0.024173	0.49174
0.034312	0.53192
0.048084	0.557065
0.055504	0.557065
0.061695	0.547854
0.067674	0.514492
0.071004	0.470767
0.073787	0.405865
0.075787	0.355972
0.079312	0.293144
0.080253	0.247699
0.08208	0.222653

(a)

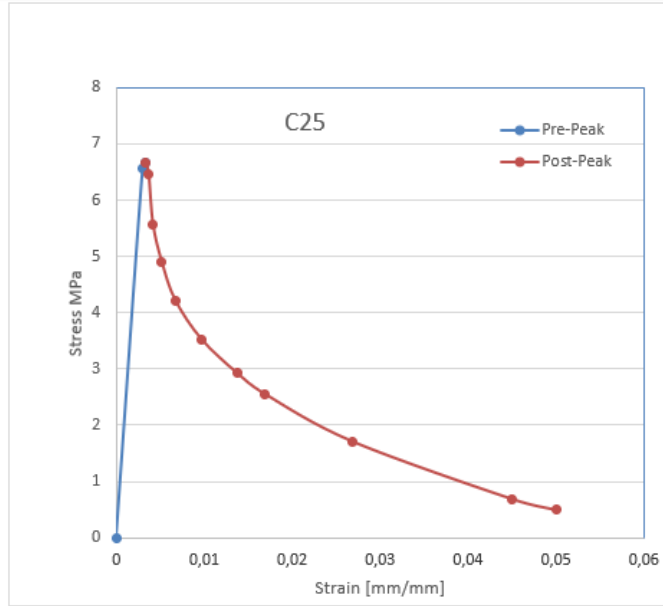


(b)

Figure 18: compressive stress–strain response of concrete with 100%, (a) coordinates of  $\epsilon$ - $\sigma$  Post-Peak, (b) diagram of compressive  $\epsilon$ - $\sigma$

C25	
Post-Peak	
$\epsilon$ [mm/mm]	$\sigma$ [Mpa]
0	0
0,002951	6,5564
<b>0,003357</b>	<b>6,6688</b>
0,003652	6,4611
0,004138	5,5681
0,005159	4,8912
0,006668	4,2217
0,009656	3,5263
0,013736	2,9240
0,016894	2,5537
0,026848	1,7121
0,045046	0,6888
0,050125	0,4942

(a)

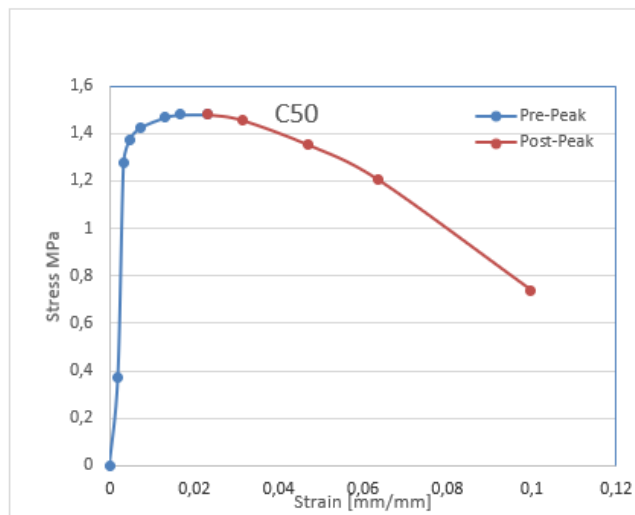


(b)

Figure 19: compressive stress–strain response of concrete with 25%, (a) coordinates of  $\epsilon$ - $\sigma$  Post-Peak, (b) diagram of compressive  $\epsilon$ - $\sigma$

C50	
Post-Peak	
$\epsilon$ [mm/mm]	$\sigma$ [Mpa]
0	0
0,00198878	0,3706
0,00335254	1,2792
0,00475608	1,3727
0,00728854	1,4244
0,01294957	1,4667
0,01648514	1,4789
<b>0,02326989</b>	<b>1,4806</b>
0,03126371	1,4567
0,04707314	1,3514
0,06347661	1,2055
0,09969062	0,7382

(a)

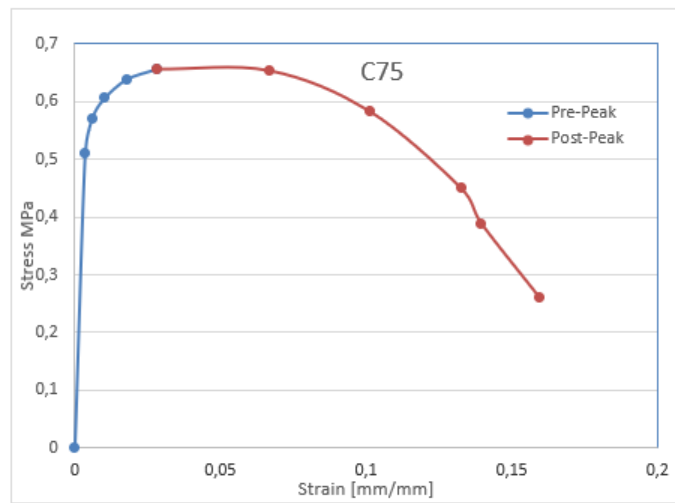


(b)

Figure 20: compressive stress–strain response of concrete with 50%, (a) coordinates of  $\epsilon$ - $\sigma$  Post-Peak, (b) diagram of compressive  $\epsilon$ - $\sigma$

C75	
Post-Peak	
$\epsilon$ [mm/mm]	$\sigma$ [Mpa]
0	0
0,00356	0,5113
0,006085	0,5722
0,010316	0,6063
0,017985	0,6390
0,028039	0,6561
0,066882	0,6534
0,101118	0,5835
0,132481	0,4504
0,13954	0,3890
0,159579	0,2601

(a)

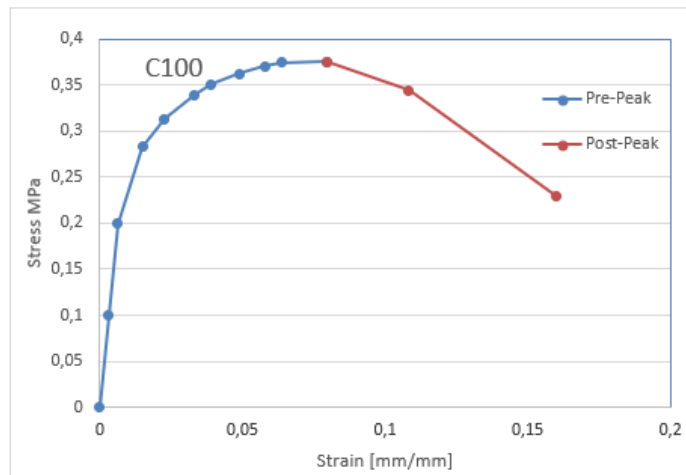


(b)

Figure 21::compressive stress–strain response of concrete with 75%,(a) coordinates of  $\epsilon$ - $\sigma$  Post-Peak,(b) diagram of compressive  $\epsilon$ - $\sigma$

C100	
Post-Peak	
$\epsilon$ [mm/mm]	$\sigma$ [Mpa]
0	0
0,003158	0,099783
0,006316	0,199567
0,015064	0,282661
0,022752	0,312901
0,033143	0,339907
0,039146	0,351145
0,048755	0,362103
0,057748	0,370557
0,063708	0,374621
0,079393	0,375759
0,108389	0,344303
0,159937	0,230049

(a)

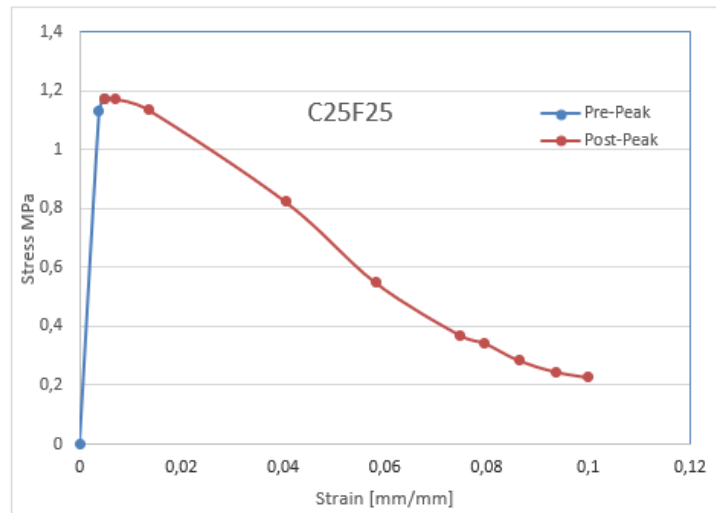


(b)

Figure 22::compressive stress–strain response of concrete with 100%,(a) coordinates of  $\epsilon$ - $\sigma$  Post-Peak,(b) diagram of compressive  $\epsilon$ - $\sigma$

C25F25	
Post-Peak	
$\epsilon$ [mm/mm]	$\sigma$ [Mpa]
0	0
0,003853	1,1306
0,004776	1,1742
0,007061	1,1726
0,01351	1,1367
0,040502	0,8241
0,058151	0,5498
0,074827	0,3699
0,079679	0,3431
0,086369	0,2843
0,093507	0,2459
0,099893	0,2266

(a)

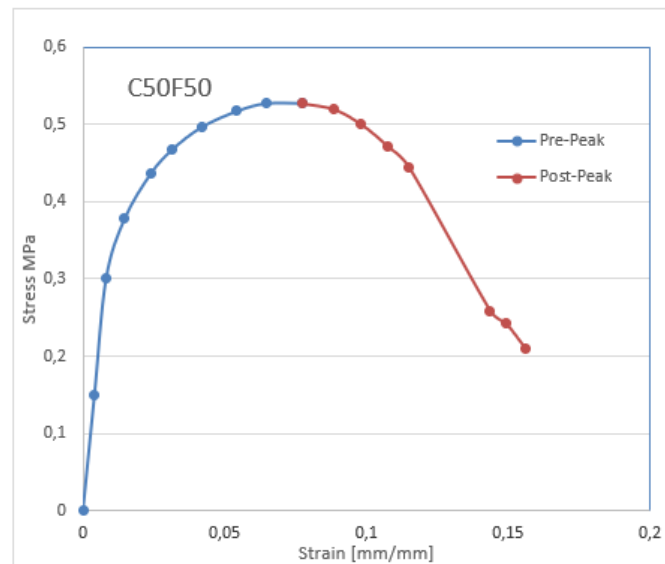


(b)

Figure 23: compressive stress–strain response of concrete with C25F25%, (a) coordinates of  $\epsilon$ - $\sigma$  Post-Peak, (b) diagram of compressive  $\epsilon$ - $\sigma$

C50F50	
Post-Peak	
$\epsilon$ [mm/mm]	$\sigma$ [Mpa]
0	0
0,004071	0,15004
0,008141	0,30008
0,014658	0,377895
0,023829	0,436098
0,031518	0,467898
0,041915	0,496874
0,054377	0,517511
0,064564	0,52733
0,077473	0,527506
0,088371	0,520014
0,09801	0,500714
0,107621	0,471438
0,115021	0,444348
0,143643	0,258335
0,149088	0,242758
0,156223	0,208888

(a)



(b)

Figure 24: compressive stress–strain response of concrete with C50F50%, (a) coordinates of  $\epsilon$ - $\sigma$  Post-Peak, (b) diagram of compressive  $\epsilon$ - $\sigma$

The curves indicate that the behavior of tire–rubber concrete is more nonlinear compared to that of plain concrete, implying a different failure type for tire–rubber concrete. The nonlinear behavior for tire–rubber concrete mixtures may also be due to the lower compressive strength of these mixtures.

A comparison between the investigated mixtures reveals that the C mixture behavior is more nonlinear than the F and CF mixtures behavior. The increased nonlinearity for tire–rubber concrete can explain the observations of the more global and well dispersed failures of the tire–rubber concrete specimens. The substitution of rubber for mineral aggregates appear to permit more uniform crack development and provide gentler crack propagation, compared to plain concrete.

Considering the stress–strain curves, tire–rubber concrete specimens experience larger deformations compared to plain concrete specimens under the same loading conditions.

Hence, these curves support the assertion that tire particle usage in concrete results in concrete failures with larger deformations and higher energy dissipation.

Failure state or softening phases of C specimens were accompanied by a larger deformation compared to F specimens at the same loading condition. C specimens exhibited higher strength compared to F specimens at the failure state for the same strain condition. This extra strength is due to the existence of fibers in coarse tire–rubber particles.

As shown in the previous Table 15-25 , the CF specimen stress–strain curves located between the C and F specimens stress–strain curves contain the same tire concentration. The combined stress–strain curve demonstrated stress values which were close to those of the F mixture, but the curve’s shape dominantly resembled the C mixture curve. This suggests that the ultimate stress of CF tire–rubber concrete depends on the fine aggregate concentration, while the shape of the stress–strain curve is primarily affected by the coarse aggregate concentration. These observations imply the stress–strain response for CF tire–rubber concrete is located between the corresponding C and F stress–strain curves equaling the total respective tire particles concentration. Hence any desired stress–strain curve between the C and F curves can be obtained by tuning coarse and fine tire concentrations.

Tire–rubber concretes are able to withstand loads beyond the peak load, which is referred to as post-failure strength.

Failure states in plain concrete specimens, as shown in Figure 25, are accompanied with the separation of pieces or slices from the specimen. For concrete containing tire particles, the failure state was not accompanied by any detachment due to the bridging of cracks by rubber particles.

Tire–rubber concrete specimens did not exhibit any detachment, despite losing a considerable amount of strength as shown by the F25 and C25 specimens in Figure 25. Tire–rubber concrete specimens present large deformations compared to plain concrete specimens. During the unloading process, the flexible behavior of tire particles decreases the internal friction among the concrete elements, and recovers extra strain. Failure properties, like discontinuities and cracks, propagated uniformly and gradually in tire–rubber concrete specimens. In contrast, the propagation of failure symptoms were abrupt and concentrated for plain concrete. Figure 25 demonstrates that the failure parameters grow uniformly from the bottom to the top of a C25 of specimen. The lateral deformations of tire–rubber concrete specimens are larger than those of plain concrete specimens; however, because of the porosity due to the substitution of tire particles, Poisson’s ratios for tire–rubber concrete are slightly more than those for plain concrete. It is important to note that the behavior of rubberized concrete is not perfectly elastic, therefore Poisson’s ratio is not constant for the entire loading process. Poisson’s ratio increases and approaches 0.5 as the behavior of rubberized concrete becomes plastic-like. As shown in Figure 25, considerable lateral deformations are observable in tire–rubber concrete specimens after an entire loading process.



Figure 25: Failure types of specimens

## 4.2. Test number Two:

In some application of concrete, it is desired that concrete should have low unit weight, high toughness and impact resistance. Although concrete is the most commonly used construction material, it does not always fulfill these requirements. To improve elastic properties of concrete and recycle the waste materials recently new applications have been realized . One of these applications is the utilization of discarded tires to replace a part of the aggregate. For this purpose, this research was conducted to investigate the physical and mechanical properties of the concrete which was obtained by incorporating pieces of discarded tires. It is thought that rubberized concrete would be an ideal material for jersey barriers which are subjected to immediate effects of impact and very high strength is not sought for. Rubberized concrete could prevent life casualties and damage to vehicles by absorbing the impact energy.

### 4.2.1. Materials and methods:

In preparation of the specimens for the experiments, ASTM C 150 type I portland cement (28- day compressive strength of 32.5 MPa) was used. In all concrete series river sand was used, which has 4 mm maximum size, 1.640 kg/dm<sup>3</sup> unit weight, 2.640 specific gravity, 1% water absorption, and 2.00 fineness modulus. In concrete, crushed limestone of 4 to 16 mm was used as coarse aggregate. The crushed stone has 1.425 kg/dm<sup>3</sup> unit weight, 2.681 specific gravity, 0.3 % water absorption, and 5.04 fineness modulus. The rubber aggregate, obtained by mechanical grinding from the outer surface of scrap tires, was sieved and separated into two grain sizes of 0/1 (fine) and 1/4 mm (coarse). The fine and coarse rubber chips had specific gravity of 0.650, unit weights of 0.472 and 0.410, fineness moduli of 1.58 and 1.91, respectively.

#### 4.2.2. Concrete mixes:

In this study, C20 control concrete without rubber and six series of concrete with rubber chips of 0/1 and 1/4 mm were used. The mix proportioning of the control concrete series was done using the absolute volume method. The other six series were prepared by replacing same volume of fine and coarse aggregates by rubber chips. The water-cement ratio of the batches were around 0.60 to get an average slump of 40-50 mm and a flow value of 420 mm. The weights and absolute volumes of the materials in 1 m<sup>3</sup> of the control concrete were as follows:

	Cement	Sand	Crashed Stone	Water	Air
Weight[Kg]	357,5	609	1148,1	222,4	0
Volume[dm <sup>3</sup> ]	113,5	230,7	428,4	222,4	5

*Table 13:Weights and absolute volumes of the materials in 1[m<sup>3</sup> ] of the control concrete*

The fine and coarse rubber chips were included by replacing 15, 30, and 45 % of the aggregate in the control concrete. The resulting concretes were designated as follows: NC (control concrete), FRC-15, FRC-30, FRC-45 (15, 30, and 45 %, by volume, 0/1 mm rubber chips replacing the aggregate), CRC-15, CRC-30, and CRC-45 (15, 30, and 45 %, by volume, 1/4 mm rubber chips replacing the aggregate).

#### 4.2.3. Results and discussion:

In order to investigate the mechanical properties of tire–rubber concrete, specimens of a cylindrical shape 15 cm in diameter \_ 30 cm in height were fabricated. These specimens were different in the content and type of tire particles as a portion of total aggregates in concrete as as demonstrated in Table 14.

To unify the rubber content, a designated percentage for each mix type was converted to a total aggregate volume percentage.

This control mix was used as the basis for preparing two rubberized concrete mixes specified by FRC and CRC mixes. In the CRC mixes, the aggregates of the control mix were replaced by 1/4mm rubber chips , and in the FRC mixes, the aggregates of the control mix were replaced by 0/1mm rubber chips.

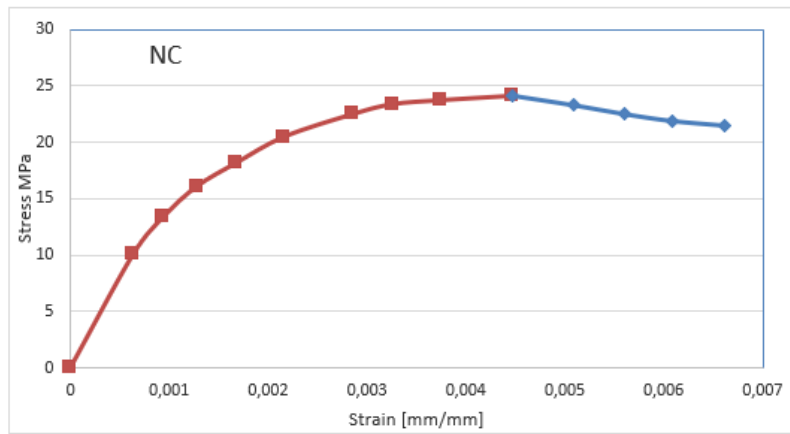
Test	Specimen	Cylinder sample		rubber content(%)by total aggregate	Fine Rubber chips(%)	Coarse rubber chips
		H[cm]	D[cm]			
#1	NC	30	15	0	0	0
#2	FRC-15	30	15	15	15	0
#3	FRC-30	30	15	30	30	0
#4	FRC-45	30	15	45	45	0
#5	CRC-15	30	15	15	0	15
#6	CRC-30	30	15	30	25	30
#7	CRC-45	30	15	45	50	45

*Table 14:Experimental Program*

The experimental results of the compressive stress–strain response of each specimen are summarized in the figure a and b as follow:

NC	
$\epsilon$ [mm/mm]	$\sigma$ [Mpa]
0	0
0,000634	10,0558
0,00094	13,3793
0,001276	16,0641
0,001681	18,1770
0,002162	20,4760
0,002853	22,4736
0,003255	23,3552
0,003738	23,7049
0,004467	24,0984
0,005086	23,2845
0,0056	22,5294
0,00608	21,9394
0,00662	21,5383

(a)

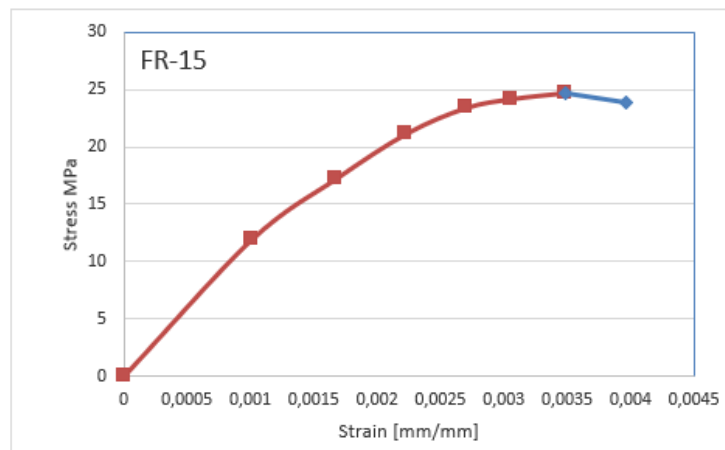


(b)

Figure 26: compressive stress–strain response of normal concrete ,(a) coordinates of  $\epsilon$ - $\sigma$  Post-Peak,(b) diagram of compressive  $\epsilon$ - $\sigma$ :

FR-15	
$\epsilon$ [mm/mm]	$\sigma$ [Mpa]
0	0
0,001006	11,9038
0,001677	17,2591
0,002229	21,1849
0,002696	23,4171
0,003058	24,2068
0,0035	24,7360
0,003962	23,8255

(a)

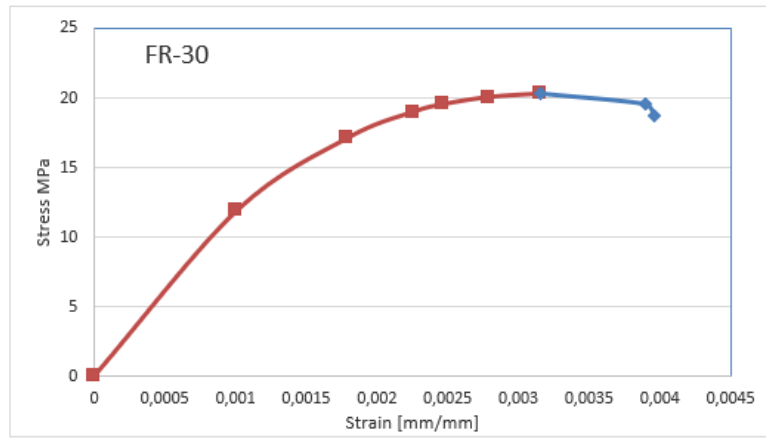


(b)

Figure 27: compressive stress–strain response of concrete with FR-15% ,(a) coordinates of  $\epsilon$ - $\sigma$  Post-Peak,(b) diagram of compressive  $\epsilon$ - $\sigma$

FR-30	
$\epsilon$ [mm/mm]	$\sigma$ [Mpa]
0	0
0,001006	11,8749
0,001791	17,1145
0,002254	18,9848
0,002466	19,5362
0,002792	20,0531
0,0032	20,2943
0,003896	19,5362
0,003961	18,7091

(a)

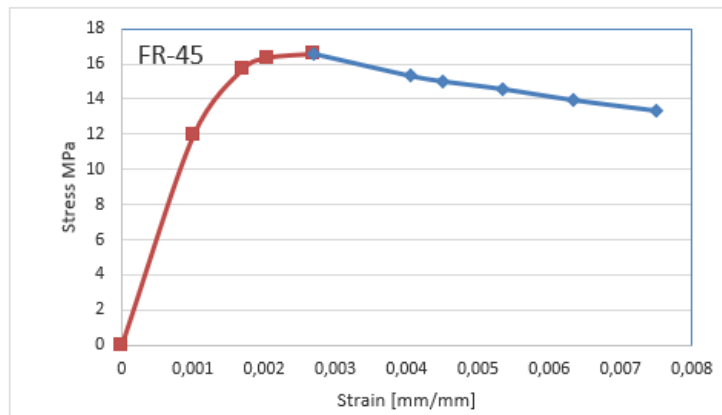


(b)

Figure 28: compressive stress–strain response of concrete with FR-30% ,(a) coordinates of  $\epsilon$ - $\sigma$  Post-Peak,(b) diagram of compressive  $\epsilon$ -  $\sigma$

FR-45	
$\epsilon$ [mm/mm]	$\sigma$ [Mpa]
0	0
0,001006	11,9038
0,001697	15,6817
0,002056	16,3489
0,0027	16,5759
0,004052	15,3349
0,004502	15,0266
0,005341	14,5899
0,006332	13,9681
0,007493	13,3700

(a)

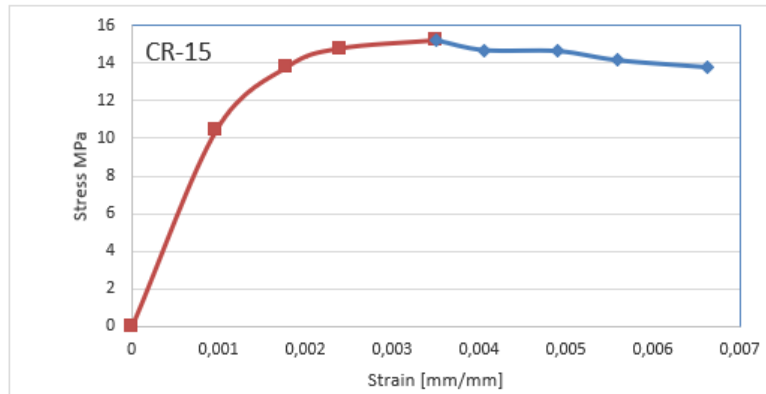


(b)

Figure 29: compressive stress–strain response of concrete with FR-45% ,(a) coordinates of  $\epsilon$ - $\sigma$  Post-Peak,(b) diagram of compressive  $\epsilon$ -  $\sigma$

CR-15	
$\epsilon$ [mm/mm]	$\sigma$ [Mpa]
0	0
0,000976	10,4772
0,001789	13,8056
0,002394	14,7724
0,003503	15,2112
0,004052	14,7035
0,004903	14,6516
0,005589	14,1812
0,00662	13,8199

(a)

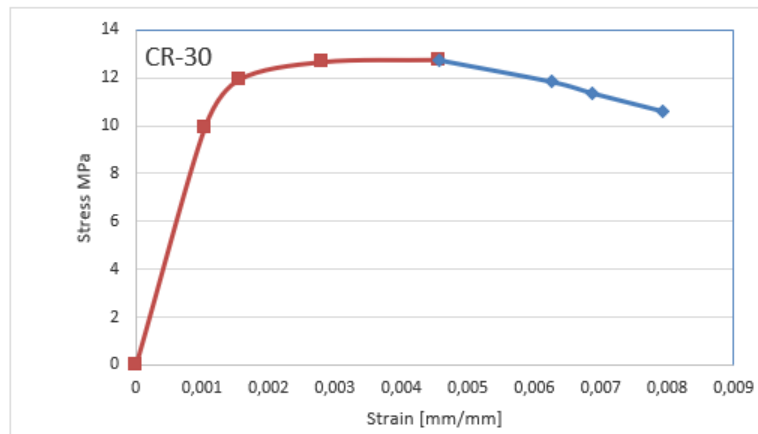


(b)

Figure 30: compressive stress–strain response of concrete with CR-15% ,(a) coordinates of  $\epsilon$ - $\sigma$  Post-Peak,(b) diagram of compressive  $\epsilon$ -  $\sigma$

CR-30	
$\epsilon$ [mm/mm]	$\sigma$ [Mpa]
0	0
0,001036	9,9344
0,001554	11,9296
0,002809	12,6632
0,004559	12,7512
0,00627	11,8304
0,006878	11,3523
0,00792	10,6053

(a)

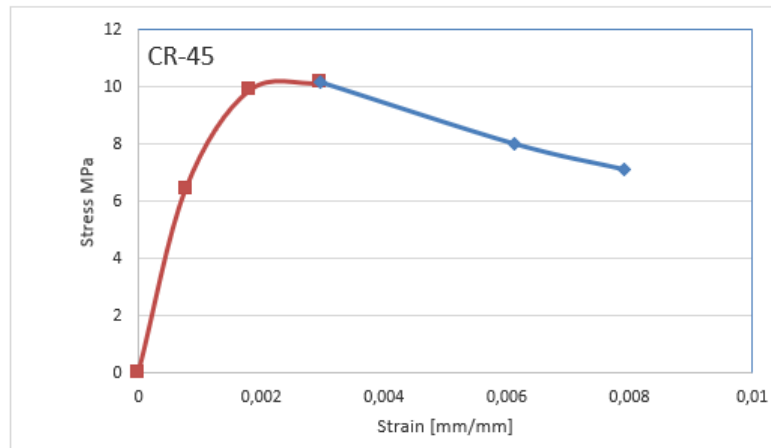


(b)

Figure 31: compressive stress–strain response of concrete with FR-30% ,(a) coordinates of  $\epsilon$ - $\sigma$  Post-Peak,(b) diagram of compressive  $\epsilon$ -  $\sigma$

CR-45	
$\epsilon$ [mm/mm]	$\sigma$ [Mpa]
0	0
0,000771	6,4443
0,001805	9,8922
0,002965	10,1573
0,006112	8,0259
0,007921	7,1204

(a)



(b)

Figure 32: compressive stress–strain response of concrete with FR-45% ,(a) coordinates of  $\epsilon$ - $\sigma$  Post-Peak,(b) diagram of compressive  $\epsilon$ - $\sigma$

Although the  $\sigma$ – $\epsilon$  diagrams of 7, 28-day and 6-month normal and rubberized concretes were tested in this study, because of their similarity only those of 28-day concretes are given in the previous figures as example. When the  $\sigma$ - $\epsilon$  diagrams of these concretes are analyzed, it can be seen that control concrete reaches the ultimate strain around 0.002. The concrete having 15 % coarse rubber mixture shows similar behavior as normal concrete. With mixture of coarse rubber particles maximum strain points fall while the strain increases at the failure point in rubberized concretes  $\epsilon$ -strain values change between 0.003 and 0.005 against maximum strains.

the rubberized concretes absorb more energy, they can show more strain at the time of fracture. Examination of  $\epsilon_{max}$  values obtained from  $\sigma$ - $\epsilon$  diagrams show that these values can reach to 0.007 and 0.008.

Tire–rubber concrete specimens present large deformations compared to plain concrete specimens. During the unloading process, the flexible behavior of tire particles decreases the internal friction among the concrete elements, and recovers extra strain.

Tire–rubber concretes are able to withstand loads beyond the peak load, which is referred to as post-failure strength.

### 4.3. Test number Three:

#### 4.3.1. Materials and method:

The base paste material in this study consisted of Type 1 ordinary Portland cement. Coarse aggregate (crushed stone) had a maximum size of 14 mm. The specific gravity of the coarse aggregate was 2.65. River sand with fineness modulus of 3.4 and specific gravity of 2.64 was used as fine aggregate. The particle size distribution is shown in Figure 33 at left. Crumb rubber used in this study is shown in Figure 33 at right .

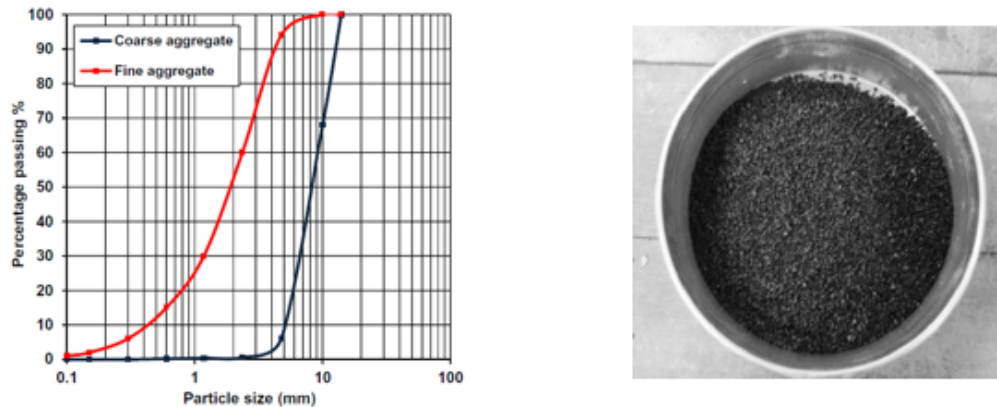


Figure 33: Particle size distribution of fine and coarse aggregate (at left), Materials used in this study: Crumb rubber (at right)

The total number of mixtures prepared was four. Each mixture differed in rubber ratio. Ordinary concrete as reference mixture designed with minimum strength of 40 MPa. The other series consisted of rubberized concrete with crumb rubber that had different replacement ratios (5%, 10%, and 15%) by partial replacement of fine aggregate (sand) by volume.

Table 15 shows the proportions of mixtures considered in this work. Each sample consisting of (200-100 mm) (Height \_ Diameter) cylinders prepared according to ASTM C192 for compression and stress-strain behaviour.

Mix	Cement	Water	Coarse aggregate	fine aggregate	Crumb rubber
NC	430	202	907	814	0
CRC-5	430	202	907	773	11,1
CRC-10	430	202	907	732	22,2
CRC-15	430	202	907	692	33,3

*Table 15: Mix proportions in [kg/m<sup>3</sup>]*

#### 4.3.2. Test setup:

The compressive test was conducted using (200 \_ 100 mm) (Height \_ Diameter) concrete cylinders subjected to an axial load applied by a hydraulically operated machine with rate 0.3 N/mm<sup>2</sup>/s until the failure of the specimen. The test conditions were according to ASTM C39 and at age of 28 days. The stress–strain curves were determined by measuring loads that increased at a constant rate. For each stress value, the specified strain was measured and calculated immediately using the built – in system of the machine. Modulus of elasticity was calculated according to ASTM C469.

### 4.3.3. Results and discussion :

In order to investigate the mechanical properties of tire–rubber concrete, specimens of a cylindrical shape 10 cm in diameter \_ 20 cm in height were fabricated. These specimens were different in the content and type of tire particles as a portion of total aggregates in concrete as as demonstrated in Table 16.

To unify the rubber content, a designated percentage for each mix type was converted to a total aggregate volume percentage.

This control mix was used as the basis for preparing one rubberized concrete mix specified by CRC mixes. In the CRC mixes, fine aggregate (sand) of the control mix were replaced by crumb rubber that had different replacement ratios (5%, 10%, and 15%) .

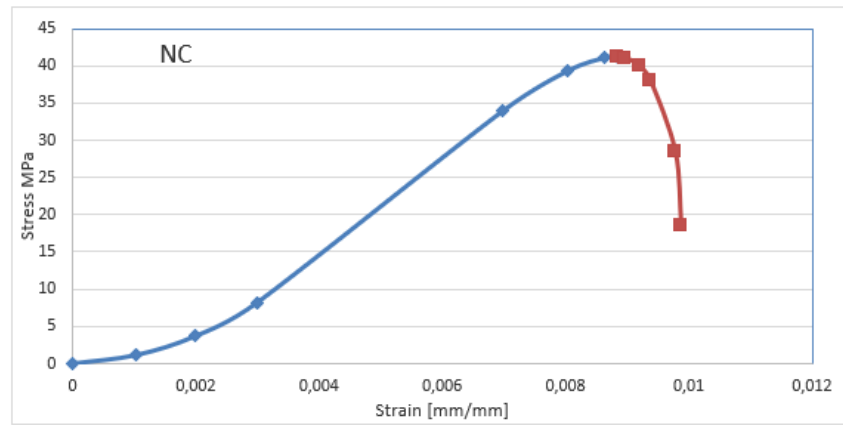
Test	Specimen	Cylinder sample		Crumb tire aggregate(%)
		D[cm]	H[cm]	
#1	NC	10	20	0
#2	CRC-5	10	20	5
#3	CRC-10	10	20	10
#4	CRC-15	10	20	15

Table 16:Experimental program

The experimental results of the compressive stress–strain response of each specimen are summarized in the figure a and b as follow:

NC	
$\epsilon$ [mm/mm]	$\sigma$ [Mpa]
0	0
0,001031	1,1468
0,001989	3,6824
0,002987	8,1537
0,006979	33,9398
0,008035	39,3101
0,00864	41,0664
0,008835	41,2189
0,00896	41,0231
0,009199	39,9093
0,009381	37,8863
0,00979	28,4285
0,009886	18,4482

(a)

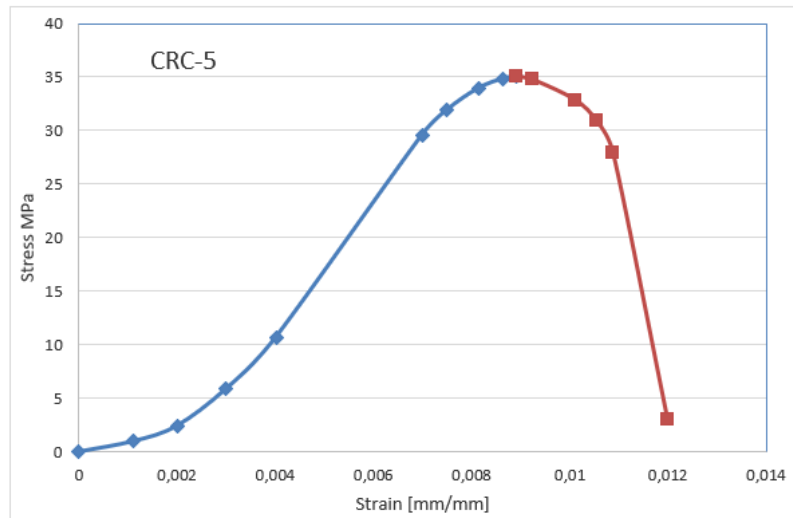


(b)

Figure 34: compressive stress–strain response of normal concrete ,(a) coordinates of  $\epsilon$ - $\sigma$  Post-Peak,(b) diagram of compressive  $\epsilon$ - $\sigma$

CRC-5	
$\epsilon$	$\sigma$
0	0
0,001116	0,9843
0,001994	2,4003
0,003	5,8725
0,004012	10,6832
0,006996	29,6105
0,007502	31,9227
0,008132	33,9169
0,00864	34,8252
0,00891	34,9964
0,009235	34,7465
0,010101	32,8459
0,010539	30,8873
0,010872	27,9267
0,01198	2,9981

(a)

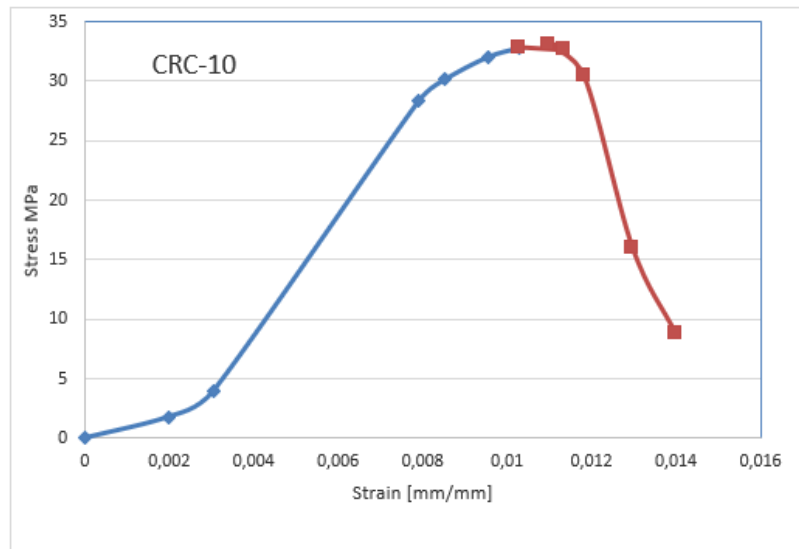


(b)

Figure 35: compressive stress–strain response of concrete with CRC-5% ,(a) coordinates of  $\epsilon$ - $\sigma$  Post-Peak,(b) diagram of compressive  $\epsilon$ - $\sigma$

CRC-10	
$\epsilon$ [mm/mm]	$\sigma$ [Mpa]
0	0
0,001998	1,8078
0,003038	3,9526
0,007908	28,3943
0,008533	30,1926
0,009535	32,0598
0,010287	32,8474
0,011344	32,6401
0,010976	33,0685
0,011816	30,4294
0,012964	15,9840
0,013979	8,8245

(a)

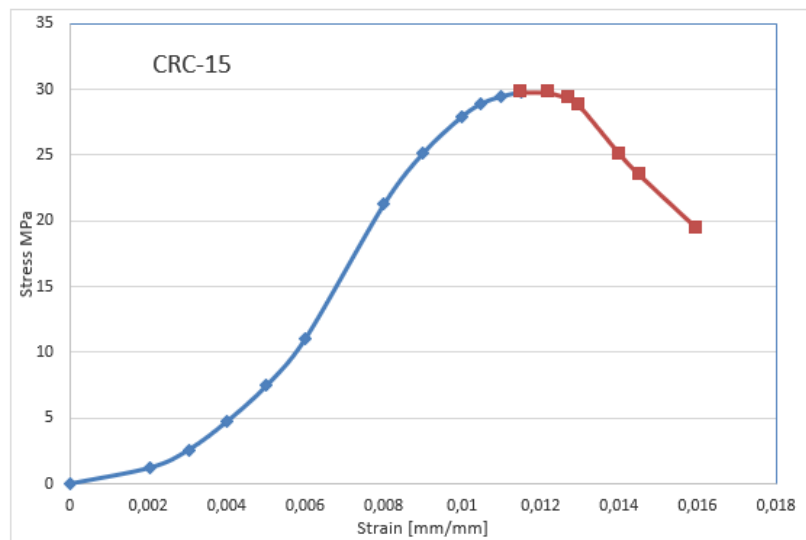


(b)

Figure 36: compressive stress–strain response of concrete with CRC-10% ,(a) coordinates of  $\epsilon$ - $\sigma$  Post-Peak,(b) diagram of compressive  $\epsilon$ -  $\sigma$

CRC-15	
$\epsilon$ [mm/mm]	$\sigma$ [Mpa]
0	0
0,002054	1,2379
0,003028	2,5919
0,004004	4,7506
0,005015	7,4861
0,005999	11,0309
0,008008	21,2700
0,008997	25,1171
0,009982	27,8880
0,010488	28,8983
0,010984	29,4478
0,011504	29,7845
0,012194	29,7463
0,01272	29,2898
0,012974	28,8274
0,014019	25,0770
0,014523	23,4968
0,015994	19,3936

(a)



(b)

Figure 37: compressive stress–strain response of concrete with CRC-15% ,(a) coordinates of  $\epsilon$ - $\sigma$  Post-Peak,(b) diagram of compressive  $\epsilon$ -  $\sigma$

The complete stress–strain curves for the cylinders tested in this work are shown in the previous Figures. The average values for rubberized normal concrete fibre concrete are presented. Each curve represents the average results of three tests conducted at the same age and conditions. The measurement of strain was limited to 2%.

For the normal concrete with crumb rubber, the increase in rubber crumb content led to increasing strain during the reduction in maximum stress.

A change in the shape of the stress–strain curves was also observed. The behaviour of rubberized concrete specimen differed from that of normal concrete, which exhibited ductile behaviour rather than the brittle one. This behaviour was concluded by comparing the shapes of rubberized concrete curves with those of normal concrete. A further increase in rubber content led to increase in the ductility. The failure state of rubberized concrete was accompanied by high deformations in descending curves. Another difference between rubberized concrete curves was the increase in strain capacity (which can be defined as the strain at the maximum stress).

Hence, the rubberized concrete mixtures showed a decrease in the slope of the descending portion of the stress–strain curve by the addition of crumb rubber. A high strain was measured at the peak stress, although the maximum stress was reduced with rubber replacement ratio. The change in the shape of the stress–strain curves would also affect the energy absorbed.

the rubberized concretes absorb more energy, they can show more strain at the time of fracture. Examination of  $\varepsilon_{max}$  values obtained from  $\sigma$ - $\varepsilon$  diagrams show that these values can reach to 0.012 and 0.016, while in the normal concrete specimen is only 0.0098.

## 4.4. Test number Four :

### 4.4.1. Materials methods:

Table 17 summarizes the mix proportions of the concrete mixes considered in this paper. The materials used were: general purpose cement (manufactured by Adelaide Brighton Cement), 20 mm and 10 mm stone, natural sand (from Hallett Concrete), water and super-plasticizer (Glenium 107 Suretec from BASF), crumbed rubber (nominal size of 1.18 mm and 2.36 mm mixed at a weight ratio of 1:1) from waste tyres sourced from Chip Tyre Pty Ltd (Figure 38). The concrete was mixed as required by AS 1012.2 . All aggregate

was air dried before mixing to reduce the moisture content to a minimum. Crumbed rubber was clean and contained no steel belting or steel fibres. The specific gravity (relative density) of stone, sand and rubber were 2.73, 2.6 and 0.85 respectively. For all mixes, rubber particles were pre-treated with Sodium Hydroxide (NaOH) solution and then pre-coated with cement before being added into the concrete mixture. Other research has shown alternative treatment methods, such as water treatment, can also improve concrete compressive strength. The target compressive strength at 28 days of the TC mix design

was 45–50 MPa. For all mixes the water cement ratio was kept as 0.5. Doses of super-plasticizer (SP) were adjusted and used for each mix to ensure all mixes obtained similar slumps of approximately 75 mm.



*Figure 38:Rubber Particles*

Mix	Rubber percentage[%]	Cement[kg/m <sup>3</sup> ]	20mm stone[kg/m <sup>3</sup> ]	10mm stone[kg/m <sup>3</sup> ]	Sand[kg/m <sup>3</sup> ]	Water[kg/m <sup>3</sup> ]	Rubber[kg/m <sup>3</sup> ]	Rubber treatment
TC	0	400	865	215	687	200	0	
CRC6	6	400	865	215	646	200	13.5	NaOH
CRC12	12	400	865	215	605	200	27	NaOH
CRC18	18	400	865	215	563	200	40.5	NaOH

Table 17: Mix proportions

#### 4.4.2. Specimen preparation and testing:

In this study, one TC mix and three CRC mixes were used. The three CRC mixes were designated as CRC6, CRC12 and CRC18, which represents crumb rubber content of 6%, 12% and 18% (replacement of sand at volume percentages). For each mix three 100 mm \_ 200 mm unconfined cylindrical specimens were tested

under uniaxial displacement-controlled compression loading at a rate of 0.001[mm/s]. Linear Variable Differential Transformers (LVDT) were used to measure the platen to platen displacement which was taken as the total vertical displacement of the specimen and used for analysis.

The cylinder specimens were cast for each mix, TC, CRC6, CRC12 and CRC18 following requirements in AS 1012.8.1. 24 h after casting, the cylinders were demoulded and then continuously moist-cured in the fog room, for 28 days. At 28 days of age before testing started, specimens were measured for dimension and

weight, and then both ends were ground flat and parallel. For each concrete mix three specimens were prepared for tests and analysis.

The tests were carried out on a Baldwin compression machine , connected to a computer for data logging. The loading process, visible deformations, crack propagation process and failure modes of specimens were also recorded by two cameras and displayed on the screen by Grasshopper software. At the beginning of the test the upper platen was lowered and a very small seating load was exerted on the specimen. Displacement-controlled load was applied to the specimen at a constant loading rate of 0.001 mm/s throughout the test according to the RILEM standard. A LVDT was used to measure the platen to platen displacement. It was contact-free to the specimen so that the test data was not disturbed by the cracking and spalling of the specimen. The duration of the test until strength failure of a specimen was approximately 50 min. When the strain reached around 0.005 or the load reached a nearly constant value during the softening stage, loading was stopped.

#### 4.4.3. Results and discussion:

In order to investigate the mechanical properties of tire–rubber concrete, specimens of a cylindrical shape 10 cm in diameter \_ 20 cm in height were fabricated. These specimens were different in the content and type of tire particles as a portion of total aggregates in concrete as as demonstrated in Table 18.

one normal concrete mix and three CRC mixes were used. The three CRC mixes were designated as CRC6, CRC12 and CRC18, which represents crumb rubber content of 6%, 12% and 18% (replacement of sand at volume percentages).

To unify the rubber content, a designated percentage for each mix type was converted to a total aggregate volume percentage.

This control mix was used as the basis for preparing one rubberized concrete mix specified by CRC mixes. In the CRC mixes, fine aggregate (sand) of the control mix were replaced by crumb rubber that had different replacement ratios (5%, 10%, and 15%) .

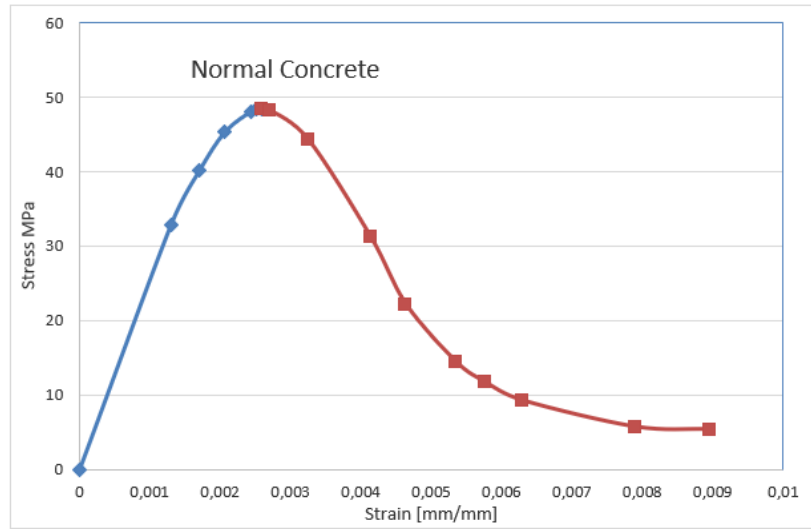
Test	Specimen	Cylinder sample		Crumb Rubber content(%)by total aggregate
		H[cm]	D[cm]	
#1	NC	20	10	0
#2	CRC6	20	10	6
#3	CRC12	20	10	12
#4	CRC18	20	10	18

*Table 18:Experimental program*

The experimental results of the compressive stress–strain response of each specimen are summarized in the figure a and b as follow:

NC	
$\epsilon$ [mm/mm]	$\sigma$ [Mpa]
0	0
0,001299	32,9087
0,001702	40,1531
0,002062	45,3170
0,002435	48,0922
0,002506	48,3179
0,002582	48,3928
0,002705	48,1875
0,003245	44,2778
0,00413	31,2724
0,004637	22,1299
0,005351	14,3982
0,005758	11,7226
0,006295	9,2260
0,007896	5,6947
0,008954	5,3421

(a)

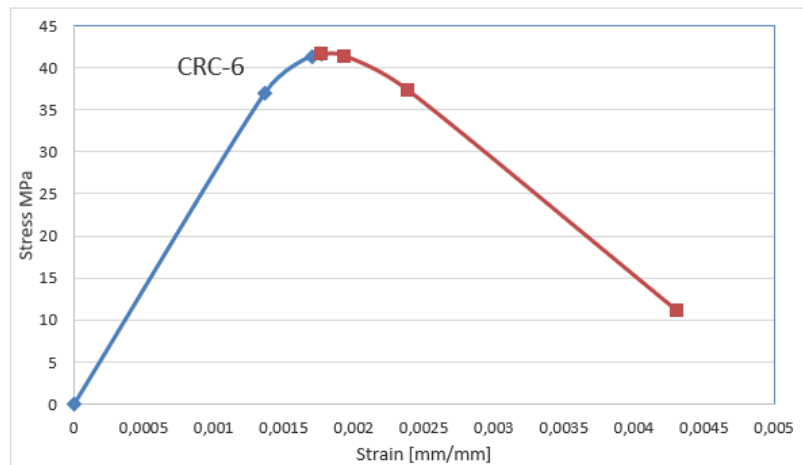


(b)

Figure 39: compressive stress–strain response of normal concrete, (a) coordinates of  $\epsilon$ - $\sigma$  Post-Peak, (b) diagram of compressive  $\epsilon$ - $\sigma$

CRC-6	
$\epsilon$ [mm/mm]	$\sigma$ [Mpa]
0	0
0,001364	36,9419
0,001698	41,3682
0,00177	41,6316
0,001936	41,3786
0,002383	37,3551
0,004311	11,0629

(a)

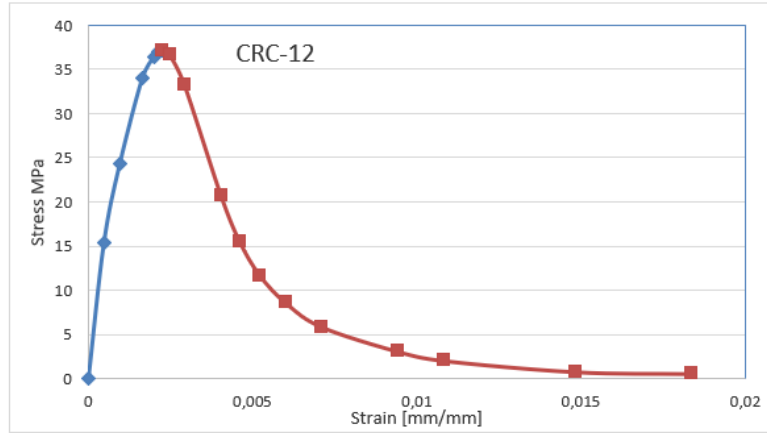


(b)

Figure 40: compressive stress–strain response of concrete with CRC-6%, (a) coordinates of  $\epsilon$ - $\sigma$  Post-Peak, (b) diagram of compressive  $\epsilon$ - $\sigma$

CRC-12	
$\epsilon$ [mm/mm]	$\sigma$ [Mpa]
0	0
0,000472	15,3382
0,000962	24,3656
0,001652	34,0629
0,002004	36,4639
0,00213	37,0222
0,00226	37,1865
0,002483	36,6602
0,002929	33,3307
0,00405	20,7252
0,004619	15,5113
0,005236	11,6736
0,006017	8,6082
0,0071	5,8900
0,009408	3,1164
0,010829	2,0568
0,014837	0,7895
0,018347	0,5844

(a)

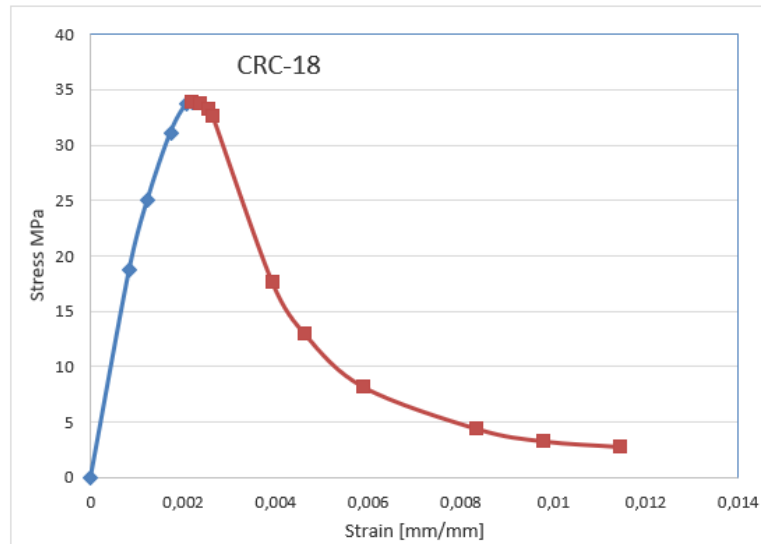


(b)

Figure 41: compressive stress–strain response of concrete with CRC-12% ,(a) coordinates of  $\epsilon$ - $\sigma$  Post-Peak,(b) diagram of compressive  $\epsilon$ -  $\sigma$

CRC-18	
$\epsilon$ [mm/mm]	$\sigma$ [Mpa]
0	0
0,000835	18,6690
0,001234	25,0633
0,00173	31,0947
0,002069	33,6650
0,002205	33,8361
0,002379	33,7168
0,002553	33,1666
0,002642	32,6332
0,003933	17,5967
0,004642	12,8972
0,005905	8,1466
0,008349	4,3834
0,009787	3,2623
0,011451	2,7585

(a)



(b)

Figure 42: compressive stress–strain response of concrete with CRC-18% ,(a) coordinates of  $\epsilon$ - $\sigma$  Post-Peak,(b) diagram of compressive  $\epsilon$ -  $\sigma$

The complete stress strain curves of individual tested specimens of each group are presented in the previous figures Figure 39-42 respectively.

It can be seen that all the stress-strain curves from different mixes followed a similar trend. The initial part of the curve is linear then the stress increased more slowly up to the peak stress. The descending portion tended to reach a constant stress level at higher strains.

The post-peak behavior presents other differences. For reference mix or the normal concrete, the softening branch has a high reduction of stiffness, when compared with rubberized concrete. With increased rubber content this post peak behavior has an increase in the softening stiffness leading to a higher ultimate strain varying between 0.004 and 0.011.

However, mixes with rubber fail with less pronounced cracks, in more uniform manner, which is in accordance with previously analyzed strain-strain curves, i.e., post peak behavior. Namely, after reaching peak stress test specimens could withstand further increase of strain without sudden loss of force.

Stiffness is greater and curvature smaller for reference NC mixes, with a reverse proportional tendency with increase of rubber content. These differences can be seen in the previous figures, where four characteristic curves are presented, one for normal and the others for rubberized concrete. The post-peak behavior presents other differences. For reference mixes, the softening branch has a high reduction of stiffness, when compared with rubberized concrete. With increased rubber content this post peak behavior has an increase in the softening stiffness leading to a higher ultimate strain.

## 4.5. Test number Five:

### 4.5.1. Materials:

The rubber particles used in the rubberised concrete mixes were obtained from two sources. Rubber aggregates with dimensions up to 10 mm, produced from car tyre recycling. They were supplied in the following size ranges: 0–0.5 mm, 0.5–0.8 mm, 1.0–2.5 mm, 2–4 mm and 4–10 mm, and were used in the concrete mix in the 5%, 5%, 15%, 20% and 10% ratio of the total added rubber content, respectively, with remaining 45% being comprised of particles with sizes in the range 10–20 mm.

The larger rubber particles were produced from truck or bus tyre recycling, with typically higher density than car tyre particles. This portion was identified following a study of the workability of rubberized concrete within a wider European research project. These proportions resulted from a detailed study on 40 mixes carried out by Raffoul et al. in which the best balance between workability and strength loss was sought. All rubber particles are reported to have 25% content of carbon black, polymers in the range of 40–55%, whereas the remaining constituents are softeners and fillers. The specific gravity of rubber was 1.1, whereas the water absorption 7.1% for 4–10 mm particles and 1.05 for 10–20 mm particles.

Sand and gravel aggregates, from naturally occurring rock deposits consisting of combinations of various minerals, were used for the concrete mix. The fine aggregates with sizes up to 5 mm had a specific gravity of 2.65 and a moisture content of 5%, whereas the coarse aggregate (5–10 mm) had a specific gravity of 2.65 and a moisture content of 3%. The particle size distribution of mineral aggregates and rubber particles was determined following EN 933-1:2012. In the trial mixes, CEM I 52.5N and CEM II 32.5N were used to assess their influence on the compressive concrete strength at 7 and 28 days. However, in the tests used for the assessment of the constitutive behaviour, the higher strength cement was used.

### 4.5.2. Mix design and testing arrangement :

A reference normal concrete mix with target compressive strength of 60 MPa, typically used in bridge piers as provided by an industrial partner of the project based on practical experience, was prepared the following mix ratios. This included also the amount of admixtures that they use in practice. The normal concrete (NC) reference mix had 425 kg/m<sup>3</sup> of cement, 820 kg/m<sup>3</sup> of sand, 1001 kg/m<sup>3</sup> of gravel, 149 L of tap water, with 2.5 L/m<sup>3</sup> of plasticiser and 5.1 L/m<sup>3</sup> of super-plasticiser. In

the rubberized concrete mixes, 20% of the cement was replaced in equal quantities with EN 450-1 fineness category S fly ash and Grade 940 silica fume . They were primarily added to improve workability, segregation and slump, and to optimize the particle packing of the mixture. Rubberized concrete mixes with 20%, 40% and 60% rubber replacement by volume of mineral aggregates were produced to assess the full constitutive characteristics of rubberized concrete.

The rubber quantities used in the mixes were 110 kg/m<sup>3</sup>, 220 kg/m<sup>3</sup> and 330 kg/m<sup>3</sup>, respectively.

The rationale behind the mix design reported in this paper and used throughout the above-mentioned European research project was to develop an environmentally friendly concrete, primarily provided with high deformability capacities even for significant strength losses which are recovered by external confinement. This was achieved with replacement ratios of 60% of both fine and coarse aggregates using the rubber particle sizes reported in this paper and 2–4 layers of AFRP jacket confinement for applications in bridge piers and/or base isolation systems.

In this investigation, preliminary tests were carried out at 7 days, yet the fundamental observations from tests are made at 28 days from compression tests on 100 mm \_ 200 mm cylinders.

The cylindrical specimens, used in the pilot tests and for assessing the full constitutive behaviour, were tested in a stiff four-post Instron Satec 3500 kN machine. These tests were carried out in displacement control with a compressive displacement rate of 0.1 mm/min .

### 4.5.3. Results and discussion:

In order to investigate the mechanical properties of tire–rubber concrete, specimens of a cylindrical shape 10 cm in diameter \_ 20 cm in height were fabricated. These specimens were different in the content and type of tire particles as a portion of total aggregates in concrete as as demonstrated in Table 19.

one normal concrete mix and three RC mixes were used. The three RC mixes were designated as RC20, RC40 and RC60, which represents rubber content of 20%, 40% and 60% (replacement of mineral aggregate at volume percentages).

To unify the rubber content, a designated percentage for each mix type was converted to a total aggregate volume percentage.

This control mix was used as the basis for preparing a rubberized concrete mixes with 20%, 40% and 60% rubber replacement by volume of mineral aggregates were produced to assess the full constitutive characteristics of rubberized concrete.

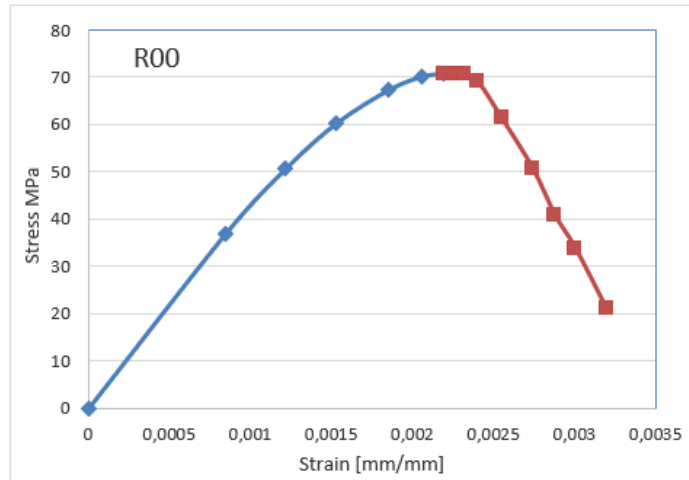
Test	Specimen	Cylinder sample		Rubber content(%)by total aggregate
		H[cm]	D[cm]	
#1	RC0	20	10	0
#2	RC20	20	10	20
#3	RC40	20	10	40
#4	RC60	20	10	60

*Table 19:Experimental program*

The experimental results of the compressive stress–strain response of each specimen are summarized in the figure a and b as follow:

R00	
$\epsilon$ [mm/mm]	$\sigma$ [Mpa]
0	0
0,000845	36,8343
0,001219	50,7058
0,001532	60,2536
0,001855	67,2615
0,002056	70,0143
0,002189	70,6728
0,002256	70,7452
0,002318	70,5745
0,002402	69,1086
0,002551	61,3461
0,002741	50,7298
0,002877	40,9118
0,003004	33,8827
0,003195	21,1453

(a)

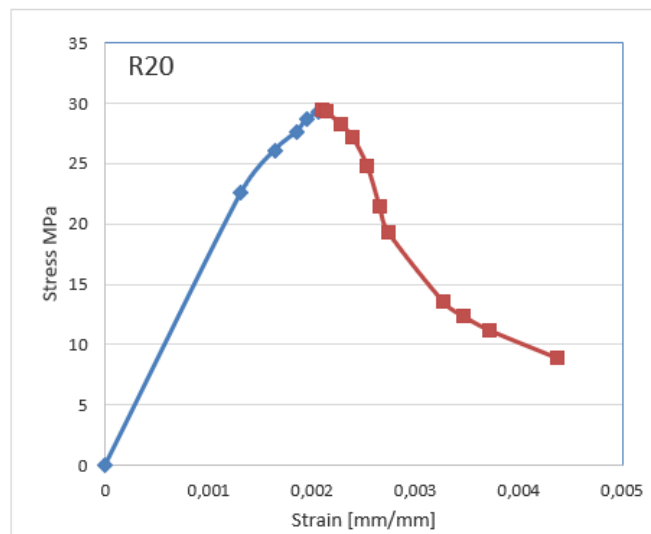


(b)

Figure 43: compressive stress–strain response of normal concrete ,(a) coordinates of  $\epsilon$ - $\sigma$  Post-Peak,(b) diagram of compressive  $\epsilon$ - $\sigma$

R20	
$\epsilon$ [mm/mm]	$\sigma$ [Mpa]
0	0
0,001312	22,5485
0,001637	26,0595
0,001851	27,6138
0,001945	28,6202
0,002067	29,2720
0,002104	29,3336
0,00214	29,2617
0,002282	28,1578
0,002391	27,1720
0,002537	24,6987
0,002654	21,4115
0,002744	19,2045
0,003272	13,5102
0,003465	12,3396
0,003726	11,1421
0,004379	8,8477

(a)

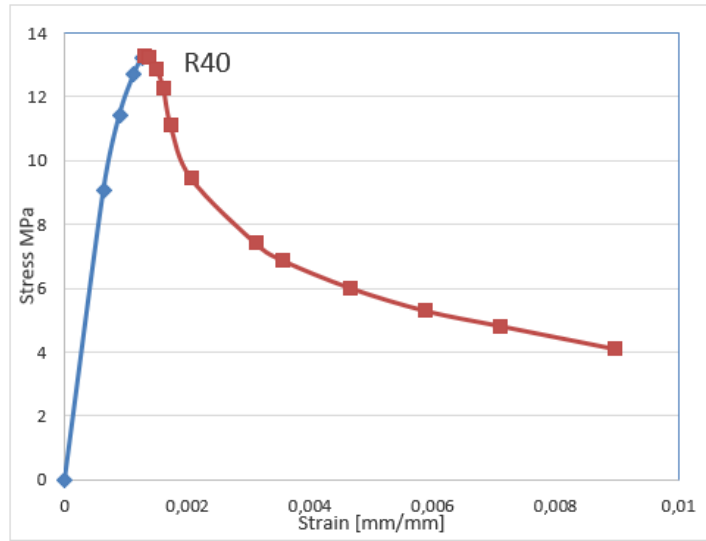


(b)

Figure 44: compressive stress–strain response of concrete with R-20% ,(a) coordinates of  $\epsilon$ - $\sigma$  Post-Peak,(b) diagram of compressive  $\epsilon$ - $\sigma$

R40	
$\epsilon$ [mm/mm]	$\sigma$ [Mpa]
0	0
0,000635	9,0789
0,000893	11,4177
0,001129	12,7041
0,001261	13,2175
0,001321	13,2509
0,001383	13,2143
0,001511	12,8180
0,001615	12,2485
0,001734	11,0824
0,002066	9,4345
0,003124	7,3863
0,003555	6,8636
0,004666	5,9918
0,005889	5,2812
0,00712	4,7994
0,008967	4,0898

(a)

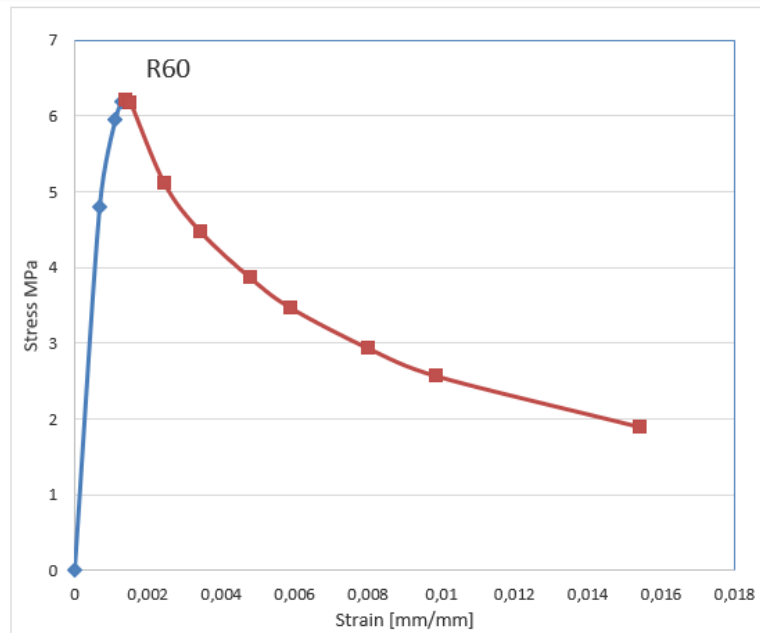


(b)

Figure 45: compressive stress–strain response of concrete with R-40% ,(a) coordinates of  $\epsilon$ - $\sigma$  Post-Peak,(b) diagram of compressive  $\epsilon$ -  $\sigma$

R60	
$\epsilon$ [mm/mm]	$\sigma$ [Mpa]
0	0
0,000674	4,8001
0,001096	5,9532
0,001262	6,1808
0,001381	6,2102
0,001505	6,1770
0,002437	5,1062
0,003424	4,4686
0,004782	3,8621
0,005889	3,4649
0,008026	2,9270
0,009858	2,5684
0,015404	1,8972

(a)



(b)

Figure 46: compressive stress–strain response of concrete with R-60% ,(a) coordinates of  $\epsilon$ - $\sigma$  Post-Peak,(b) diagram of compressive  $\epsilon$ -  $\sigma$

Material characterisation tests on rubberised concrete and normal concrete cylinders were carried out to assess the influence of rubber content on the constitutive behaviour. The investigated rubber replacement ratios were 20%, 40% and 60% of the total aggregate volume, as described previously in this section.

The previous figures depict the average lateral stress-strain recorded test curves. The stress-strain curves include both pre-peak and post-peak behaviour as recorded in the tests. The post-peak response is plotted down to 30% of the compressive strength  $f_{cr}$ .

Beyond this value, an approximate response band is plotted with reference to the negative stiffness of the descending branch.

The comparative assessment of  $\sigma - \varepsilon$  curves from the previous figures shows clear reductions in strength and stiffness with the increase of rubber content. The strength is approximately halved with each 20% increment increase of aggregate replacement. The compressive strength of concrete  $f_{cr}$  with  $\rho_{vr} = 0.6$  (R60) is about 10% of the normal concrete R00.

the post-peak axial compression behaviour exhibits increased softening with the decrease in strength. Tests showed softer post-crushing behaviour which typically leads to similar or higher energy dissipation in the post-peak regime.

Tire-rubber concretes are able to withstand loads beyond the peak load, which is referred to as post-failure strength.

With increased rubber content this post peak behavior has an increase in the softening stiffness leading to a higher ultimate strain varying between 0.004 and 0.015.

## 5. Characterization of post-peak branch :

### 5.1. The normalized stress and the inelastic displacement diagram:

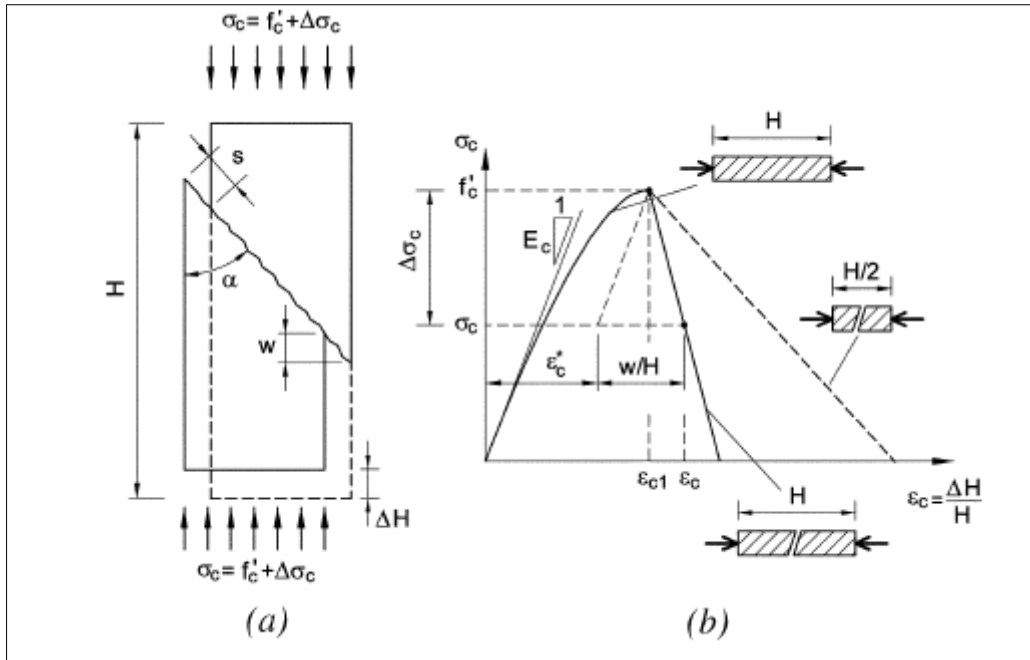


Figure 47: The stress-strain relationships of cement-based materials in compression

In the post-peak phase, the formation of an inclined cracked band is evidenced, which subdivides the cylindrical specimen into two progressively sliding blocks (Figure 47(a)).

The stress-strain relationships of cement-based materials in compression can be divided into two parts (Figure 47(b)). In the first part, when the stress is lower than the strength

$f'_c$  (and  $\epsilon_c < \epsilon_{c1}$ ), the specimen can be considered undamaged, while in the second part when the stress is also lower than the strength  $f'_c$  (and  $\epsilon_c > \epsilon_{c1}$ ), the specimen starts to have inelastic displacement  $w$  and consequent sliding  $s$  of the blocks along the sliding surface.

In the case of plain concrete (concrete containing no steel reinforcing bars or wire or containing not more than two tenths of one percent of reinforcing), the ascending branch of  $\sigma_c - \epsilon_c$  can be defined by the Sargin's relationship proposed by the CEB-FIP Model Code.

As soon as the peak stress is reached, localized damage develops and strain softening begins. In this stage, the progressive sliding of two blocks of cement-based material is evident.

the angle between the vertical axe of the specimen and the sliding surfaces is assumed to be  $\alpha = 18$  degrees, according to the experimental observations of Fujita et al. In the case of compressed concrete, a similar value of  $\alpha$  is obtained through the Mohr- Coulomb failure criterion, if the tensile strength is assumed to be 1/10 of that in compression ( $f_{ct} = 0.1f'_c$ ). For this reason, the value of  $\alpha$  only depends on the strength of materials and, therefore, can change only in the presence of efficient confinement (that is, the presence of stirrups in reinforced concrete beams). As shown by Fantilli et al. however, ordinary values of confinement do not significantly change the value of  $\alpha$ .

The inelastic displacement  $w$  of the specimen and the consequent sliding  $s$  of the blocks along the sliding surface rule the average post-peak compressive strain  $\varepsilon_c$  of the specimen (Figure 47). Referring to the specimen depicted in Fig. 46(a), post peak strains can be defined by the following equation (1) :

$$\varepsilon_c = \varepsilon_c^* + \frac{w}{H} = \varepsilon_{c1} - \frac{\Delta\sigma_c}{E_c} + \frac{w}{H} \quad (1)$$

Where  $\varepsilon_{c1}$  is the strain at compressive strength  $f'_c$ ,  $\Delta\sigma_c$  is the stress decrement after the peak, and  $H$  is the height of the specimen.

In all the stress-strain relationships seen before in the compression tests, as soon as the peak stress is reached, localized damage develops and strain softening begins.

During softening, the sliding of the blocks along the sliding surface, and the consequent inelastic displacement  $w$  of the specimen, are the parameters governing the average post-peak compressive strain  $\varepsilon_c$  of the specimen.

the inelastic displacement can be defined by the following equation:

$$w = H(\varepsilon_c - \varepsilon_c^*) = H\left(\varepsilon_c - \varepsilon_{c1} - \frac{f'_c - \sigma_c}{E_c}\right) \quad (2)$$

In this way, a new material property, defined by the non-dimensional function  $\sigma/f_c - w$ , can be introduced to reproduce univocally the post-peak stage of a generic cement-based material in compression.

## 5.2. The area A(f):

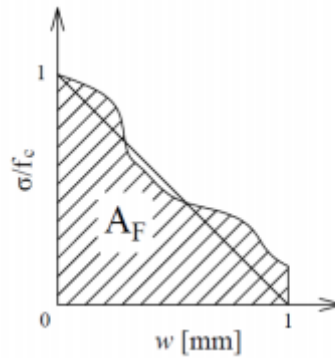


Figure 48: Post-peak response in terms of relative stress vs. inelastic shortening  $w$

Post-peak stage of the concrete mixtures is described before and they will be reported in the next figures by the  $\sigma/f_c$ - $w$  curves, while the area  $A_F$  under the curves (i.e., the ductility in compression) will be described in the following:

All the curves are limited to  $w = 1$  mm and the corresponding values of  $A_F$ , computed in the range  $w \sim 0$ -1 mm are reported, then the area's differences  $\Delta A$  of each specimen have been computed.

In order to study the ductility in compression of the rubberized concrete I need to find the area  $A_F$  under the  $F(w)$  curve in the inelastic displacement range ( $0 \leq w \leq 1$ ) as shown in the Figure 48:

$$A_F = \int_0^1 F(w) dw \quad (3)$$

Using the equation (3) Suppose that:

- $A_{NC} = \int_0^{W_{max}} F(w) dw$ : is the area of the normal concrete specimen under the  $F(w)$  curve.

- $A_R = \int_0^{W_{max}} F(w) dw$ : is the area of the rubberized concrete specimens under the  $F(w)$  curve.

- $\Delta A = A_R - A_{NC}$ : is the area difference of the normal and rubberized concrete specimens under the  $F(w)$  curve.

And finally I used the area difference  $\Delta A$  in order to study the ductility behavior in the post-peak stage.

### 5.3. The experimental results:

It is difficult to avoid the occurrence of cracks in concrete members. If the cracks appear, water and corrosive substances can enter into the interior of the concrete through the cracks. This can lead to leakage of concrete structure, so it is of great significance to carry out the study of concrete cracks.

To do so I used the equations (2) and (3) in order to study the post-peak stage of the concrete mixtures by plotting the  $\sigma/f_c$ - $w$  curves and the area AF under the curves (i.e., the ductility in compression).

#### 5.3.1. Test number One:

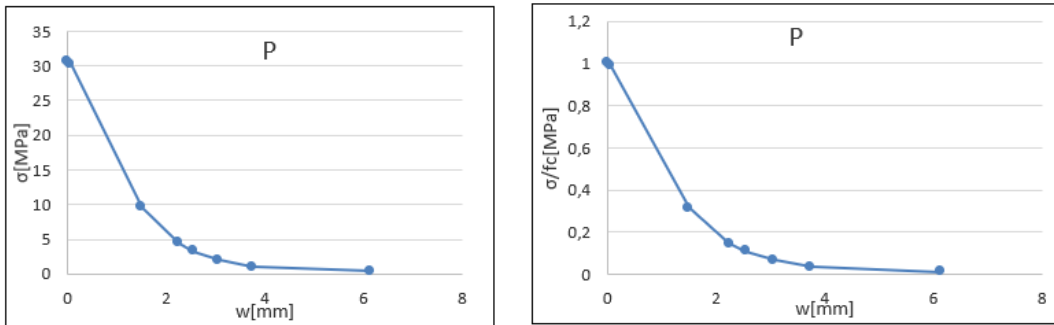


Figure 49:  $\sigma$ - $w$  diagram for normal concrete specimen P (at right),  $F(w)$ - $w$  diagram for normal concrete specimen P (at left)

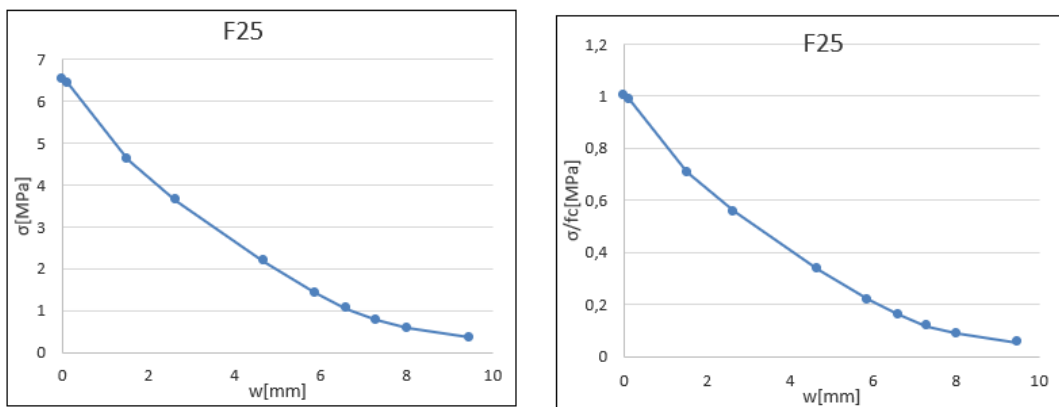


Figure 50:  $\sigma$ - $w$  diagram of the specimen F25 (at right),  $F(w)$ - $w$  diagram of the specimen F25 (at left)

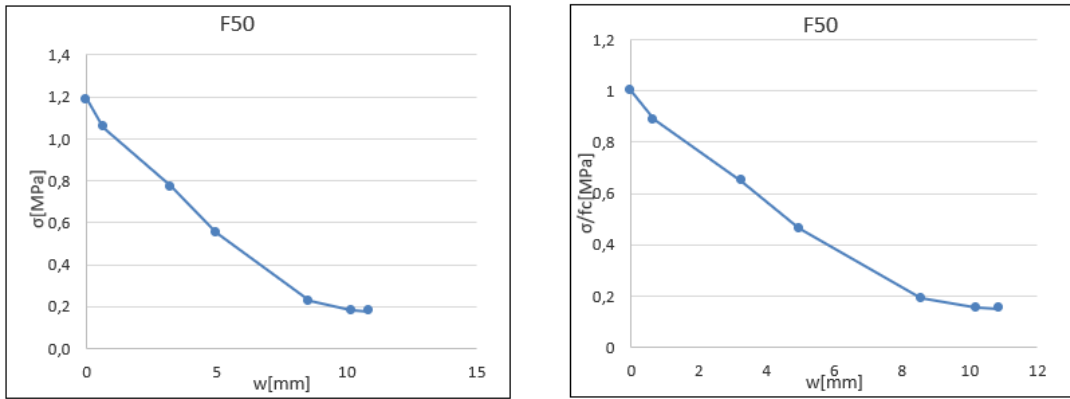


Figure 51:  $\sigma$ -w diagram of the specimen F50(at righth ),  $F(w)$ -w diagram of the specimen F50(at left )

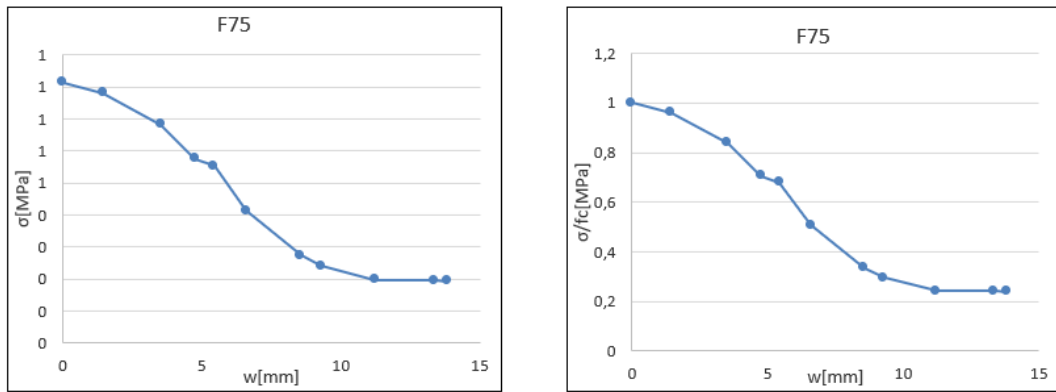


Figure 52:  $\sigma$ -w diagram of the specimen F75 (at righth ),  $F(w)$ -w diagram of the specimen F75 (at left )

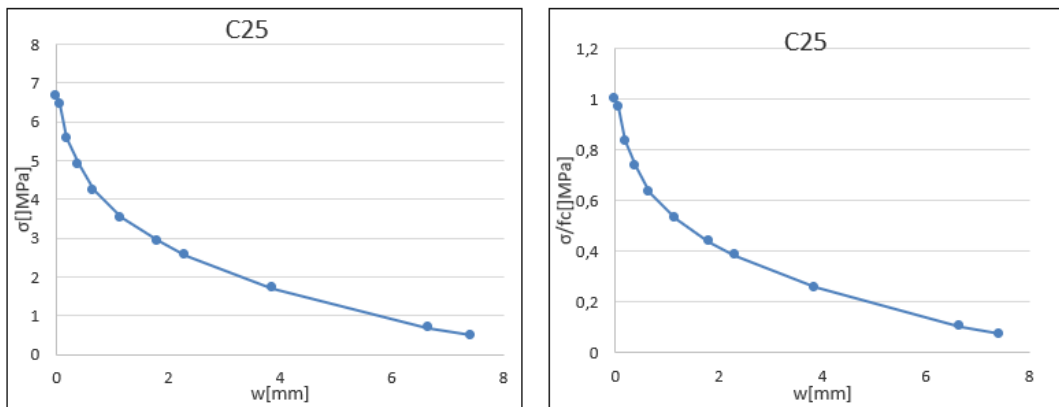


Figure 53:  $\sigma$ -w diagram of the specimen C25 (at righth ),  $F(w)$ -w diagram of the specimen C25(at left )

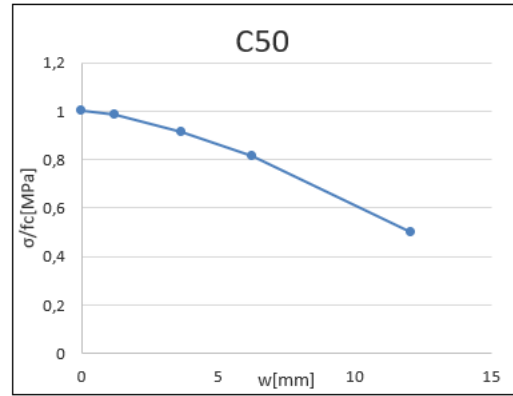
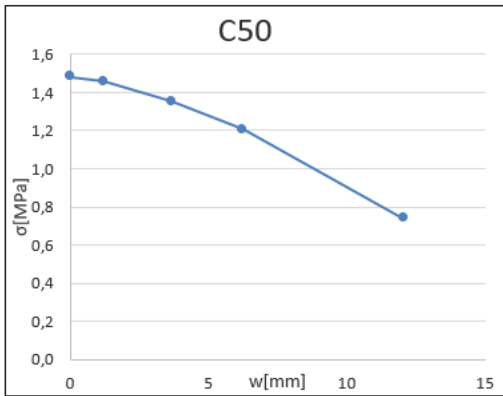


Figure 54:  $\sigma$ -w diagram of the specimen C50 (at right),  $F(w)$ -w diagram of the specimen C50 (at left)

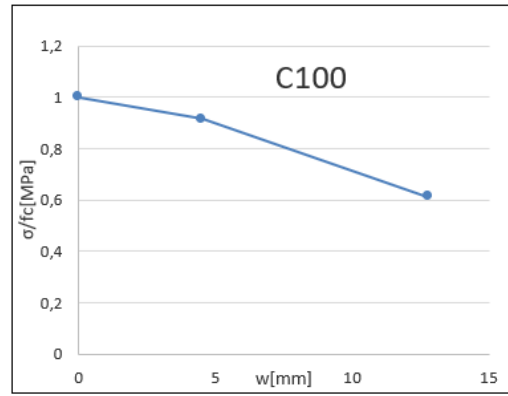
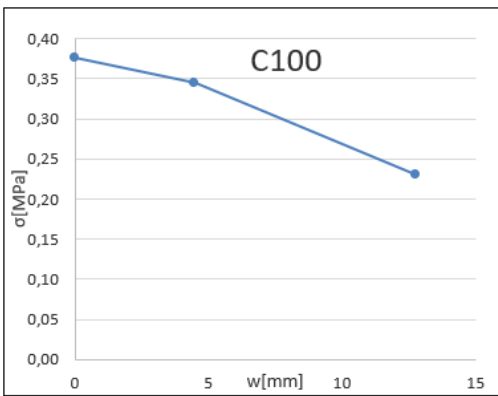


Figure 55:  $\sigma$ -w diagram of the specimen C100 (at right),  $F(w)$ -w diagram of the specimen C100 (at left)

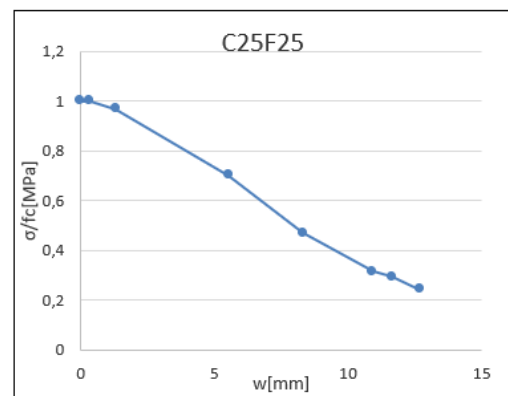
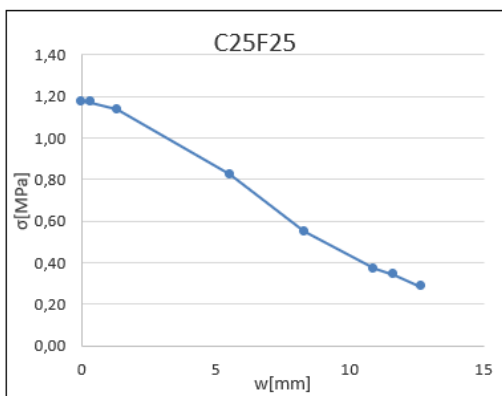


Figure 56:  $\sigma$ -w diagram of the specimen C25F25 (at right),  $F(w)$ -w diagram of the specimen C25F25 (at left)

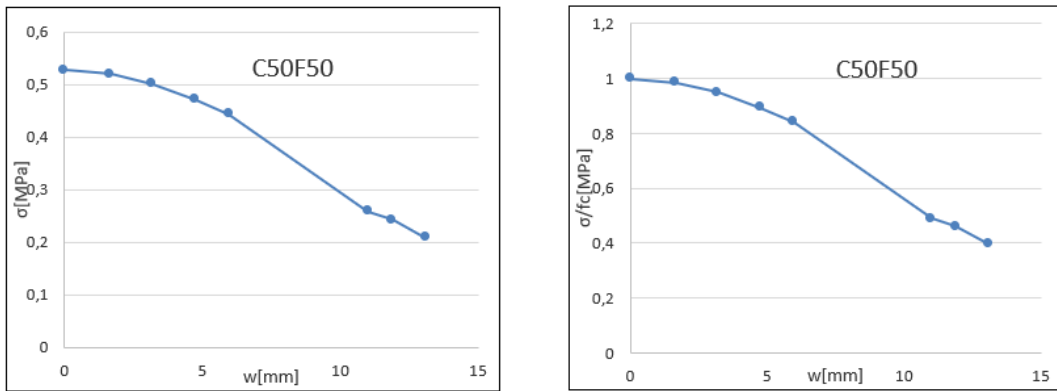


Figure 57:  $\sigma$ - $w$  diagram of specimen C50F50(at right ),  $F(w)$ - $w$  diagram of the specimen C50F50(at left )

In the observed range ( $0 \leq w \leq 1$ ) I plot the :

$$-\Delta A = A_R - A_{NC} = \int_0^1 F_R(w)dw - \int_0^1 F_{NC}(w)dw$$

All the curves are limited to  $w = 1$  mm and the corresponding values of AF, computed in the range  $w \sim 0-1$  mm for each specimen and then it is calculated the area difference of the rubberized concrete with respect to the normal concrete specimen.

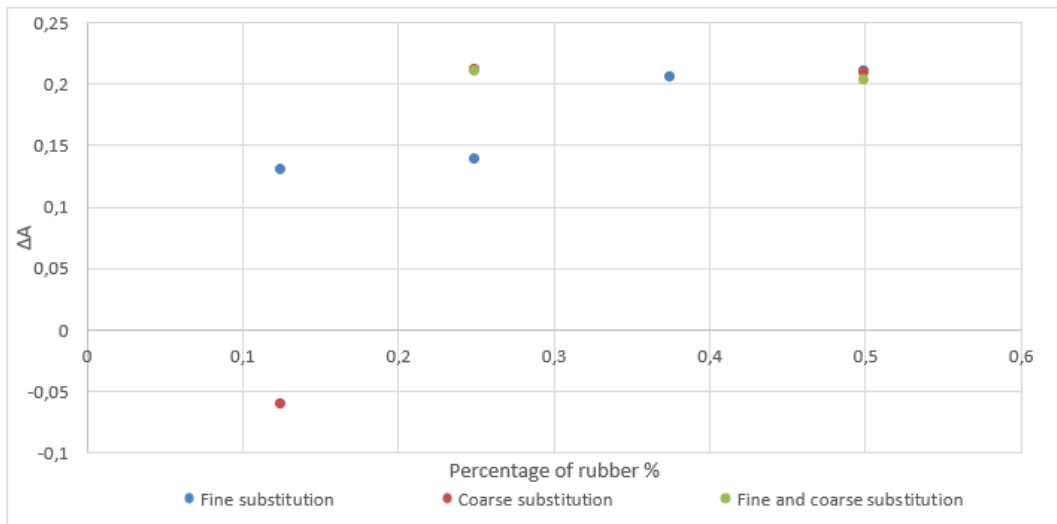


Figure 58: The area difference under  $F(w)$

Here from the  $F(w)$ - $w$  curves In all the tests the relative stress  $F(W)$  decreases with  $w$ , and as the percentage of the crumb or chips rubber increases, even if the strength of concrete cylinders decreases, the inelastic displacement increases due to energy absorption of rubber particles, curves clearly shows that after the failure also cylinders will take load.

The inelastic displacement of the Portland cement concrete (the specimen P) is limited to  $w_{max} = 6$  mm in correspondence of which the normalized stresses in the post-peak branch is nearly zero.

In the F specimens where the sand in the control mix was replaced by crumb rubber the maximum inelastic displacement is between 9[mm] and 14[mm] , while In the C mixes, where the coarse aggregates of the control mix were replaced by rubber chips, the maximum inelastic displacement is between 8[mm] and 13[mm].

For the C25F25 mix, where crumb rubber replaced 25% of the sand volume and tire chips replaced 25% of the coarse aggregate volume , and a C50F50 mix, where crumb rubber replaced 50% of the sand volume and tire chips replaced 50% of the coarse aggregate volume, the maximum inelastic displacement is more or less 13[mm].

Rubberized concrete mixtures with 50% and 100% where the coarse aggregates of the control mix were replaced by rubber chips show a higher increasing in ductility compared to normal concrete and the other rubberized concrete specimens .

The increase in plastic deformation is observed in stress-strain curves as the percentage of rubber aggregates increases in concrete ,and this increase became even greater as the rubber size increased.

Noting also that the slope is greater in the normal concrete graph with respect to the other graphs and this leads to decreasing in the ductility ,even if its mechanical strength is higher.

The slope of the softening is becoming lower as the percentage of the crumb rubber increases and this leads to a remarkable increase in ductility .

the results of the parametric study indicate that the ductility ratio is significantly affected the percentage of the rubber substitution ,but slightly influenced by the type of the rubber .

As  $F(w)$  is a relative stress normalized with respect to the compressive strength  $f_c'$  , a comparison between all the cement-based composites, under compression test , is possible in terms of  $\Delta A$  in the range of  $(0 \leq w \leq 1)$  . Higher values of  $\Delta A$  are attained in concretes capable of maintaining high loads after failure (that is, in the case of ductile materials).

Obviously, Here as the percentage of the rubber increases , the  $\Delta A$  increases due to energy absorption of rubber particles and this leads to a remarkable increase in ductility.

### 5.3.2. Test number Two:

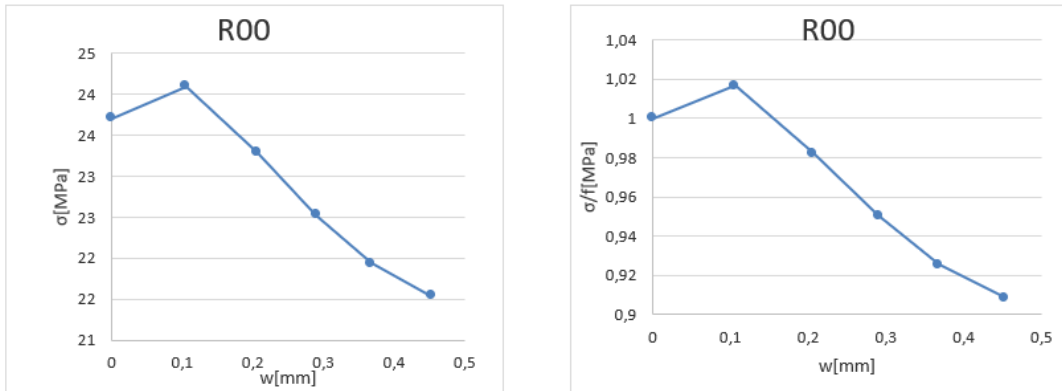


Figure 59:  $\sigma$ - $w$  diagram for normal concrete specimen R00 (at right),  $F(w)$ - $w$  diagram for normal concrete specimen R00 (at left)

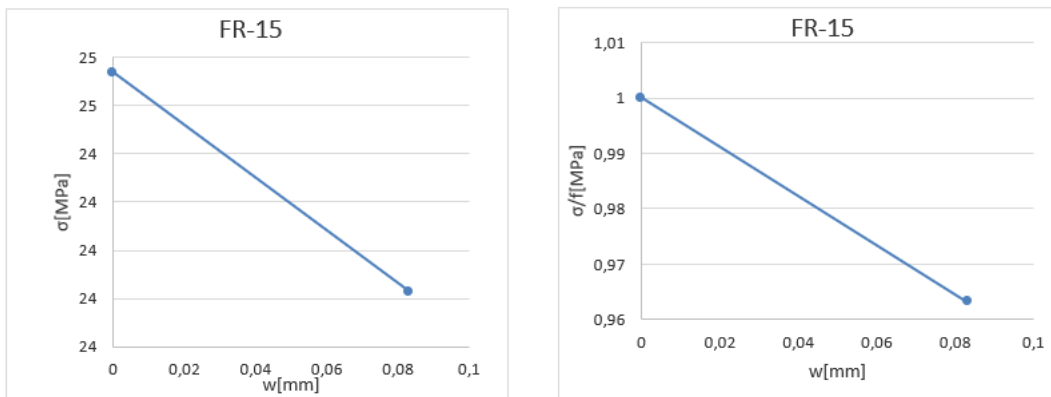


Figure 60:  $\sigma$ - $w$  diagram the specimen FR-15 (at right),  $F(w)$ - $w$  diagram for normal concrete specimen FR-15 (at left)

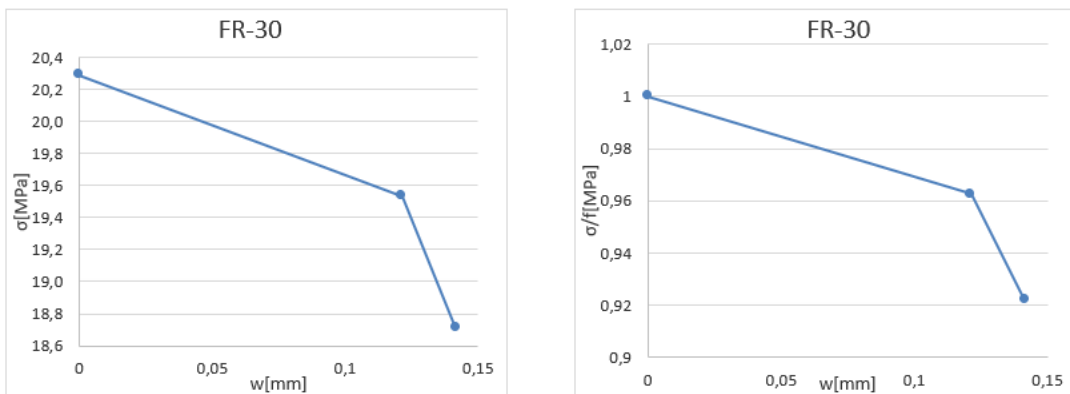


Figure 61:  $\sigma$ - $w$  diagram the specimen FR-30 (at right),  $F(w)$ - $w$  diagram for normal concrete specimen FR-30 (at left)

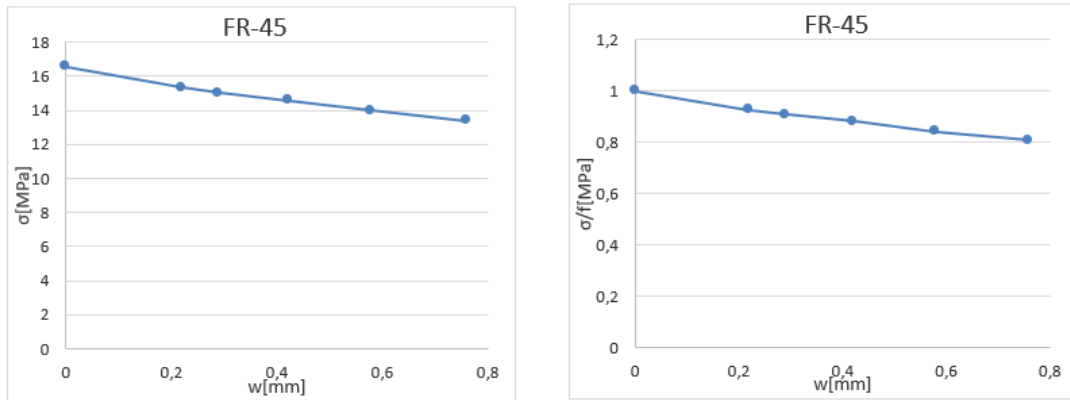


Figure 62:  $\sigma$ -w diagram THE specimen FR-45(at right),  $F(w)$ -w diagram for normal concrete specimen FR-45(at left)

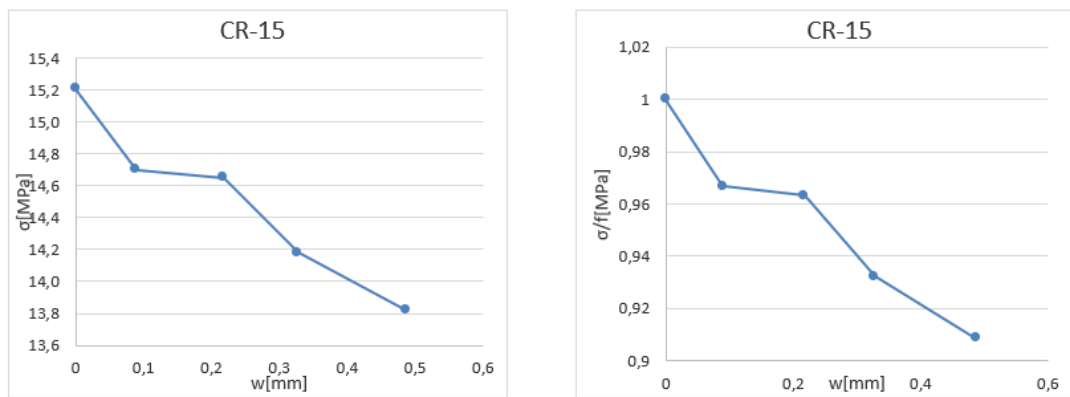


Figure 63:  $\sigma$ -w diagram THE specimen CR-15(at right),  $F(w)$ -w diagram for normal concrete specimen CR-15(at left)

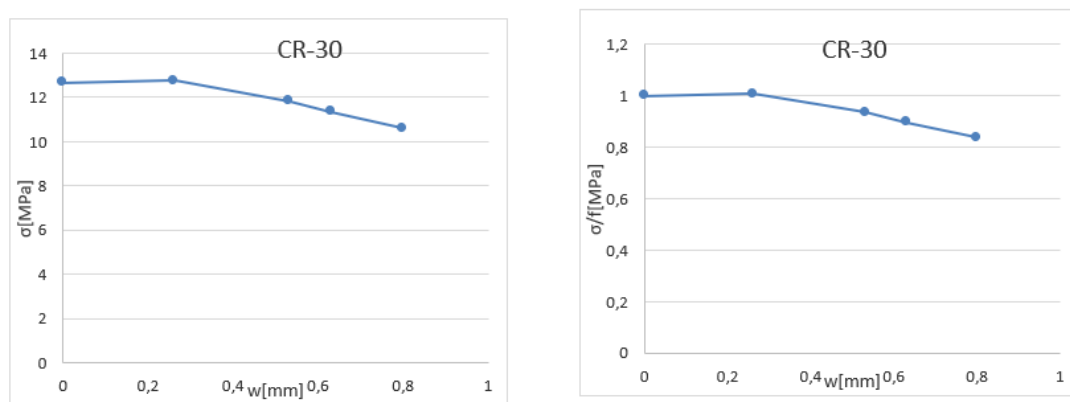


Figure 64:  $\sigma$ -w diagram THE specimen CR-30(at right),  $F(w)$ -w diagram for normal concrete specimen CR-30(at left)

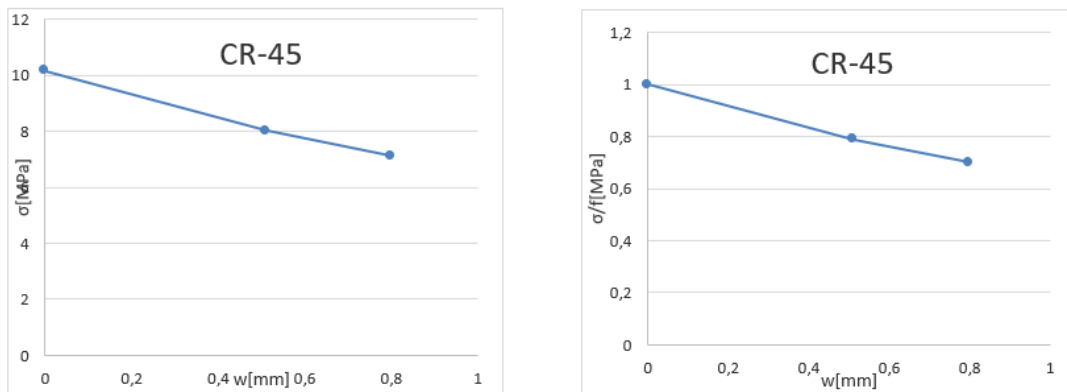


Figure 65:  $\sigma$ -w diagram for the specimen CR-45 (at right),  $F(w)$ -w diagram for the specimen CR-45 (at left)

In all the tests the relative stress  $F(w)$  decreases with  $w$ , the inelastic displacement of the Portland cement concrete (the specimen P) is limited to  $w_{max} = 0.45$  [mm] in correspondence of which the normalized stresses in the post-peak branch is nearly 0.9 [MPa].

in the FRC-15 and FRC-30 specimens where 15 and 30%, by volume, 0/1 mm rubber chips replacing the aggregate), the maximum inelastic displacement is between 0.08 [mm] and 0.14 [mm] while the FRC-45 specimen has an maximum inelastic displacement equal to 0.8 [mm] and their slopes of the softening is higher than the slope of the normal concrete.

While in the CRC-15, CRC-30, and CRC-45 (15, 30, and 45 %, by volume, 1/4 mm rubber chips replacing the aggregate) the maximum inelastic displacement is between 0.5 [mm] and 0.8 [mm].

Here as the percentage of the rubber chips increases, even if the strength of concrete cylinders decreases, the inelastic displacement increases due to energy absorption of rubber particles. Graph clearly shows that after the failure also cylinders will take load. Noting also that the slope is greater in the normal concrete graph with respect to the other graphs and this leads to decreasing in the ductility. The increase of the ductility is becoming remarkable when the 30%, by volume, 0/1 mm rubber chips replacing the aggregate.

The slope of the softening is becoming lower as the percentage of the crumb rubber increases and this leads to a remarkable increase in ductility.

NB: in all the previous curves there are no values in the observed range ( $0 \leq w \leq 1$ ), so it not possible to calculate the area AF under the curves (i.e., the ductility in compression).

### 5.3.3. Test number Three:

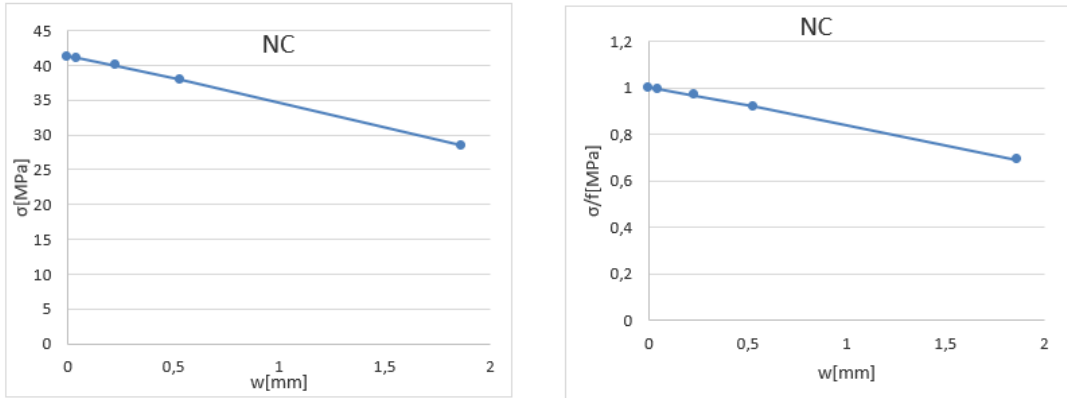


Figure 66:  $\sigma$ - $w$  diagram for the specimen NC (at right),  $F(w)$ - $w$  diagram for the specimen NC (at left)

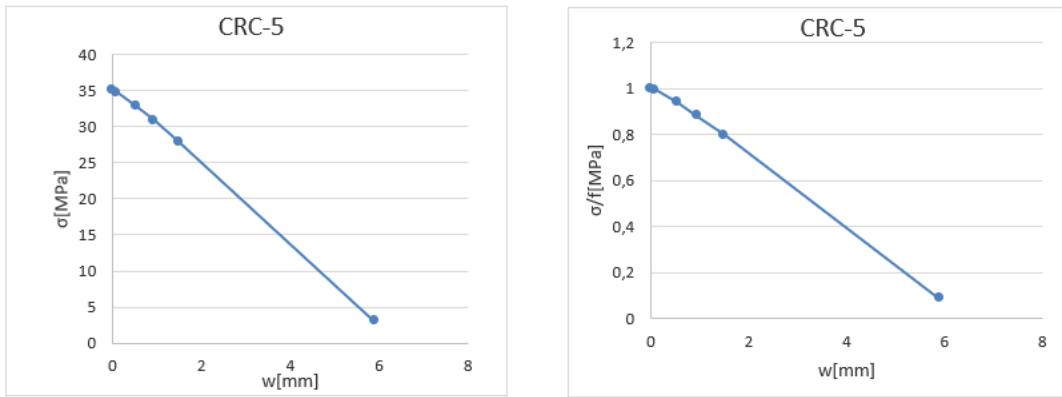


Figure 67:  $\sigma$ - $w$  diagram for the specimen CRC-5 (at right),  $F(w)$ - $w$  diagram for the specimen CRC-5 (at left)

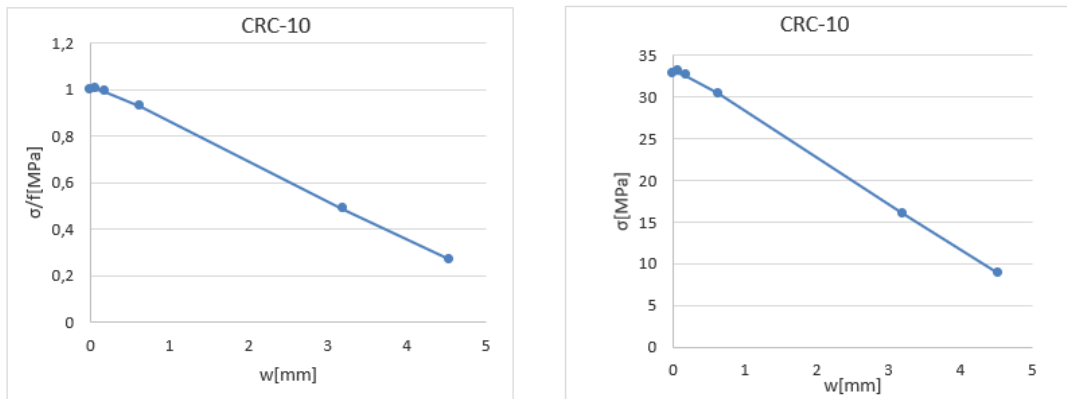


Figure 68:  $\sigma$ - $w$  diagram for the specimen CRC-10 (at right),  $F(w)$ - $w$  diagram for the specimen CRC-10 (at left)

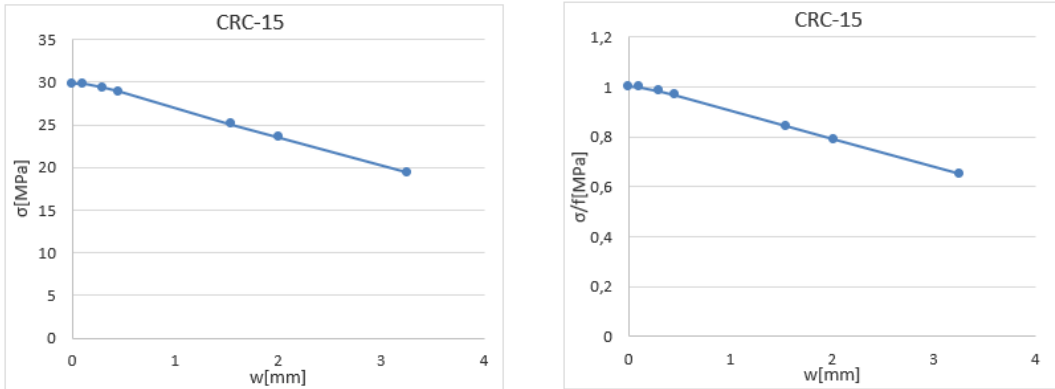


Figure 69:  $\sigma$ - $w$  diagram for the specimen CRC-15 (at right),  $F(w)$ - $w$  diagram for the specimen CRC-15 (at left)

In the observed range ( $0 \leq w \leq 1$ ) I plot the :

$$-\Delta A = A_R - A_{NC} = \int_0^1 F_R(w)dw - \int_0^1 F_{NC}(w)dw$$

All the curves are limited to  $w = 1$  mm and the corresponding values of AF, computed in the range  $w \sim 0-1$  mm for each specimen and then it is calculated the area difference of the rubberized concrete with respect to the normal concrete specimen.

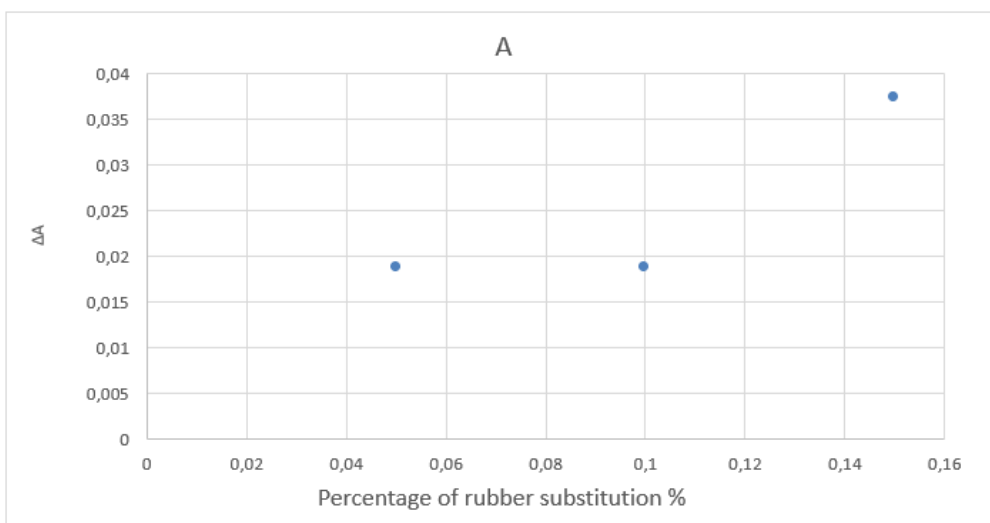


Figure 70: The area difference under  $F(w)$

In all the tests the relative stress  $F(W)$  decreases with  $w$ , the inelastic displacement of the Portland cement concrete (the specimen NC) is limited to  $w_{max} = 1.8$  [mm] in correspondence of which the normalized stresses in the post-peak branch is nearly 0.6 [MPa].

Noting also that the slope is greater in the normal concrete graph with respect to the other graphs and this leads to decreasing in the ductility, even if its mechanical strength is higher.

In the CRC-5, CRC-10, and CRC-15 (5, 10, and 15 %, by volume, crumb rubber replacing the fine aggregate (sand)) the maximum inelastic displacement is between 3 [mm] and 6 [mm].

Here as the percentage of the crumb rubber increases, even if the strength of concrete cylinders decreases, the inelastic displacement increases due to energy absorption of rubber particles. Graph clearly shows that after the failure also cylinders will take load.

The slope of the softening is becoming lower as the percentage of the crumb rubber increases and this leads to a remarkable increase in ductility.

Obviously, Here as the percentage of the rubber increases, the  $\Delta A$  increases due to energy absorption of rubber particles and this leads to a remarkable increase in ductility.

### 5.3.4. Test number Four :

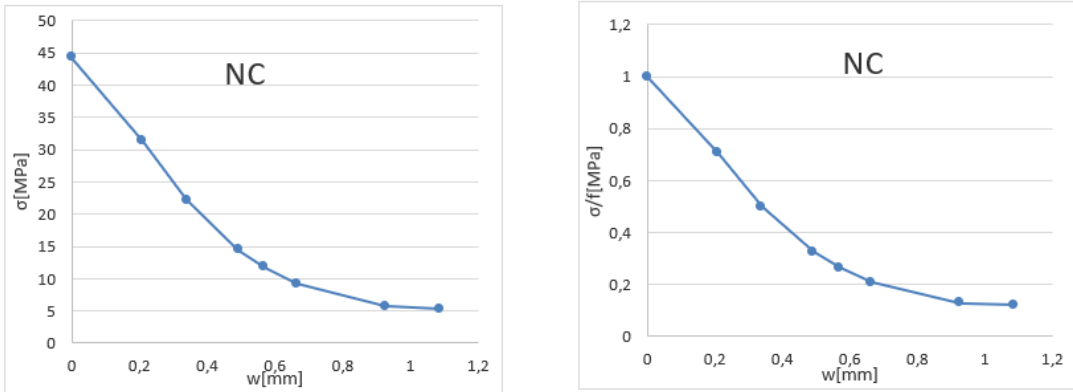


Figure 71:  $\sigma$ - $w$  diagram for the specimen NC (at right),  $F(w)$ - $w$  diagram for the specimen NC (at left)

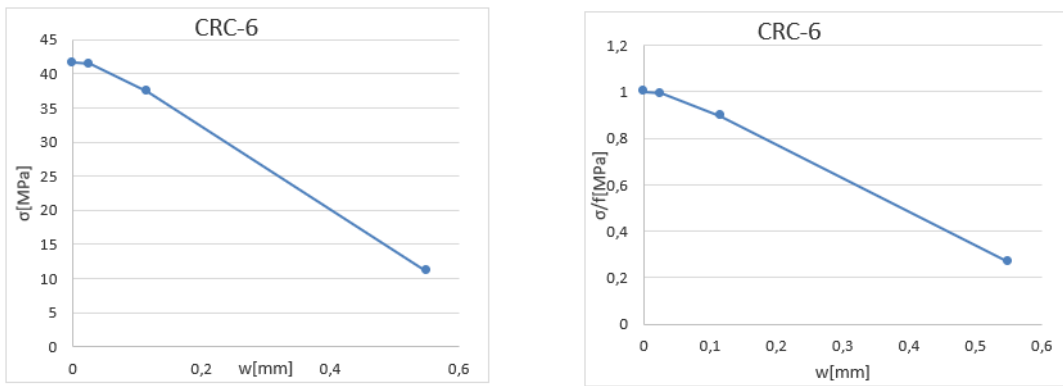


Figure 72:  $\sigma$ - $w$  diagram for the specimen CRC-6 (at right),  $F(w)$ - $w$  diagram for the specimen CRC-6 (at left)

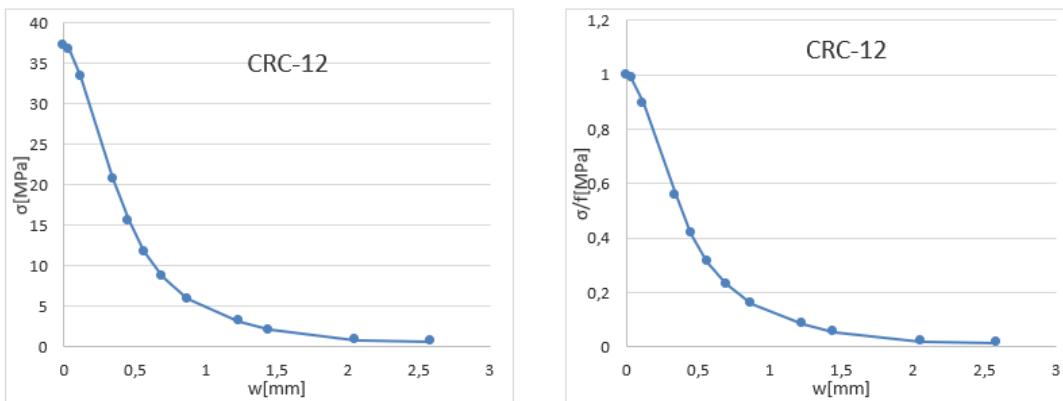


Figure 73:  $\sigma$ - $w$  diagram for the specimen CRC-12 (at right),  $F(w)$ - $w$  diagram for the specimen CRC-12 (at left)

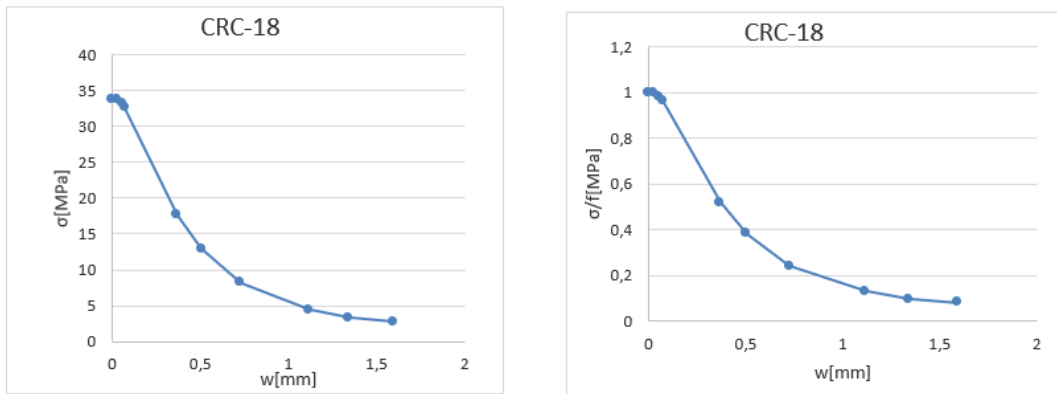


Figure 74:σ-w diagram for the specimen CRC-18 (at right), F(w)-w diagram for the specimen CRC-18 (at left)

In the observed range ( $0 \leq w \leq 1$ ) I plot the :

$$-\Delta A = A_R - A_{NC} = \int_0^1 F_R(w)dw - \int_0^1 F_{NC}(w)dw$$

All the curves are limited to  $w = 1$  mm and the corresponding values of AF, computed in the range  $w \sim 0-1$  mm for each specimen and then it is calculated the area difference of the rubberized concrete with respect to the normal concrete specimen.

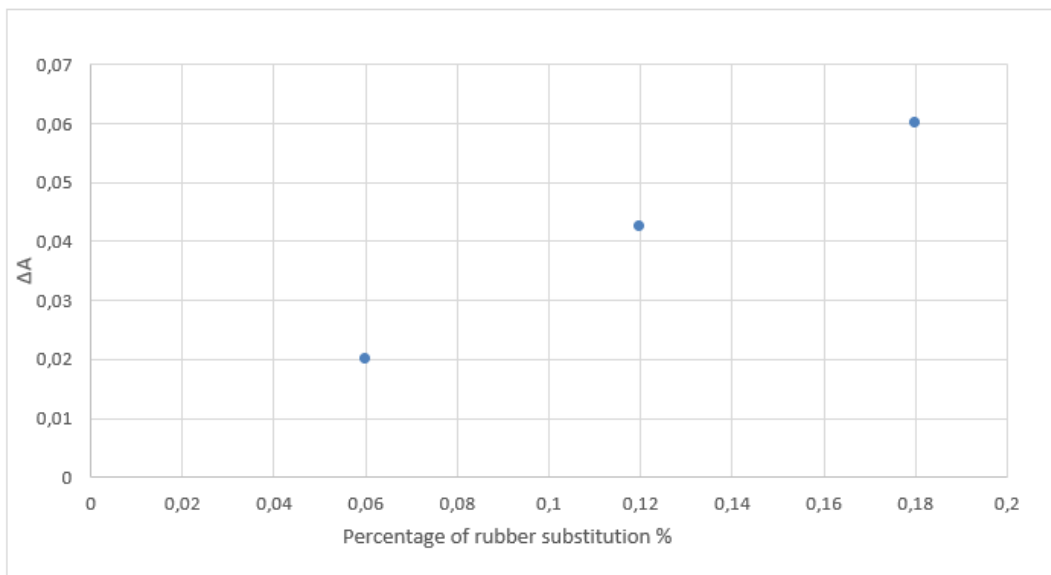


Figure 75:The area difference under F(w)

In all the tests the relative stress  $F(W)$  decreases with  $w$ , the inelastic displacement of the Portland cement concrete (the specimen NC) is limited to  $w_{max} = 1.08$  [mm] in correspondence of which the stress in the post-peak branch is nearly 5 [MPa].

in the CRC6, CRC12 and CRC18 specimens, which represents crumb rubber (nominal size of 1.18 mm and 2.36 mm mixed at a weight ratio of 1:1) content of 6%, 12% and 18% (replacement of sand at volume percentages). the maximum inelastic displacement is between 0.5 [mm] and 2.5 [mm].

Here as the percentage of the rubber crumb rubber increases, even if the strength of concrete cylinders decreases, the inelastic displacement increases due to energy absorption of rubber particles. Graph clearly shows that after the failure also cylinders will take load.

Noting also that the slope is greater in the normal concrete graph with respect to the other graphs and this leads to decreasing in the ductility, even if its mechanical strength is higher.

So the slope of the softening is becoming lower as the percentage of the crumb rubber increases and this leads to a remarkable increase in ductility.

Also here the same thing can be noticed, as the percentage of the rubber increases, the  $\Delta A$  increases due to energy absorption of rubber particles and this leads to a remarkable increase in ductility.

### 5.3.5. Test number Five:

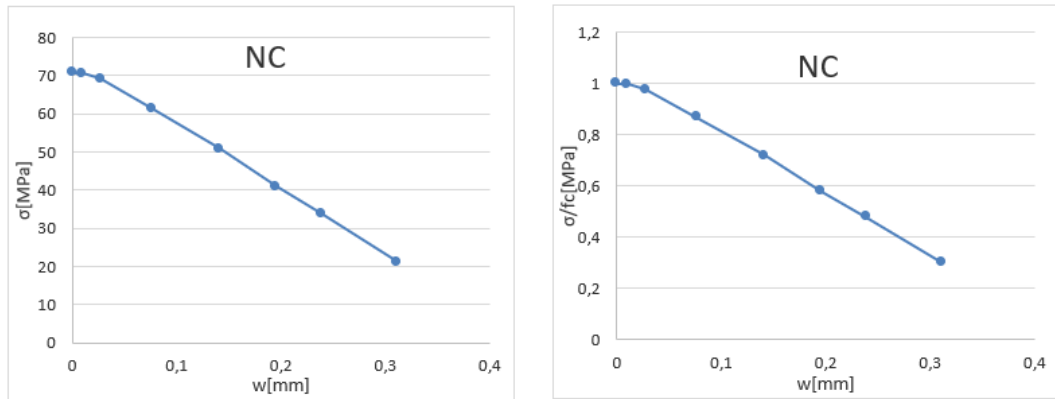


Figure 76:  $\sigma$ - $w$  diagram for the specimen NC (at right),  $F(w)$ - $w$  diagram for the specimen NC (at left)

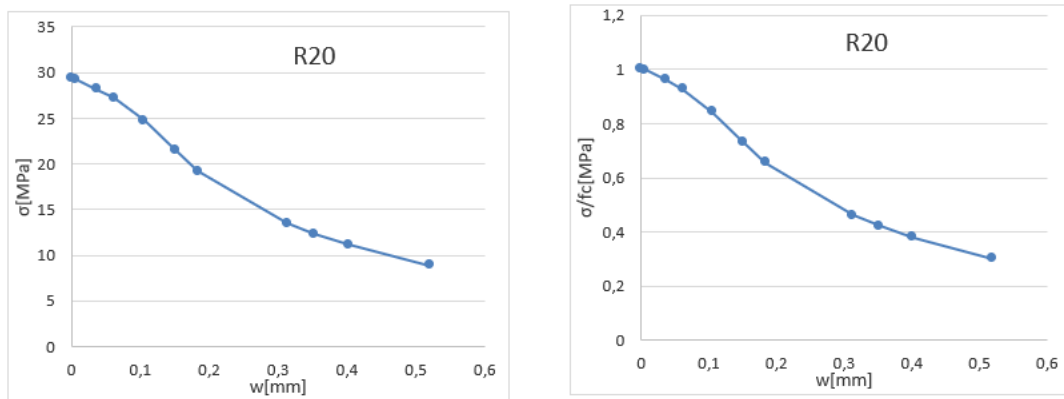


Figure 77:  $\sigma$ - $w$  diagram for the specimen R20 (at right),  $F(w)$ - $w$  diagram for the specimen R20 (at left)

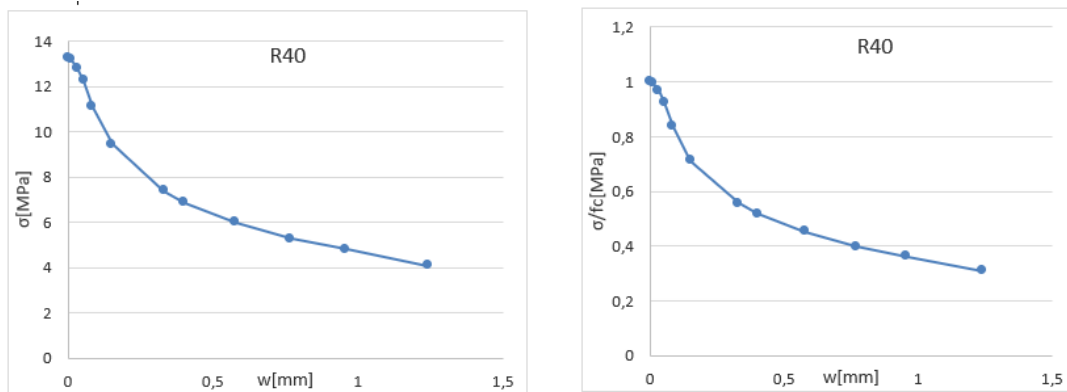


Figure 78:  $\sigma$ - $w$  diagram for the specimen R40 (at right),  $F(w)$ - $w$  diagram for the specimen R40 (at left)

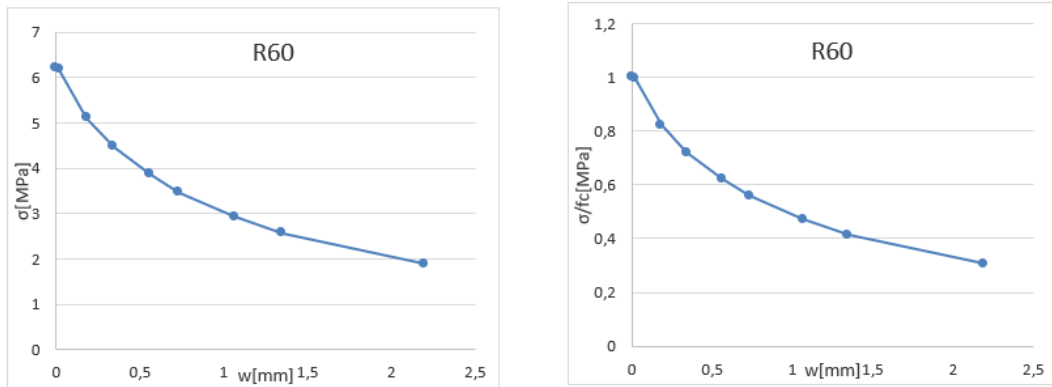


Figure 79:  $\sigma$ -w diagram for the specimen R60 (at right),  $F(w)$ -w diagram for the specimen R60 (at left)

In all the tests the relative stress  $F(W)$  decreases with  $w$ , the inelastic displacement of the Portland cement concrete (the specimen NC) is limited to  $w_{max} = 0.3$  [mm] in correspondence of which the stresses in the post-peak branch is nearly 21[MPa].

in the R-20, R-40 and R-60 specimens where mixes with 20%, 40% and 60% rubber particles with dimensions up to 10 mm replacing the aggregate, has an maximum inelastic displacement between 0.5[mm] and 2[mm].

Noting also that the slope is greater in the normal concrete graph with respect to the other graphs and this leads to decreasing in the ductility, even if its mechanical strength is higher.

Here as the percentage of the rubber particles increases, even if the strength of concrete cylinders decreases, the inelastic displacement increases due to energy absorption of rubber particles. Graph clearly shows that after the failure also cylinders will take load.

The slope of the softening is becoming lower as the percentage of the rubber particles increases and this leads to a remarkable increase in ductility.

NB: in all the previous curves there are no values in the observed range ( $0 \leq w \leq 1$ ), so it not possible to calculate the area AF under the curves (i.e., the ductility in compression).

Additionally, a detailed analysis of a database on average tests results from several rubberized concrete mixtures and their reference concrete mixes, including tests undertaken in their studies, was carried out. In this way, Several authors defined a series of prediction expressions to estimate the compressive strength and the area  $A(F)$  under the curves (i.e., the ductility in compression) of rubberized concrete materials as a function of its volumetric rubber ratio. In Figure 80 it is showed a comparison between compressive strength degradation curve and the increasing of the ductility in compression as a function of rubber ratio.

The strength reduction factor is defined as the ratio between the compressive strength of the rubbercrete with a certain percentage of rubber and the compressive strength of the concrete without rubber.

Considering in a single figure (Figure 80) all the SRF values corresponding to different percentages of replacement, a “fan shaped” point cloud is obtained. Regression analyses have been carried out to calculate the upper and the lower bound curves of this point cloud, which are in blue and green respectively. Also the ductility in compression which defined as the difference between the area under the curve  $F(w)$  of the rubbercrete with a certain percentage of rubber and the area under the curve  $F(w)$  of the concrete without rubber (is defined in red lines).

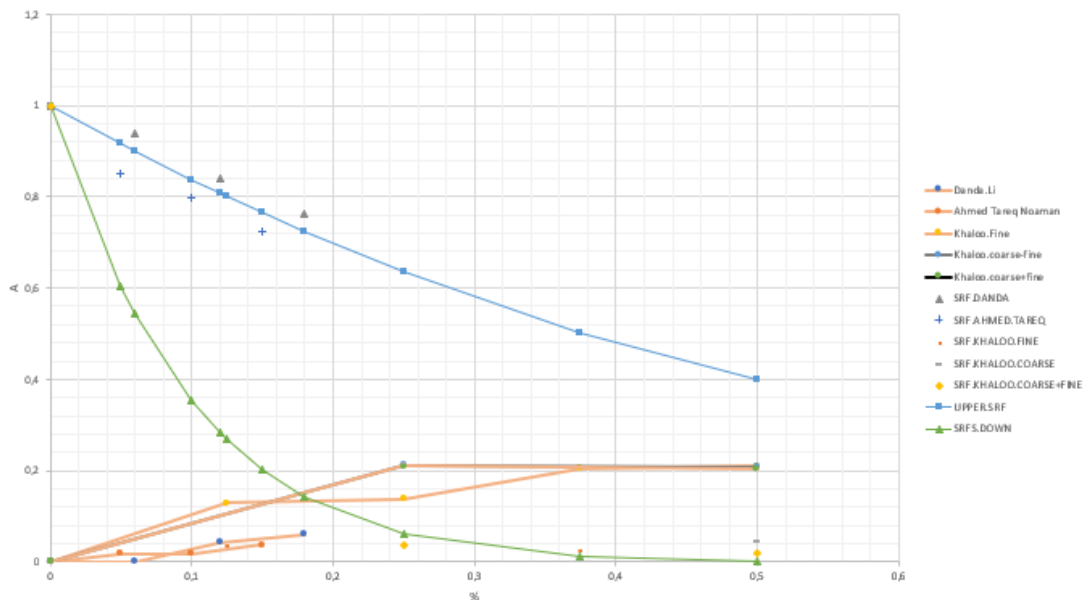


Figure 80: Whole dataset of the Strength reduction factor – SRF and the ductility in compression  $\Delta A$  vs. the content (by volume)

Test results indicate that while the  $\Delta A$  is increased, compressive strength is reduced when proportion of rubber aggregates is increased, and beyond the 30% of rubber the compressive strength and the  $\Delta A$  remain constant .

From compression strength tests it comes out that there are substantial differences occurred between stress-strain response of ordinary concrete and rubberized concrete. In fact, all the rubberized concrete mixtures exhibited a lower compressive strength and modulus of elasticity values with respect to the ordinary Portland control mixture.

Obviously, Here The results indicate that use of larger rubber chips reduces dynamic modulus, and specimens showed higher toughness and were less brittle since the energy generated is plastic. In addition, specimens showed a gradual failure of splitting and shearing and sudden, abrupt failure was not seen.

This study has exclusively focused on the mechanical and physical properties of tire-rubber concrete for fine, coarse, and combined rubber replacements of mineral aggregates, and it is reported that the substitution of mineral aggregates with tire-rubber particles in concrete results in large reductions in ultimate strength and the tangential modulus of elasticity. Due to the considerable decrease in ultimate strength, rubber concentrations exceeding 25% are not recommended. Pretreatment of tire particle surfaces should be considered for possible improvement of tire-rubber concrete mechanical properties.

More ductile behavior is observed for rubberized concrete compared to plain concrete specimens under compression testing. Unlike plain concrete, the failure state in rubberized concrete does not occur quickly and does not cause any detachment in the specimen's elements. Crack width in rubberized concrete is smaller than that of plain concrete, and the propagation of failure symptoms is more gradual and uniform. The failure state in tire-rubber concrete compared to plain concrete is characterized by more deformation.

## 6. Conclusion :

The experimental research presented in this work examined the mechanical properties and the behavior of concrete materials incorporating rubber particles, obtained from recycled tires, as a replacement for mineral aggregates. A complete overview on the main mechanical properties and behavior in both the pre and post peak stages have been purposed about many different concrete mixtures: an ordinary Portland control mixture, used as reference in results analysis, and other rubberized concrete mixtures obtained by replacing a certain aggregates volume with rubber. The mechanical properties that have been investigated was compressive strength, modulus of elasticity, and also the behavior of rubberized concrete in the post-peak stage has been investigated .

From compression tests it comes out that there are substantial differences occurred between stress-strain response of ordinary concrete and rubberized concrete. In fact, all the rubberized concrete mixtures exhibited a lower compressive strength and modulus of elasticity values with respect to the ordinary Portland control mixture.

This difference in results between stress-strain response of normal concrete and rubberized concrete is mainly due to the modality with which the substitution was made and to the reduced size of rubber particles used (from 0.15mm to a maximum of 30 mm). In fact, as described before, substitution was made between specific fractions of aggregate and rubber with the same dimension after a phase of accurate sieving of material. Regarding post-peak response, rubberized concrete mixtures exhibited a more ductile behavior than ordinary concrete. This is due to the fact that fracture propagation in concrete is slower by the presence of rubber particles .

from these studies , it can be observed that there is linear increase of stresses until it reaches its peak before energy is released by specimen's fracture. For this case, the specimens behaved like a brittle material of which the total energy generated upon fracture is elastic energy. However, nonlinear behavior is seen for the other specimens which containing a certain rubber percentage. Here, once the peak stress is reached, the specimen continues to yield, as represented by the branch-line. This behavior is similar to the behavior of the tough materials having most of its energy generated upon fracture as plastic energy ,Plastic energy is defined as the amount of energy required to produce a specified deformation after the elastic

range, which increased the ability of the material to support loads even after the formation of cracks. Therefore, it can be stated that concrete with a higher percentage of rubber possess high toughness, since the generated energy is mainly plastic.

From the case studies it can be concluded that the waste tyre rubber in the form of crumb and chipped rubber in replacement of coarse and fine aggregate is possible in the concrete but it is still not recommended for structural uses because of the low compressive strength comparing with the normal concrete containing natural rock aggregates. In some cases, it was observed that the compressive strength of concrete is decreases as we increased the percentage of rubber in concrete also there are several properties that can be improved by adding rubber aggregate to the concrete. .This waste material exists in the environment with almost no cost. The use of rubber in concrete is an excellent choice for feaseability, a cleaner environment, and a reduction in insulation cost.

Even though the rubberized concrete mixture has generally a reduced compressive strength that may limit its use in certain structural applications, it possesses a number of desirable properties, such as lower density, higher toughness, and higher impact resistance, compared to conventional concrete , For this reasons, rubbercrete represents a suitable material mostly for non-structural

purposes, including insulating screeds, lightweight masonry, external enclosure walls and filling materials.

## Bibliography:

- Ayesha Siddika , Md. Abdullah Al Mamun , Rayed Alyousef , Y.H. Mugahed Amran , Farhad Aslani , Hisham Alabduljabbar, Properties and utilizations of waste tire rubber in concrete: A review, *Construction and building materials*, volume 224, pages 711-731.
- Khaloo, A.R.; Dehestani, M.; Rahmatabadi, P. (2008). "Mechanical properties of concrete containing a high volume of tire-rubber particles." *Waste Management*, Volume 28, Issue 12, December 2008, 2472-2482.
- Siddique, R.; Naik, T. R. (2004). "Properties of concrete containing scrap-tyre rubber – an overview." *Waste Management* 24(6), 563–569.
- Topçu, I.B. (1995). "The properties of rubberized concretes." *Cement and Concrete Research*, Volume 25, Issue 2, February 1995, 304-310.
- Li, D.; Zhuge, Y.; Gravina, R.; Mills, J.E. Compressive stress strain behavior of crumb rubber concrete (CRC) and application in reinforced CRC slab. *Constr. Build. Mater.* 2018, 166, 745–759.
- Alessandro P. Fantilli, Hirozo Mihashi, Paolo Vallini, and Bernardino M. Chiaia. Equivalent Confinement in HPRCC Columns Measured by Triaxial Test. *ACI materials journal Technical paper* Title no. 108-M18.
- Ahmed Tareq Noaman , B.H. Abu Bakar , Hazizan Md. Akil . Experimental investigation on compression toughness of rubberized steel fibre concrete. *Construction and Building Materials* 115 (2016) 163–170
- Ilker Bekir Topçu. The properties of rubberized concretes. *Cement and Concrete Research*. Volume 25, Issue 2, February 1995, Pages 304-310.
- Alessandro P. Fantilli , Paolo Vallini , Bernardino Chiaia . Ductility of fiber-reinforced self-consolidating concrete under multi-axial Compression. *Cement & Concrete Composites* xxx (2011) xxx–xxx
- Ayman Moustafa, Mohamed A. ElGawady . Mechanical properties of high strength concrete with scrap tire rubber. *Construction and Building Materials* 93 (2015) 249–256.
- Bompa, D.V.; Elghazouli, A.Y.; Xu, B.; Stafford, P.J.; Ruiz-Teran, A.M. Experimental assessment and constitutive modelling of rubberised concrete materials. *Constr. Build. Mater.* 2017, 137, 246–260.
- A.Gregori<sup>1</sup>, C. Castoro<sup>2</sup>, G.C. Marano<sup>3</sup>, R. Greco<sup>4</sup>. Compressive Strength of Concrete containing Rubber Aggregates from Waste Tyres. *The New Boundaries of Structural Concrete Concrete with Recycled and Non-Traditional Materials*.
- Alessandro P. Fantilli, Hirozo Mihashi, and Paolo Vallini. Post-Peak Behavior of Cement-Based Materials in Compression. *ACI materials journal Technical paper* Title no. 104-M55.